# APPLICATIONS OF CARBON DIOXIDE WAVEGUIDE LASERS TO INFRARED SATURATION SPECTROSCOPY

a dissertation submitted by David Crocker
of Downing College, Cambridge
for the Ph.D. degree

# Applications of Carbon Dioxide Waveguide Lasers to Infrared Saturation Spectroscopy

## Abstract

The development of tunable lasers has made possible spectroscopy at a resolution previously unattainable. Although continuous-wave broadly tunable sources in the 10 μm region do not yet exist, waveguide carbon dioxide lasers offer a useful tunability about a large number of emission lines in this part of the spectrum.

The first part of this thesis contains a review of waveguide $CO_2$ laser theory and previous work on these devices. A design intended for high resolution spectroscopy is then described. Two of these lasers have been used in a spectrometer, using a saturated fluorescence to provide a stable and calibrated reference and a microprocessor-based system for control and monitoring of the tunable source. The general principles and resolution limits of sub-Doppler saturation spectroscopy are also covered.

The second part is a compendium of measurements taken and insights gained using the completed spectrometer. Collisional transitions between the hyperfine components of a methyl iodide absorption have been observed. Precise measurements of phosphine absorption frequencies indicate that far-infrared lasers may be pumped much further from resonance than has been assumed hitherto. Measurements on the allene molecule have provided improved constants for the $v_9=1$ state; the splitting of states by K- or l-doubling has also been observed, confirming theoretical predictions. Finally, a postulated Coriolis interaction between two modes of formic acid has been verified and quantified, and improved constants obtained for both modes in a study bringing together measurements taken using the waveguide laser spectrometer and the microwave and submillimetre measurements of others.

## Preface

The work described in this dissertation was carried out by the author at the Cavendish Laboratory, Cambridge, between February 1978 and November 1980. Except where explicit reference is made to the work of others, the ideas expressed are my own.

Although the concept of an offset-locked laser as a spectroscopic source is not new and parallel development of similar systems has taken place in France, it appears that the following have not been attempted outside this laboratory: the development of high stability carbon dioxide lasers using boron nitride waveguides (chapter 2) and the use of a microcomputer to control such a system and carry out real-time performance analysis (chapter 5). The spectroscopic measurements described in chapters 7 to 10 are also entirely unique to this work.

I am indebted to Mr. A. Page for his workshop skills, particularly in machining boron nitride waveguides and cutting small diffraction gratings from a master ruling. Analysis of the formic acid spectra (chapter 10) in the short time available was made possible by a computer program which Dr. B.M. Landsberg very kindly provided and modified. I am grateful to the Science Research Council for supporting me by way of a research studentship and for providing a grant for the purchase of the equipment required, and to Downing College for giving additional support in the form of a Bye-Fellowship. Finally, I am thankful for the guidance and constant encouragement of my supervisor, Dr. R.J. Butcher, to whom the conception of this project was also due.

No part of this dissertation has been or is being submitted for any degree, diploma or qualification at any other University.

D. Crocker, December 1980.

# Applications of Carbon Dioxide Waveguide Lasers to Infrared Saturation Spectroscopy

## Contents



Contents

# 1. THE CARBON DIOXIDE LASER

## 1.1 Introduction

This chapter begins with a brief review of $CO_2$ laser theory; a history and more detailed account of the subject has been given by Duley (1976). The principles of waveguide lasers will then be discussed, with emphasis on features relevant to the design of tunable $CO_2$ lasers.

## 1.2 Basic principles of $CO_2$ lasers

The essential features of a conventional low power continuous-wave $CO_2$ laser are shown in Fig. 1.1. A mixture of $CO_2$, $N_2$ and He is excited by an electrical discharge. Nitrogen molecules raised to excited vibrational states in this way cannot relax to the ground state via radiative transitions since, for a homonuclear diatomic molecule, there is no dipole moment associated with the vibration; hence relaxation is mainly by collision with other molecules. The energy of the v=1 state in nitrogen is only 18 $cm^{-1}$ less then that of the $(00^01)$ vibration in $CO_2$ (Fig. 1.2), so the population of $CO_2$ molecules in this state is greatly enhanced by such collisions. Inversion is achieved between the $(00^01)$ and the two $(10^00,02^00)$ states; these latter states are so designated because of the strong Fermi resonance between the component vibrations. The gain tube is placed in a Fabry-Perot resonator to provide optical feedback; one of the mirrors is partially transmitting to yield an output beam.

Since each vibrational state bears a manifold of rotational sub-levels, oscillation is possible on a large number of vibration-rotation transitions in each of the two bands. Individual transitions are labelled by the angular momentum quantum number J of the lower state. Emissions of the form J-1 → J are written P(J) while transtions J+1 → J are written R(J). Due to the symmetry of the molecule and the absence of nuclear spin in $^{16}O$, alternate states are absent; thus the possible emissions are P(2), P(4), P(6) ... and R(0), R(2), R(4) ... in each band. The band $(00^01) \rightarrow (10^00,02^00)_I$ is centred around 10.4 μm and the band $(00^01) \rightarrow (10^00,02^00)_{II}$ is centred near 9.4 μm, so to distinguish between these bands the transition may be prefixed by 10 or 9.

Transition strengths vary with J due to a 2J+1 degeneracy term and the Boltzmann factor $\exp(-BJ(J+1)/kT)$, peaking at values of J near 20. The 10.4 μm band is stronger than the 9.4 μm band, and the P-branches are stronger than the R-branches. A laser of the type shown in Fig. 1.1 will oscillate on one or a small number of lines near 10P(20), weaker lines being inhibited by competition. To ensure operation on a single line and to obtain the weaker lines, one of the Fabry-Perot mirrors may be replaced by a diffraction grating in the Littrow configuration, where the first-order reflection returns along the tube axis (Fig. 1.3). Emission may sometimes be obtained on transitions associated with higher vibrational states also.

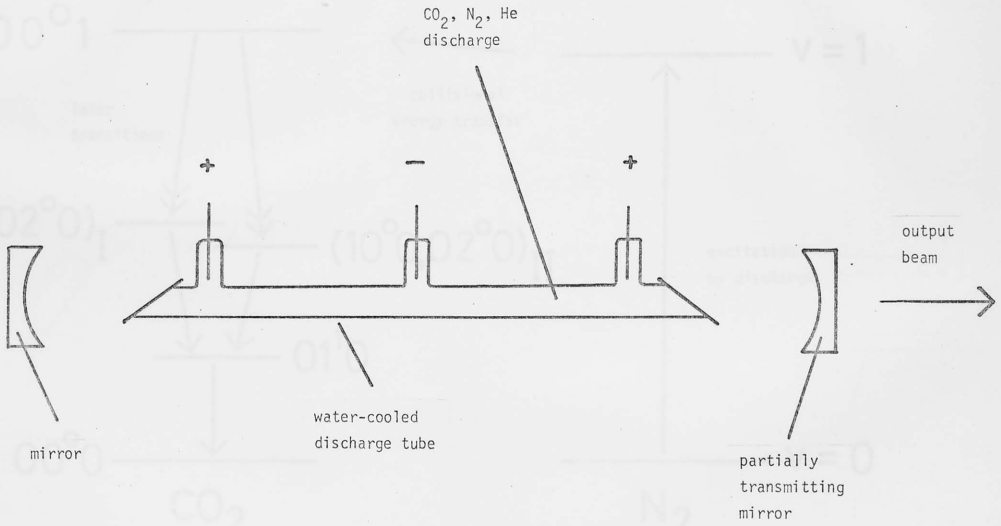


Fig. 1.1: A basic carbon-dioxide laser

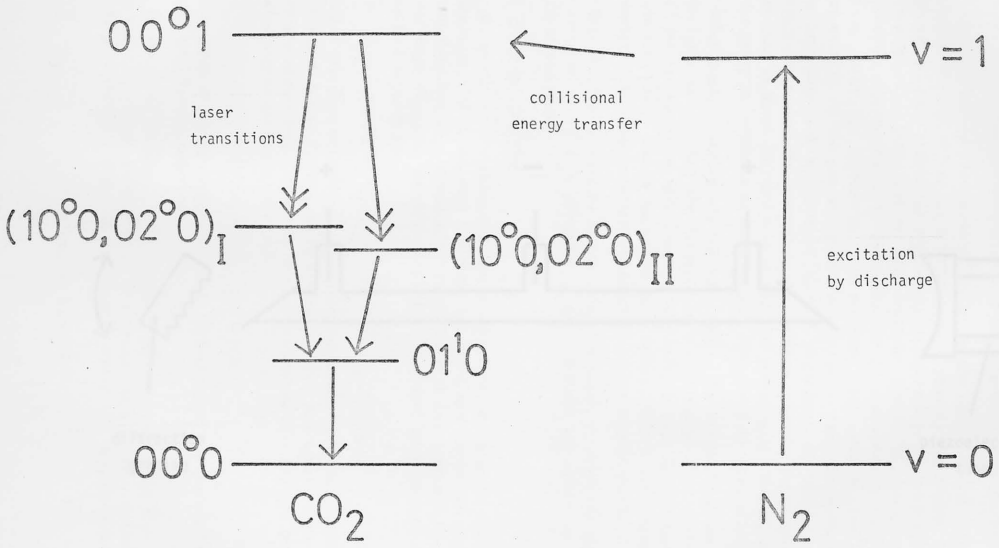


Fig. 1.2: Mechanism of carbon dioxide laser

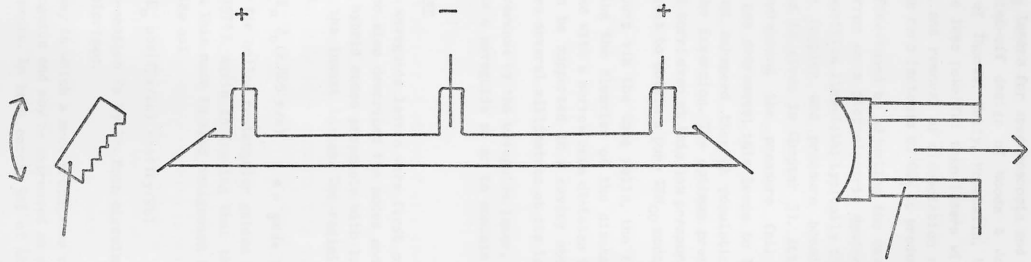


Fig. 1.3: Basic frequency-controlled $CO_2$ laser

High stability $CO_2$ lasers for spectroscopic and other applications are typified by the sealed-off design of Woods & Joliffe (1976) and the flowing gas design of Thomas, Kelly, Monchalin, Kurmit & Javan (1980). Sealed-off lasers are less powerful than lasers with gas flow due to the enhanced gas cooling and removal of dissociation products in the latter, but may be operated on rare isotopes of $CO_2$ to produce more emission lines.

The laser may be fine-tuned by adjusting the cavity length, usually by mounting the end mirror on a piezoelectric device. The tuning range is determined by the transition linewidth; typically this is about 60 MHz and arises equally from Doppler and pressure broadening (an account of broadening mechanisms is given in Chapter 3). Attempts to increase the tuning range by increasing the pressure fail because the thermal conductivity of the gas decreases; this leads to high temperatures near the tube axis and an enhanced thermal population of the lower laser levels, destroying the inversion. The optimum pressure for a sealed-off 8 mm tube is about 14 torr; even at this low pressure, the thermal gradient often makes it difficult to obtain a pure $TEM_{00}$ mode of oscillation.

Since cooling occurs via the tube walls, the thermal problem may be alleviated by reducing the diameter of the discharge tube. However, the diffraction associated with a narrow beam dictates that the smallest free-space mode which can be supported in a cavity about a metre long has a diameter which reaches several millimetres at its largest point.

This problem is overcome by the waveguide laser, in which the gain tube is designed to act as a waveguide so as to contain the radiation without diffraction loss.

## 1.3 The waveguide laser

Hollow-dielectric waveguide lasers were first proposed by Marcatili & Schmeltzer (1964), who also described the modes and losses for a circular guide. Only the $EH_{nm}$ hybrid modes propagate with low loss and the lowest order mode $EH_{11}$ has the lowest losses. The radial distribution of this mode is described by:

$$E(r) = E_o \, J_o(2.405 \, r/a) \qquad a = \text{guide radius} \qquad (1.1)$$

Similar calculations for hollow rectangular guides have been published by Laakmann & Steier (1976), again indicating that the lowest order hybrid mode propagates best. This mode is also designated $EH_{11}$ and the amplitude varies across the guide as:

$$E(x,y) = E_o \cos(\pi x/2a) \cos(\pi y/2b) \qquad (1.2)$$

for a guide of cross-section 2a by 2b. Both circular and rectangular $EH_{11}$ modes are linearly polarised.

To calculate the way in which a mode propagates on leaving a waveguide, the field at the waveguide end may be expressed as a linear combination of Gaussian free-space modes. In both cases, 98% of the $EH_{11}$ waveguide mode

couples into the $TEM_{00}$ free-space mode.

Single-frequency waveguide lasers are almost always designed to operate in the $EH_{11}$ mode. Suppression of other modes is desirable since they have slightly different propagation constants and hence lead to different frequencies if allowed to oscillate.

## 1.4 Waveguide laser resonators

A self-oscillating waveguide laser may be made by reflecting radiation back into the guide at its ends. In order to obtain oscillation in the $EH_{11}$ mode, the radiation in this mode must be returned to the same mode (i.e. it must not be appreciably scattered into higher modes). The efficiency with which various mirror-waveguide combinations achieve this has been investigated for circular waveguides by Degnan & Hall (1973) and for square ones by Avrillier & Verdonck (1977). In both cases, three low-loss situations were found (Fig. 1.4). Case I consists of a flat mirror at the waveguide end. All modes are coupled back to themselves, if the mirror is perpendicular to the waveguide axis. If the mirror is actually a small distance d from the guide end, losses occur due to diffraction. The $EH_{11}$ loss is lowest and is about $605(d/ka^2)^{3/2}\%$ for a circular guide of radius a if $d/ka^2 < 0.1$, or $1310(d/ka^2)^2\%$ for a square guide of side 2a if $d/ka^2 < 0.05$; k is $2\pi/\lambda$ where $\lambda$ is the free-space wavelength.

Case II comprises mirrors with large radius of curvature C centred on the guide end, i.e. d = C. Losses are less than 1% if $C > 3ka^2$; however, the separation d becomes more critical as C is increased. Again, all modes are coupled to themselves; $EH_{11}$ may be favoured by limiting the mirror aperture, at the cost of higher losses.

Case III comprises mirrors of radius C at a distance d = C/2 from the guide, with $ka^2/C = 2.415$ (circular) or 2.073 (square). The $EH_{11}$ losses for large aperture mirrors are 1.38% and 1.58% respectively, but other modes suffer much greater losses (e.g. $EH_{12}$ suffers 78% loss in the circular case). Hence this configuration gives good mode discrimination; also, mirror positioning is much less critical than for Case II. For these reasons, and because less cavity space is wasted, Case III is generally preferred to Case II.

## 1.5 Materials for $CO_2$ laser waveguides

Several constraints severely restrict the number of materials suitable for $CO_2$ laser waveguides. The main properties required are good electrical insulation, chemical inertness in the presence of a $CO_2/N_2/He$ discharge, high thermal conductivity (to provide good discharge cooling), good vacuum properties, a 10 um refractive index giving low guiding losses, and machinability to allow the fabrication of smooth, small bore waveguides. For large bore guides, the refractive index is less important since losses are proportional to $1/a^3$; the thermal problem is also eased since wall area increases with bore size while power input per unit length remains

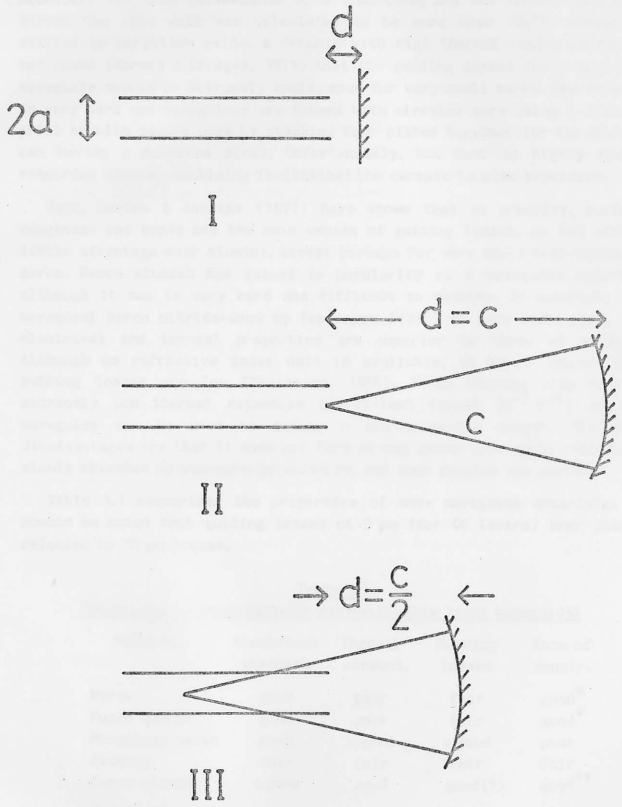


Fig. 1.4: Low-loss waveguide to mirror coupling cases

constant.

Early waveguide $CO_2$ lasers used Pyrex capilliary tubing (Bridges, Burkhardt & Smith, 1972); however, it was found that cooling to -70°C was necessary for best performance of a 1 mm tube, and the temperature drop across the tube wall was calculated to be more than 100°C. Attention shifted to beryllium oxide, a ceramic with high thermal conductivity. It was shown (Abrams & Bridges, 1973) that the guiding losses for a good BeO waveguide should be extremely small, even for very small bores. The ceramic is very hard and waveguides are formed with circular bore using a diamond drill or with square bore by stacking four plates together (or two plates, one having a machined slot). Unfortunately, BeO dust is highly toxic, requiring special machining facilities; the ceramic is also expensive.

Hall, Gorton & Jenkins (1977) have shown that in practice, surface roughness and bends are the main causes of guiding losses, so BeO offers little advantage over alumina, except perhaps for very small well-machined bores. Hence alumina has gained in popularity as a waveguide material although it too is very hard and difficult to machine. In contrast, the hexagonal boron nitride used by Papanayou (1976) is very soft; also, its electrical and thermal properties are superior to those of alumina. Although no refractive index data is available, it would appear that guiding losses are low (Papanayou, 1976). Boron nitride also has an extremely low thermal expansion coefficient (about $10^{-7}$ $K^{-1}$) so the waveguide can be used to define a stable cavity length. Its main disadvantages are that it does not form strong bonds with epoxy resins, is slowly attacked by atmospheric moisture, and some samples are porous.

Table 1.1 summarises the properties of some waveguide materials. It should be noted that guiding losses at 5 μm (for CO lasers) bear little relation to 10 μm losses.

Table 1.1

Properties of materials for carbon dioxide laser waveguides

| Material | Electrical strength | Thermal conduct. | Guiding losses | Ease of constr. |
|---|---|---|---|---|
| Pyrex | good | poor | fair | good* |
| Fused quartz | good | poor | fair | good* |
| Beryllium oxide | good | v.good | v.good | poor |
| Alumina | fair | fair | fair | fair |
| Boron nitride | v.good | good | good(?) | good** |

* using drawn tubes

** for flowing-gas designs

## 1.6 Scaling laws for waveguide $CO_2$ lasers

Abrams & Bridges (1973) have summarised the plasma scaling laws relating to $CO_2$ lasers. Provided the pressure is high enough to broaden the transition homogeneously, discharges in waveguides of various diameters d will be 'similar' if the gas pressure p and the current density J vary as 1/d. The discharge voltage and current will then vary as 1/d and d respectively, the saturation flux density as $1/d^2$, while the small-signal gain, power input and potential power output per unit length will be constant (ignoring waveguide losses). However, tuning range is proportional to pressure and hence to 1/d, so small bores are needed if tunability is wanted. These laws are very helpful when designing new waveguide lasers since the performance and optimum operating conditions can be predicted from data on existing lasers.

## 2. DESIGN OF CARBON DIOXIDE WAVEGUIDE LASERS FOR SPECTROSCOPY

### 2.1 Introduction

The first part of this chapter considers the main constraints and decisions involved in the design of tunable $CO_2$ lasers for spectroscopy. After a review of similar lasers developed elsewhere, the design adopted for the spectrometer system is described and its performance assessed.

### 2.2 Design criteria

The properties required of the laser radiation source in the high resolution spectrometer are high stability, wide tunability, controllability, good output mode shape and sufficient power to saturate transitions (Chapter 3).

Output power is not a problem since waveguide $CO_2$ lasers can easily provide several hundred milliwatts even on the weaker lines. Good output mode shape can be obtained by ensuring oscillation in the $EH_{11}$ waveguide mode only.

The problem of providing the best possible tunability on all lines is not easily solved. Using a conventional two-reflector cavity, the tuning range is limited by the cavity free spectral range (f.s.r.) as well as by the transition linewidth. The f.s.r. is equal to c/2l where l is the cavity length; hence a 1 GHz tuning range requires a cavity of length 150 mm or less. Since a wide tuning range also requires a long gain path so as to maintain oscillation as far into the wings of the gain vs. frequency curve as possible, it is appropriate to provide gain over the whole cavity length; hence Case I mirror-waveguide coupling is preferred. Reducing cavity length to increase the f.s.r. also reduces the gain; thus the cavity length is a critical compromise between these two factors, and its optimum value is strongly dependent on which laser line is being tuned.

In principle, this conflict may be resolved by introducing an auxilliary mode selecting device, thus removing the constraint on cavity length. A prototype laser using a Michaelson interferometer has been described by van Lerberghe, Avrillier & Borde (1978) but does not appear to have been developed. Leeb (1975) has performed a theoretical study of waveguide $CO_2$ lasers with internal etalons, concluding that a solid etalon would give a 50% increase in tuning range under typical conditions. In another paper (Leeb, 1976) he considers the use of a thin metal film close to one of the end reflectors as a mode selecting device, a configuration which appears to have lower losses than an etalon. It is also claimed that such a device can replace the grating as a line selector, with lower losses. Unfortunately, any mode selecting device considerably complicates the apparatus required for stabilising and tuning the laser as the positions of two cavity elements must be varied; however, this problem has been overcome in other laser systems, e.g. c.w. dye lasers.

When any waveguide $CO_2$ laser is to be tuned well into the wings of the gain curve, great care must be taken to avoid oscillation on other waveguide modes or on adjacent lines, as the cavity may be tuned near the peak of the gain curve for one of these. If the grating is placed close to the waveguide end for Case I coupling, the resolution obtained may be inadequate owing to the small number of grating lines illuminated by radiation from the narrow bore. A rectangular bore with the long side perpendicular to the grooves of the grating should give some improvement, at the expense of a non-circular output beam. It is possible to expand the beam on to the grating using a lens positioned for Case II coupling, but this method introduces reflection losses, typically 1% from each antireflection-coated surface.

In conclusion, the needs of spectroscopy would probably best be met by a long waveguide laser using Case III coupling in at least one place for transverse mode discrimination and some auxilliary device such as a metal film filter for longitudinal mode selection; some means of improving line selection would also be required. Such a laser and its control system would require considerably more development time than was available for this part of the spectrometer project.

## 2.3 Review of other designs

Abrams (1974) has described a sealed-off laser using a 95 mm by 1 mm square section beryllium oxide waveguide with a grating close to one end of the guide and a flat mirror at the other. A remarkable tunability of 1200 MHz was obtained on the 10P(20) line at a pressure of 260 torr; however, no details are given concerning the tunability on other lines or the total number of lines available. It is evident from Fig. 3 of the paper that competition from other lines is a problem; this would be much more severe in the R-branches where line separation is reduced. A short term stability of 100 kHz is quoted, with an f.m. noise peak at 2.2 kHz; experience suggests that the mechanical resonance invoked to explain this is that of the piezoelectric bimorph used to tune the laser.

A flowing-gas laser using a 200 mm by 1.65 mm bore Pyrex tube has been described by Lyszyk, Herlemont & Lemaire (1977). This device achieved tunability equal to the cavity f.s.r. of 700 MHz on three lines in the 10 um P-branch using a grating and flat mirror, and oscillation was obtained on about 60 lines. However, the authors have now changed to a design using a 150 mm by 1.5 mm bore beryllium oxide tube (Herlemont, Lyszyk, Lemaire, Lambeau & Fayt, 1979). Using a grating at one end and a curved mirror corresponding to neither of the low-loss $EH_{11}$ situations at the other, 900 MHz tunability was obtained on the strongest lines.

Another beryllium oxide design has been described by van Lerberghe, Avrillier & Borde (1978). The 1 mm square guide is about 120 mm long and coupled to the grating in Case II using a lens. The curved mirror at the other end is also coupled in Case II; the large amount of space thus wasted

limits the tunability to the cavity f.s.r. of 545 MHz. However, a very high stablity of a few kHz has been obtained from this laser and extensive spectra of $SF_6$ and other molecules recorded. Discussion with one of the authors revealed that the lens is thought to introduce a significant loss; in particular, lenses with different coatings are required for the 9 and 10 μm bands. Unlike other designs, piezoelectric cylinders are used for tuning instead of a bimorph.

After the completion of the lasers for the spectrometer, a similar design using 150 mm or 300 mm boron nitride waveguides was published by Evans, Prunty & Sexton (1980). The performance described is similar to that obtained here, except that the tunability quoted is somewhat lower; this may be due to the inclusion of antireflection-coated windows at the waveguide ends, which are absent in the design to be described.

2.4 Design of lasers used in the saturation spectrometer

Boron nitride was chosen as the waveguide material as it is superior in many respects to other materials (except beryllium oxide) and could be machined in the laboratory workshop. A flowing-gas design was chosen after encountering porosity problems; although this prohibits the use of rare isotopes of $CO_2$, the resulting system has a better and more consistant performance than a sealed-off arrangement and is easier to use; in particular, the gas composition and pressure can be changed whenever required.

For maximum versatility and ease of maintenance, the lasers were constructed in the form of five sub-assemblies, namely the waveguide, grating assembly, output mirror, heatsink and frame.

The frame is a rigid structure consisting of 10 mm thick aluminium alloy end plates joined by four 20 mm diameter invar or stainless steel bars. It is bolted to the table, from which it is insulated by a spacer to avoid earth loops. The frame supports the grating assembly and heatsink directly; it can also support an output mirror or other auxilliary optics if necessary.

2.5 Grating assembly

The grating assembly (Fig. 2.1) is bolted to the end plates; the outer casing is a stainless steel cylinder which is gas-tight when the waveguide assembly is attached. Three micrometers with non-rotating shafts penetrate the removable end flange via O-ring seals; these support a pair of circular knife edges holding a disc of piezoelectric bimorph, to which a small wedge of 150 line/mm diffraction grating is attached. The wedge was cut from a large original copper grating, blazed for 10 μm and gold coated (PTR Optics type ML303). Two of the spherical tips of the micrometer shafts are located in recesses in the bimorph holder; a spring holds the assembly in place, making an electrical connection between one knife edge and an insulated feedthrough in the end flange. A second weaker spring

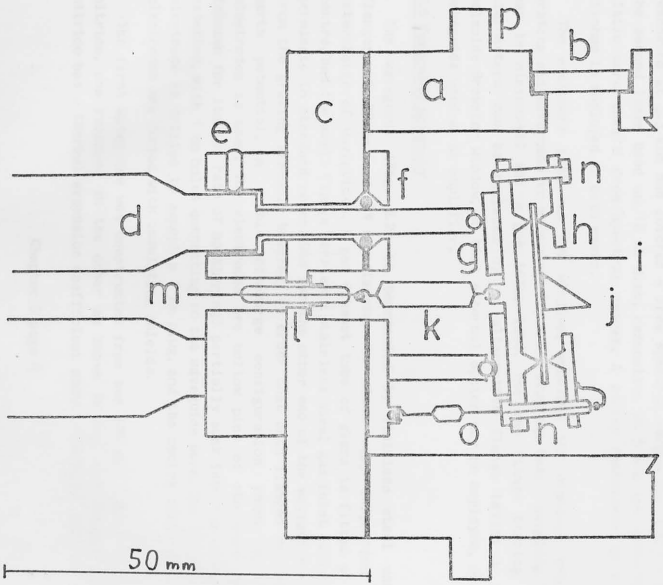


a - cylindrical housing
b - glass window
c - vacuum flange
d - micrometer (1 of 3)
e - micrometer clamp
f - shaft seal
g - PTFE plate
h - stainless steel plate with knife edge
i - bimorph
j - grating
k - main spring
l - insulating feedthrough
m - tuning voltage connection
n - nylon screw
o - earthing spring
p - fixing ring

Fig. 2.1: Grating assembly

earths the other knife edge to the wall of the enclosure.

The bimorph comprises two oppositely poled discs of piezoelectric ceramic bonded together, with silvered faces. When a voltage is applied between these faces, the resulting field causes one disc to contract and the other to expand. The disc buckles like a bimetallic strip, and since the disc is held by knife edges at the periphery, the centre portion bearing the grating translates. Compared to the piezoelectric tubes commonly employed in larger lasers, the bimorph assembly is smaller and requires much lower voltages, e.g. 50 V for one f.s.r. (5 μm movement) as opposed to typically 2 kV for a 50 mm long tube. The disadvantages are that the translation for a given voltage is dependent on the pressure applied via the knife edges, and that the fundamental resonance of the loaded disc has a high Q-factor and a relatively low frequency of a few kHz. The frequency can be raised by using a small disc, with some loss of sensitivity, while some damping may be provided by carefully choosing the output resistance of the amplifier providing the electrical drive.

In practice the use of bimorphs has proved satisfactory. The first laser (now used as the reference laser) employed a 26 mm disc which resonated at 3.3 kHz and covered 4 free spectral ranges for 160 V drive; the second laser used an 18 mm disc, resonating at 5 kHz and covering a little more than 2 free spectral ranges. A series resistance of a few kilohms is employed in both cases.

The enclosure also has two windows, enabling the distance between grating and waveguide to be viewed (in order that the Case I coupling loss may be minimised) and a gas inlet tube. The end flange bearing the micrometers can be replaced by an alternative flange having a zinc selenide Brewster window, so that external optics may be employed, or the waveguide used as an amplifier.

## 2.6 Waveguide assembly

The waveguide (Fig. 2.2) is terminated by stainless steel vacuum flanges of 70 mm and 34 mm diameter to allow easy inspection and interchange of waveguides. A gas exhaust tube of glass is fitted at the centre, and the small flange carries a stainless steel gas inlet tube; both terminate in standard cones. Gas for the other end of the waveguide comes from the grating assembly housing. In order that both flanges may be at earth potential, a double discharge configuration requiring four electrodes is used. The electrodes are hollow pins of stainless steel (chosen for its low rate of sputtering) partially sunk into the waveguide exterior, with 1 mm holes connecting to the waveguide bore. The top of each electrode is drilled to accept a 2 mm plug, and the centre (high voltage) electrodes are fitted with insulating shields.

The first waveguide was constructed from two 300 mm lengths of boron nitride, one recessed in the other as shown in Fig. 2.3. Because boron nitride has a thermal expansion coefficient about 1000 times smaller than

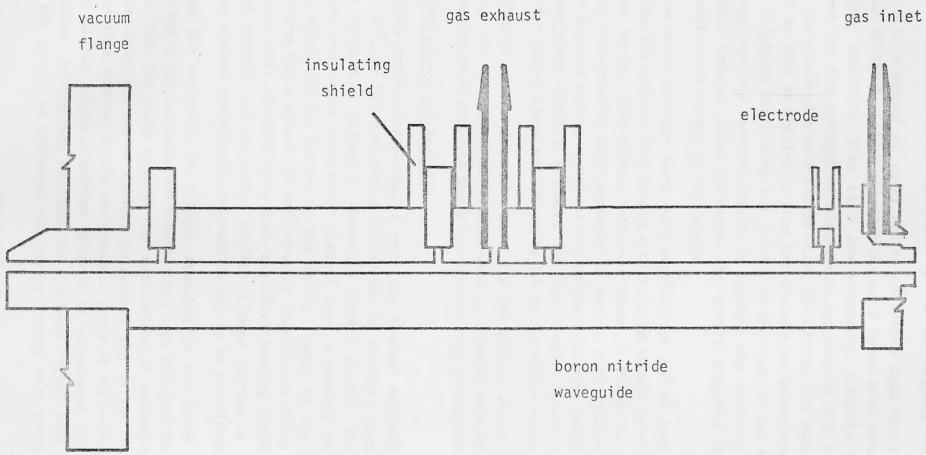


Fig. 2.2: Waveguide assembly

that of epoxy resins, the adhesive used to fill the gaps between the two pieces will tend to shrink away from the walls on cooling. Since epoxies do not form very strong bonds with boron nitride, it was necessary to use a highly flexible adhesive (Eccogel 1265 from Emerson & Cuming Ltd.). This problem was avoided in later waveguides built to the design of Fig. 2.4, in which the thickness of the adhesive layer is not tightly constrained.

Tests on a number of epoxy resins indicated that Araldite MY753 with Hardener HY1456GB yielded superior strength bonds with boron nitride than the other adhesives. This is a low viscosity, slightly flexible epoxy intended for the potting of electrical components. All waveguide parts except the electrodes were bonded using this resin. The adhesive was cured at 35°C so that on cooling to room temperature the stainless steel flanges shrank slightly, tightening the joints. In the case of the electrodes, the shrinkage has the reverse effect so bonding was achieved using Eccogel 1265, with reduced joint strength. The entire assembly was designed to avoid mechanical stress at all joints.

Since boron nitride bars were supplied in 300 mm lengths, the first waveguide was made to this length with a 1.6 mm square bore; this was later assigned to the line-centre reference laser. A 150 mm by 1 mm waveguide was also constructed; this appeared to have a bore smaller than optimum, but was damaged during modifications before extensive tests were possible. The waveguides finally produced for the tunable laser were 150 mm by 1.2 mm for strong lines and 300 mm by 1.4 mm for weaker ones.

Diffusion of air into the bore via the porous walls was reduced by spraying the waveguide assemblies with a plastic anti-corona compound; this coating also protects the boron nitride from atmospheric moisture.

2.7 Output mirror and heatsink

Because boron nitride has a very low thermal expansion coefficient (about $10^{-7}$ per °C), the output mirror can be directly mounted on the end of the waveguide, giving a thermally stable cavity. The flat cadmium telluride mirror is epoxied or clamped over a central hole in a 34 mm flange, which can be bolted to the mating flange on the waveguide. The intervening Viton gasket is sufficiently flexible to allow adjustment of the mirror tilt. Flanges have been assembled bearing mirrors of 95%, 98% and 99% nominal reflectivity. Another flange carries a zinc selenide Brewster window, enabling an external mirror to be used instead.

Since the waveguide is rigidly attached to the frame via the large flange, the aluminium heatsink assembly has been designed for good removal of heat from the guide without the application of mechanical force. This is achieved by the use of springs to support the weight of the heatsink, which is then clamped to the waveguide. A layer of silicone grease between the two allows relative motion. Coolant is circulated via two flexible nylon tubes joining the heatsink to a stress relief bush bolted to the table; the latter is connected via larger tubing to a refrigerator in an

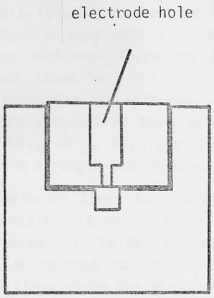


Fig. 2.3: Waveguide cross-section, original design

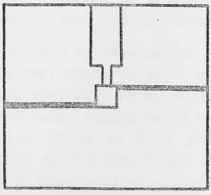

Fig. 2.4: Waveguide cross-section, final design

adjoining room.

A photograph of the complete laser is shown in Fig. 2.5.

## 2.8 Operating conditions and performance

The centre electrodes are driven from a supply of up to 20 kV through 1.8 MΩ ballast resistors. Optimum current for the 300 mm waveguides varies from 2 mA on low-J lines to more than 4 mA in the 11 μm hot band, in each of the two discharge sections. Operating pressure ranges from about 50 torr on the weakest lines to 220 torr on the strongest, for maximum tunability. At these pressures and with correct alignment, oscillation is always in the $EH_{11}$ mode although at lower pressures the 1.6 mm bore laser will switch between $EH_{11}$, $EH_{12}$, $EH_{13}$ and sometimes other modes if the cavity is scanned over a strong P-branch line.

Competition from adjacent lines is evident when attempts are made to tune the laser well away from line centre, although this can normally be suppressed in the P-branches. In the R-branches a combination of high pressure and careful adjustment of the cavity length usually succeeds, except for very low-J lines where the stronger line at J+2 often persists. These competition problems only occur when the cavity is tuned; only one line oscillates at a time. Likewise only one mode oscillates at a time (i.e. the output is single-frequency), except near the edges of the tuning curve, when mode beats may occasionally be seen on a fast detector.

The total number of lines observed in the 9 and 10 μm bands is greater than 80; a few lines in the 11 μm hot-band can also be obtained. Using the 300 mm waveguide, several lines in the 9 μm P-branch and in each of the 10 μm branches can be tuned over the cavity f.s.r. of 470 MHz, using the 99% reflector. Maximum output power was 2.5 W using the 95% mirror and it is clear that greater output would be possible using lower reflectivity; in practice, however, operation on weak lines is more important than power so the 98% and 99% reflectors are used.

The performance of the 150 mm by 1.2 mm waveguide is disappointing; the maximum tuning range obtained is 790 MHz on 10P(20), and fewer lines can be obtained. For these reasons, and because of the time taken to change from one waveguide and heatsink to another, only the 300 mm by 1.4 mm waveguide has been used for spectroscopic studies.

The width of the beat note between two of the waveguide lasers is about 100 kHz when free-running, measured over 1 second after a few minutes warm-up. To obtain this stability it was necessary to modify the Hartley Measurements 421 series power supply units to reduce the output ripple; a peak ripple current of 15 μA in 4 mA from the unmodified supplies increased the beat width to 200 kHz. It was also necessary to improve the signal-to-noise ratio of the amplifiers driving the laser bimorphs.

The discharge current (monitored at one of the end electrodes) shows sudden fluctuations, often several per second, which cause observable

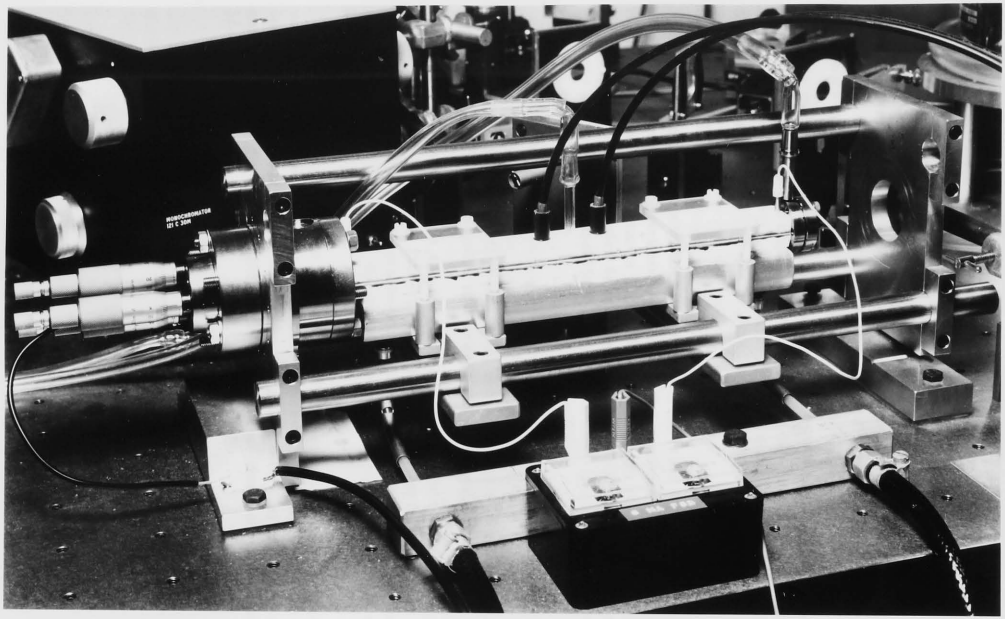

Fig. 2.5: Photograph of an assembled waveguide laser

amplitude changes in the laser output and are probably partly responsible for the linewidth. The nature of these has been investigated and the source appears to be the discharge itself, although corona discharge from the ballast resistors may be a contributory factor. It is postulated that hot spots are formed where the discharge meets the electrodes, causing the the discharge to jump to another part of the electrode surface; this phenomenon is frequently observed in the case of large tubular cathodes used in conventional $CO_2$ lasers. Electrodes in the form of pins should be less liable to this problem since they offer a smaller area than the hollow cups employed at present.

Plasma oscillations at frequencies of order 100 MHz are observed when the centre electrodes are negative with respect to the ends but are absent using the reverse polarity. The contribution of these to the linewidth seems to be small.

## 2.9 Conclusions

Although the lasers have been successfully employed in spectroscopic studies, further development would give a useful performance improvement. The elimination of discharge flicker must take first priority; the replacement of cup electrodes by pins would be worthwhile and the ballast resistors and smoothing capacitors could be immersed in oil to eliminate corona.

When fast gas flow is employed, the temperature of the incoming gas becomes more significant than that of the waveguide, so the fitting of a heat exchanger in the gas inlet line would probably improve tunability; in particular, the 150 mm waveguide might reach its 1 GHz limit.

Apart from the discharge flicker problem, the waveguide laser design described is ideal for the line-centre reference and performs well as a tunable laser, although a purpose-built laser with mode selection and better line selection could be somewhat better on the strong lines at least.

Finally, the operation of a carbon monoxide laser using a boron nitride waveguide has recently been reported (Hauck & Huffman, 1980). This indicates that adaptation of the present design to CO by cooling the inlet gas and replacing the mirror and grating by 5 μm components should produce good results.

## 3. PRINCIPLES OF THE WAVEGUIDE LASER SATURATION SPECTROMETER

### 3.1 Introduction

In this chapter, the principles of infrared saturation spectroscopy and the associated experimental techniques will be discussed. The waveguide laser spectrometer will then be described in outline; details of the stabilisation techniques employed are to be found in later chapters.

### 3.2 Resolution limits in infrared spectroscopy

The attainable resolution in conventional infrared spectroscopy is limited by the resolving power of available diffraction gratings and the brightness (power per unit bandwidth) of broadband thermal sources. Two solutions to the brightness problem have been found. One is to record data on all parts of the spectrum simultaneously, exploiting all the useful power of the thermal source instead of selecting just a small fraction. Fourier-transform spectrometers achieve this, giving higher resolution and much greater speed than grating spectrometers. The second solution is to use a radiation source producing all its power in a narrow band at a variable frequency. Although microwave spectroscopy has always used narrow-band sources, the application of this technique in the infrared had to await the development of tunable infrared lasers.

The linewidths of these lasers can be so narrow (better than 1 in $10^9$) that resolution is limited by mechanisms which broaden the transition rather than by the width of the source. In conventional spectroscopy, linewidths may be kept below the instrument resolution (except in the case of the best Fourier-transform spectrometers) by using a sample in the form of a gas at low pressure. However, once the pressure is reduced below about 5 torr, the width of the absorption becomes limited by the varying Doppler shifts seen in the incident radiation by molecules with a range of speeds. Since the number of molecules (of mass m) with a velocity component v resolved along the probe beam is proportional to $\exp(-mv^2/2kT)$, the Doppler-broadened absorption is described by:

$$I = \exp(-mc^2(f - f_o)^2/2kTf^2) \qquad (3.1)$$

where I is the absorption intensity at frequency f due to a nearby transition at frequency $f_o$. The full-width to half-maximum (FWHM) is given by:

$$f_{Doppler} = 2f_o(kT(\ln 2)/mc^2)^{1/2} \qquad (3.2)$$

which, at room temperature and 30 THz frequency (10 μm wavelength) becomes:

$$f_{Doppler} = 3.7 \times 10^8/\sqrt{M} \text{ Hz} \qquad (3.3)$$

where M is the molecular weight. A typical value would be 50 MHz, which is much greater than the linewidth of a continuous-wave $CO_2$ laser.

Doppler broadening can be eliminated by forcing a non-thermal velocity distribution on the molecules (e.g. using a molecular beam) or by selectively observing molecules in a velocity subset. One method of achieving the latter will now be described.

3.3 Saturated absorption in a standing-wave field

If a sample gas is subjected to very intense radiation at a frequency within the absorption linewidth, it is possible to maintain a non-thermal distribution of population between the two quantum states concerned. If the radiation linewidth and homogeneous broadening are much narrower than the Doppler broadening, only those molecules whose velocity component v along the beam brings them into resonance will have depleted lower state and enhanced upper state populations.

Suppose a counter-propagating beam of the same frequency is now added. Molecules with velocity -v will suffer a similar fate since their absorption is Doppler-shifted into resonance with this reverse beam. There will thus be two 'holes' in the lower state velocity distribution and two 'spikes' in the upper state, as shown in Fig. 3.1.

This situation may be realised using a suitably strong laser beam which is reflected back on itself at one end of the absorption cell. If the beam is directed at a detector after its second pass through the cell, the absorption may be monitored. As the laser is tuned, the value of v for which the molecules are in resonance with the beam changes, and the Doppler absorption profile may be traced out. However, when the laser matches the absorption frequency, only molecules with v=0 can interact with either beam; thus both beams sample the same set of molecules and due to the saturation (i.e. the existance of 'holes' and 'spikes') the total absorption is somewhat reduced. This appears as a dip at the peak of the Doppler profile (Fig. 3.2).

The dip allows resolution to be greatly increased since, at sufficiently low pressure, it is a much sharper feature than the Doppler lineshape, indicating the true position of the absorption. Many molecules have sets of absorptions which overlap when Doppler broadened; in such cases the saturation dips are usually distinct.

The relative size of the dip varies with the saturation parameter S, defined by:

$$S_{12} = (p_{12}E/\hbar R)^2 \qquad (3.4)$$

where E is the strength of the radiation electric field, $p_{12}$ is the transition dipole moment and R is the relaxation rate (i.e. the rate at which collisions and other processes tend to thermalise the relative populations of the two states). Thus strong absorptions are easier to saturate than weak ones; also, saturation is enhanced at low pressures since collisions make a large contribution to the relaxation processes.

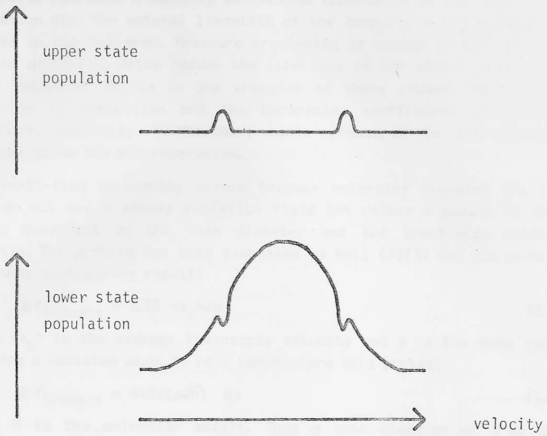


Fig. 3.1: Saturation of a transition by laser beam

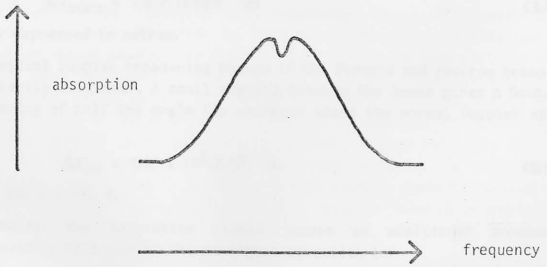


Fig. 3.2: Absorption with Lamb dip

Various residual broadening mechanisms contribute to the width of the saturation dip. The natural linewidth of the transition can generally be ignored in the infrared. Pressure broadening is caused by the collisions between molecules, which reduce the lifetimes of the states involved and cause momentary shifts in the energies of these states. The broadened lineshape is Lorentzian and the broadening coefficient is molecule-dependent, typically 10 MHz/torr; hence pressures in the region of 10 mtorr allow 100 kHz resolution.

Transit-time broadening occurs because molecules crossing the laser beam do not see a steady radiation field but rather a packet of finite length dependent on the beam diameter and the transverse molecular velocity. The problem has been discussed by Hall (1973) who has given the following approximate result:

$$\Delta f_{transit} = 0.75 \langle v_x \rangle / a \qquad (3.5)$$

where $\langle v_x \rangle$ is the average transverse velocity and a is the beam radius, assuming a Gaussian beam. At room temperature this yields:

$$\Delta f_{transit} = 940/(a\sqrt{M}) \text{ Hz} \qquad (3.6)$$

where M is the molecular weight. Thus a beam diameter of 3 mm gives typically 100 kHz broadening.

If the wavefronts of the laser beam have significant curvature, this also contributes to broadening since molecules crossing the beam see a varying Doppler shift (Letokhov & Chebotayev, 1977). The broadening is given by:

$$\Delta f_{curv} = (4kTf_o/cmr)^{1/2} \qquad (3.7)$$

where r is the wavefront radius of curvature. At 30 THz and 300 K this becomes

$$\Delta f_{curv} = 1.8 \times 10^6/\sqrt{Mr} \text{ Hz} \qquad (3.8)$$

with r expressed in metres.

Residual Doppler broadening occurs if the forward and reverse beams are not exactly collinear. A small angle $\alpha$ between the beams gives a Gaussian broadening of half the angle (in radians) times the normal Doppler width, i.e.:

$$\Delta f_{rd} = 1.85 \times 10^8 \alpha/\sqrt{M} \text{ Hz} \qquad (3.9)$$

at 30 THz and 300 K.

Finally, the saturation itself causes an additional broadening discussed by Hall (1973). The saturated linewidth is:

$$\Delta f_{sat} = f_o(1 + S)^{1/2} \qquad (3.10)$$

where $f_o$ is the homogeneous linewidth at zero power and S is the saturation parameter.

## 3.4 Detection of weak absorptions

When studying weakly absorbing molecules, the total absorption (using a few millitorr pressure) may only be a small fraction of the laser power and hence difficult to see in the presence of laser noise. Also, the saturation parameter may be so low as to render the dip very small.

The observation of such absorptions is made possible by the following method. The laser is frequency modulated over a range of several hundred kHz or less by a sinewave, usually in or somewhat above the audio-frequency range. As the laser frequency moves over the absorption profile (Fig. 3.3), the intensity of the transmitted radiation will follow this modulation. Performing a Taylor expansion of the transmittance curve T(f) about the mean frequency of the laser $f_o$, we obtain:

$$T(fo+ fdcos(wt)) = T(fo) + fdcos(wt)T'(fo) + fd^2cos^2(wt)T''(fo) + . . \qquad (3.11)$$

If the peak deviation fd is small, the main contribution at a frequency cos(nwt) will be from the term $fd^n cos^n(wt)T^{(n)}(fo)/n!$ and will therefore have amplitude:

$$A_n = fd^n T^{(n)}/2^n n! \qquad (3.12)$$

where $T^{(n)}$ is the $n_{th}$ derivative of T with respect to f. Given an electrical signal proportional to the transmitted beam, it is a simple matter to pick out one of the components using a phase-sensitive-detector (p.s.d.) fed with a reference at n times the laser modulation frequency.

The advantage of monitoring a derivative of the absorption is that small features which vary rapidly with frequency are emphasised with respect to more slowly changing backgrounds; the first derivative of a strongly saturated absorption typically gives a signal 10 times larger than that due to the larger and broader Doppler profile.

First-derivative detection is commonly used in laser Stark spectroscopy, where the laser is held at a constant frequency and the transition itself is tuned by an electric field. It is less suitable for a tunable laser spectrometer since the laser output power changes as its frequency is swept, giving rise to a background first-derivative which will mask a weak saturation dip. In this situation, third-derivative detection is used (i.e. the p.s.d. is supplied with a reference at three times the modulation frequency). The signal obtained in this way is unfortunately much smaller than a first-derivative, depending on the cube of the modulation amplitude; however, the Doppler absorption profile is virtually eliminated.

Fig. 3.3 shows the shapes of first and third derivative signals observed as a laser is scanned across a saturated absorption, ignoring the laser power variation. In both cases, the central zero-crossing coincides with the dip centre if the lineshape is symmetrical, and therefore gives the

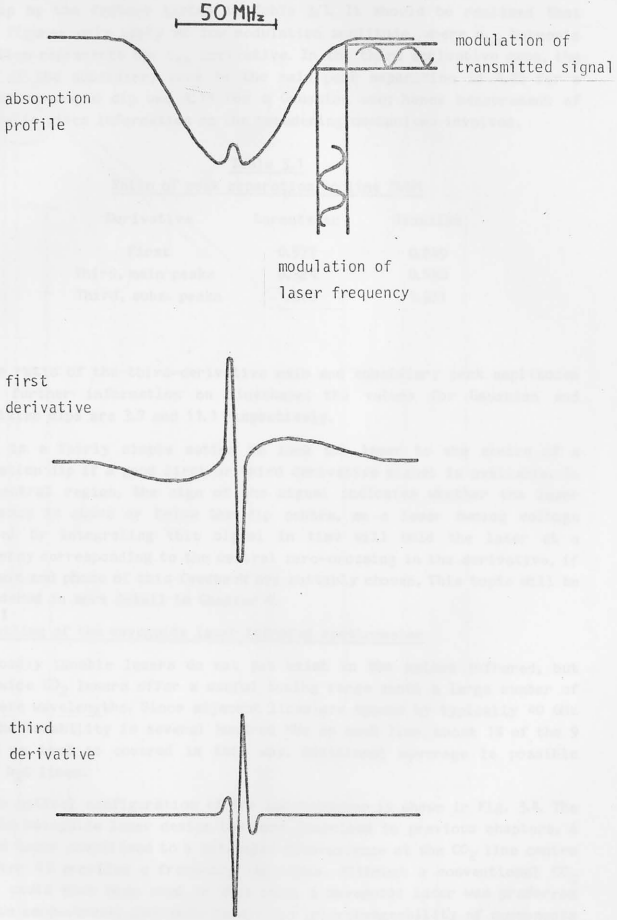


Fig. 3.3: The absorption profile and its derivatives

transition frequency.

The separation of the peaks on either side is related to the FWHM of the dip by the factors listed in Table 3.1. It should be realised that these figures only apply at low modulation amplitude, where $n_{th}$ harmonic detection represents the $n_{th}$ derivative. In the third derivative case, the ratio of the subsidiary peak to the main peak separation is 4.25 for a Lorentzian-shaped dip and 3.14 for a Gaussian one; hence measurement of this ratio gives information on the broadening mechanisms involved.

Table 3.1
Ratio of peak separation to line FWHM

| Derivative | Lorentzian | Gaussian |
|---|---|---|
| First | 0.577 | 0.849 |
| Third, main peaks | 0.324 | 0.630 |
| Third, subs. peaks | 1.376 | 1.981 |

The ratio of the third-derivative main and subsidiary peak amplitudes gives further information on lineshape; the values for Gaussian and Lorentzian dips are 3.7 and 11.1 respectively.

It is a fairly simple matter to lock the laser to the centre of a saturation dip if a good first or third derivative signal is available. In the central region, the sign of the signal indicates whether the laser frequency is above or below the dip centre, so a laser tuning voltage derived by integrating this signal in time will hold the laser at a frequency corresponding to the central zero-crossing in the derivative, if the gain and phase of this feedback are suitably chosen. This topic will be considered in more detail in Chapter 4.

## 3.5 Outline of the waveguide laser infrared spectrometer

Broadly tunable lasers do not yet exist in the medium infrared, but waveguide $CO_2$ lasers offer a useful tuning range about a large number of discrete wavelengths. Since adjacent lines are spaced by typically 40 GHz and the tunability is several hundred MHz on each line, about 1% of the 9 to 11 μm band is covered in this way. Additional coverage is possible using $N_2O$ lines.

The optical configuration of the spectrometer is shown in Fig. 3.4. The tunable waveguide laser design has been described in previous chapters. A second laser stabilised to a saturated fluorescence at the $CO_2$ line centre (Chapter 4) provides a frequency reference. Although a conventional $CO_2$ laser could have been used in this role, a waveguide laser was preferred for its compactness, good mode purity and interchangeability of components with the other laser; also, the use of a common design reduced the amount of development work required.

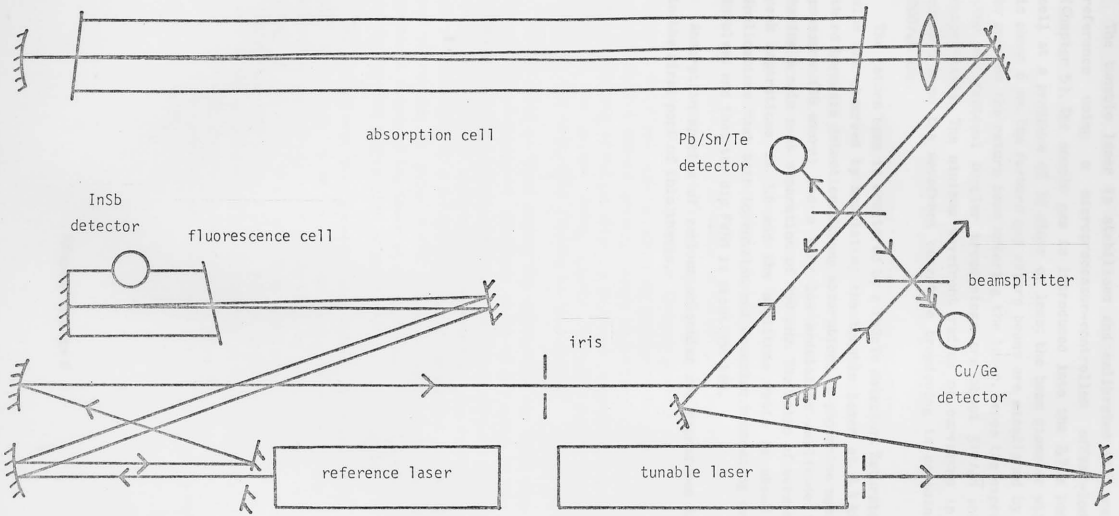


Fig. 3.4: Optical configuration of spectrometer

The tunable laser is stabilised and calibrated with respect to the reference using a microprocessor-controlled offset-locking system (Chapter 5). The sample gas is introduced into the 2.7 m long absorption cell at a pressure of 30 mtorr or less; the beam diameter within the cell is about 6 mm. The forward and return beams are misaligned by about 2 mrad to prevent the return beam entering the laser. Hence the expected transit-time and residual Doppler broadenings are about $310/\sqrt{M}$ and $370/\sqrt{M}$ kHz respectively. The minimum wavefront radius of curvature in the cell is about 5 m so the wavefront curvature broadening is certainly less than $800/\sqrt{M}$ kHz.

The return beam is monitored by a PbSnTe detector. Saturated absorption dips are observed by modulating the tunable laser at 3.3 kHz and using third harmonic detection. Strong absorptions in phosphine monitored at low pressure (15 mtorr) and a very low modulation amplitude yield traces having a main peak separation of 150 kHz. The ratio of subsidiary to main peak separations is 3.6 and the amplitude ratio is about 9, with the implications that both Lorentzian and Gaussian broadening mechanisms are involved and that the dip FWHM is about 350 kHz.

Absorption spectra of various molecules are reproduced and discussed in the final part of this thesis.

## 4. THE REFERENCE LASER STABILISATION SYSTEM

### 4.1 Introduction

The function of the reference laser is to provide a stable and known frequency with which the tunable laser can be compared. The saturated fluorescence stabilisation technique described here was chosen for this purpose because it is applicable to all $CO_2$ laser lines, and the frequencies of $CO_2$ lasers stabilised in this way are known to a precision of $\pm$50 kHz in most cases (Freed, Bradley & O'Donnell, 1980).

### 4.2 Principles of saturated fluorescence stabilisation

Consider a $CO_2$ laser beam directed into a cell also containing $CO_2$. Some molecules in the cell will be in an excited vibration-rotation state corresponding to the lower of the two levels between which the laser is operating. These molecules may resonantly absorb the laser radiation, resulting in their excitation to the upper of the two levels (Fig. 4.1). This absorption is the inverse of the lasing process.

In principle, it is possible to detect this absorption directly, but it is very weak because the lower laser vibrational level is about 1300 $cm^{-1}$ above the ground state, giving a thermal population at room temperature which is 400 times smaller than the ground state population. Fortunately, an alternative method exists, namely to monitor the spontaneous emission at a wavelength of 4.3 μm which is produced by molecules relaxing from the upper to the ground state. Liquid nitrogen cooled indium antimonide detectors are background limited in this region.

As the laser is tuned across the absorption, the fluorescence intensity has a Doppler-broadened lineshape about 50 MHz wide, if the $CO_2$ pressure is sufficently low. If the laser beam is reflected back through the cell, a saturation dip will appear in the absorption (see Chapter 3) and hence in the fluorescence. By a suitable choice of parameters, the width of this dip may be reduced to under 1 MHz. It is possible to construct a feedback system to maintain the laser at the frequency corresponding to the centre of the dip with a precision of about 1 % of the dip width.

The pioneers of this locking technique (Freed & Javan, 1970) used a $CO_2$ cell inside the laser cavity. The method has since been developed by several groups. A fairly detailed study of a system using an external cell (Woods & Joliffe, 1976) indicated that the frequencies of stabilised lasers were reproducible to $\pm$ 5kHz. A greatly improved signal-to-noise ratio in the fluorescence signal has been claimed for large external cells using a cooled elliptical reflector to increase the collection efficiency of the 4.3 μm radiation and reduce the thermal background noise (Freed & O'Donnell, 1977).

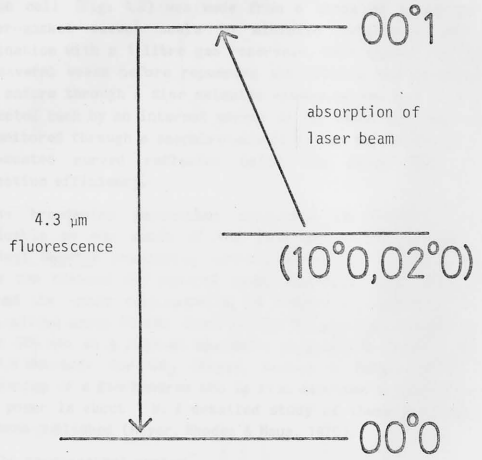


Fig. 4.1: Mechanism of laser-induced fluorescence in $CO_2$

## 4.3 Fluorescence cell

A design using a cooled reflector was considered but rejected as it required an unencapsulated InSb element of high quality as an integral part of the construction. Instead, a conventional design using an external InSb detector in a dewar with a sapphire window was used. Such detectors are available commercially with guaranteed performance. Signal-to-noise ratio is improved by using one with a large area element (7 mm square) to catch as much of the 4.3 μm radiation as possible.

The cell (Fig. 4.2) was made from a block of stainless steel using copper-gasket vacuum seals to minimise outgassing and leakage. In combination with a 1 litre gas reservoir, this allows the cell to be used for several weeks before repumping and filling are necessary. The laser beam enters through a zinc selenide window at one end of the cell and is reflected back by an internal mirror at the other end. Radiation at 4.3 um is monitored through a sapphire window at the top of the cell. An internal gold-coated curved reflector below the laser beam increases the collection efficiency.

The broadening mechanisms discussed in Chapter 3 are directly applicable to the width of the line-centre dip in the fluorescence. Residual Doppler broadening contributes about 100 kHz to the fullwidth, since the forward and reverse beams are misaligned by about 4 mrad to prevent the return beam entering the laser. The beam radius in the cell is 3 mm, giving about 50 kHz transit-time broadening. Pressure broadening is about 425 kHz at a nominal operating pressure of 50 mtorr, using a figure of 8.5 MHz/torr for $CO_2$ (Meyer, Rhodes & Haus, 1975). A saturation broadening of a few hundred kHz is also expected on strong lines where the beam power is about 1 W. A detailed study of these broadening mechanisms has been published (Meyer, Rhodes & Haus, 1975).

## 4.4 The servocontrol system

The laser is locked to the centre of the dip as follows. A 500 Hz sinewave of low amplitude is applied to the laser bimorph, giving a corresponding frequency modulation with a peak-to-peak deviation of a few hundred kHz. The intensity of the 4.3 um fluorescence shows a variation at the same frequency with an amplitude proportional to the slope of the intensity vs. frequency curve at the laser frequency (Chapter 3). Hence a phase-sensitive-detector fed from the fluorescence signal with the 500 Hz modulation as reference gives a d.c. output proportional to the first derivative of this curve. In particular, the output becomes very large on the sides of the dip, where the slope is largest. The changing sign of the derivative from one side to the other is reflected as a change in polarity of the p.s.d. output, which passes through zero at the centre of the dip. Thus the signal is a measure of the amount by which the laser frequency is in error.

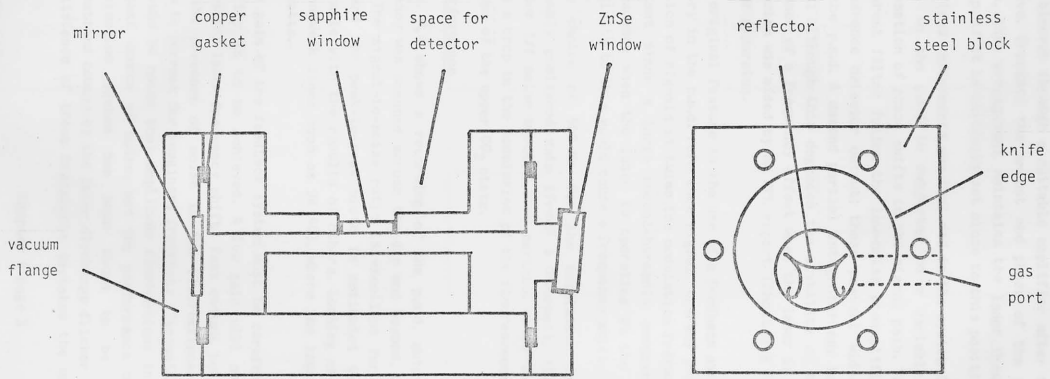


Fig. 4.2: Fluorescence cell

This error signal is applied to an integrator, whose output drives the laser bimorph through a suitable amplifier after adding the small 500 Hz sinewave. Provided the amount and phase of the feedback are correctly chosen, this arrangement maintains the laser frequency at the centre of the dip, if it is initially set close to this position.

Various refinements are included in the system (Fig. 4.3). The reference signal to the p.s.d is subjected to a variable phase shift to allow compensation of phase shifts in the signal path. Two tuned amplifiers and a coherent filter follow the low-noise preamplifier used to amplify the fluorescence detector output; these prevent wideband noise interfering with the p.s.d. A second partial integrator may be inserted at the p.s.d. output; although this degrades the stability of the loop, it avoids the existence of a frequency offset when the laser is drifting. The design of the system was aided by an NPL report (Shotton & Rowley, 1975) describing similar apparatus.

An original feature is the use of a feedback system to maintain perfect symmetry in the p.s.d. reference signal, thereby providing more than 80 db rejection of signals at twice the modulation frequency. This is especially important since a large second-harmonic component is present in the fluorescence when the laser is operating at the centre of the dip, and sensitivity to this would cause a frequency shift.

The choice of 500 Hz for the modulation frequency was based on previously published data (Freed & O'Donnell, 1977). At low frequencies detector 1/f noise becomes more serious, while increasing the frequency causes a drop in the modulation of the fluorescence signal due to the long lifetime of the upper $CO_2$ state.

## 4.5 Performance

Fig. 4.4 shows a recording of the p.s.d. output taken as the laser frequency was scanned across the dip and beyond, using the 10P(20) laser line. The signal-to-noise ratio is excellent for a simple cell of this type and the peak-to-peak width is estimated to be 800 kHz, a figure comparable with the results of others. Locking of the laser is possible even on weak lines such as 9R(40), where the laser output is only a few milliwatts.

The gain of the feedback system must be carefully adjusted if maximum stability is to be achieved. A low gain will not allow the system to correct for laser frequency shifts fast enough, but if the gain is set too high the presence of noise in the fluorescence signal will cause the system to correct for imaginary frequency fluctuations. In this connection it should be noted that amplitude fluctuations in the laser beam are an important source of noise, and the performance of the reference laser stabilisation system has been found to be limited by transient fluctuations caused by the laser discharge flicker described in Chapter 2. The existence of these transients dictates the use of a low loop gain.

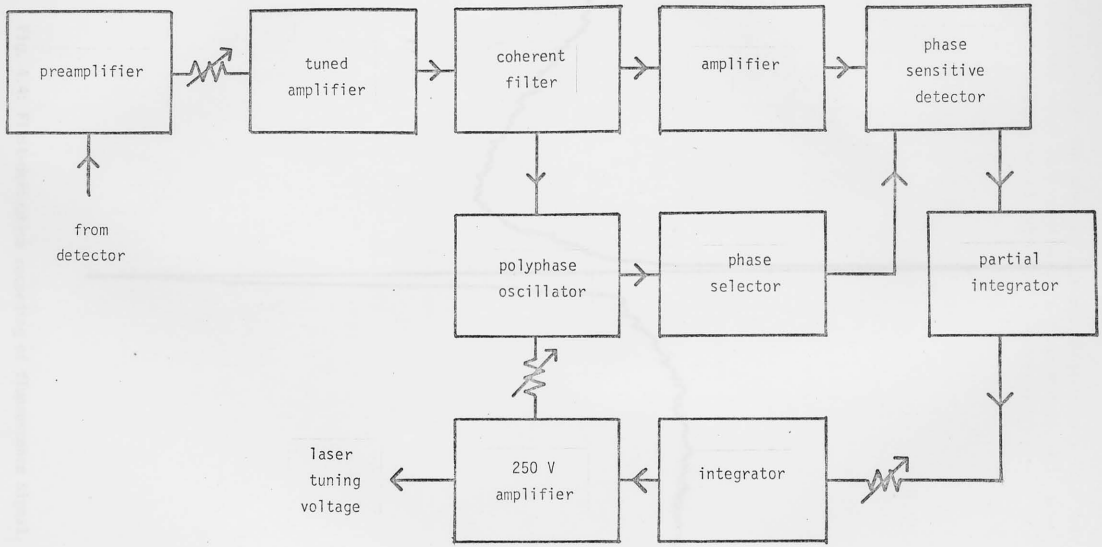


Fig. 4.3: Reference laser servocontrol unit

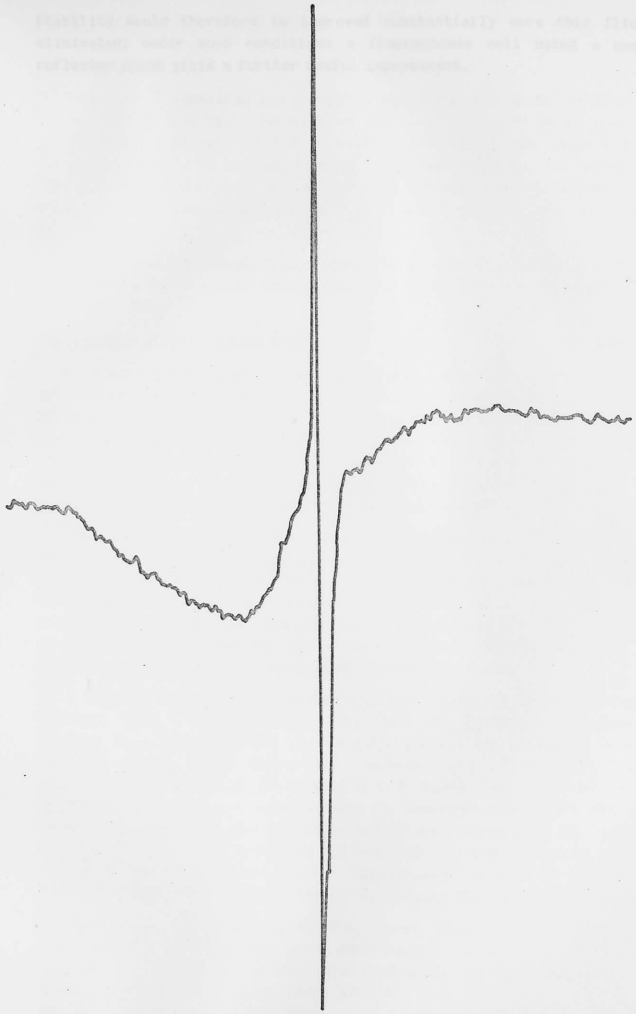

Fig. 4.4: First-derivative recording of fluorescence signal.

Stability would therefore be improved substantially were this flicker eliminated; under such conditions a fluorescence cell using a cooled reflector might yield a further useful improvement.

## 5. THE TUNABLE LASER CONTROL SYSTEM

### 5.1 Introduction

This chapter describes the apparatus used to stabilise and control the tunable laser. The basic function of the control system is to hold the laser at the frequency of the stabilised reference laser plus a given frequency offset, a technique known as offset-locking. The offset is monitored by illuminating a fast infrared detector with collinear beams from the two lasers, giving an electrical signal at the difference frequency.

The microprocessor-controlled system to be described allows the offset to be varied from 1 to 320 MHz (positive or negative) in 5 kHz steps, given a suitable laser.

### 5.2 Previous offset locking systems

A spectrometer similar to the system described here has been constructed at the Laboratoire de Physique des Lasers, Paris (van Lerberghe, Avrillier & Borde, 1978). Their stabilisation system (Fig. 5.1) uses an analogue offset-locking method in which the difference frequency is applied to a frequency-to-voltage convertor. The output from this is compared with a voltage representing the required offset and the difference is integrated to produce a laser correction voltage.

The accuracy and stability of such a system is necessarily poor since it will be sensitive to ageing and temperature drift in a number of components and the frequency-to-voltage convertor may possess appreciable non-linearity. Thus the system is satisfactory for short-term stabilisation only, and spectra obtained must be calibrated using a frequency meter to monitor the offset frequency. Systems in which the comparison is achieved digitally overcome these problems.

A digital offset-locking system has been described in an NPL report (Rowley, 1977) . In this design (Fig. 5.2), the difference frequency is applied to a prescaler and programmable divider to produce a nominal 62.5 kHz signal, which drives the count-up input of a 12-bit binary counter. A 62.5 kHz reference derived from a crystal oscillator drives the count-down input of the same counter. The counter outputs are fed to a digital-to-analogue convertor, whose output thus represents the integral of the difference in frequency between the 62.5 kHz reference and the output of the programmable divider. This voltage is used to correct the laser. The offset frequency is varied by changing the ratio of the divider.

The system as described in the report (Rowley 1977) is clearly unsuitable for a waveguide laser spectrometer as both its range (5 to 75 MHz) and resolution (5 MHz) are inadequate. Although modifications could give improvements on these figures, more serious problems arise. First, the loop gain of the system varies inversely with the divider ratio

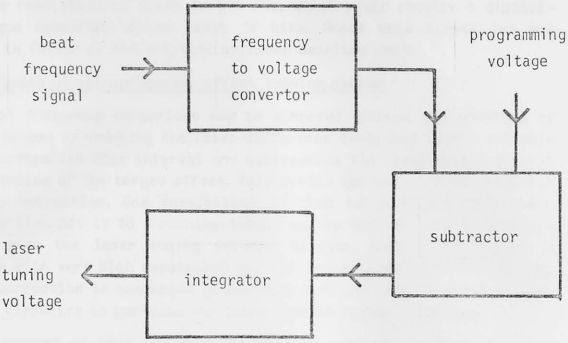


Fig. 5.1: Basic offset-lock system using analogue techniques

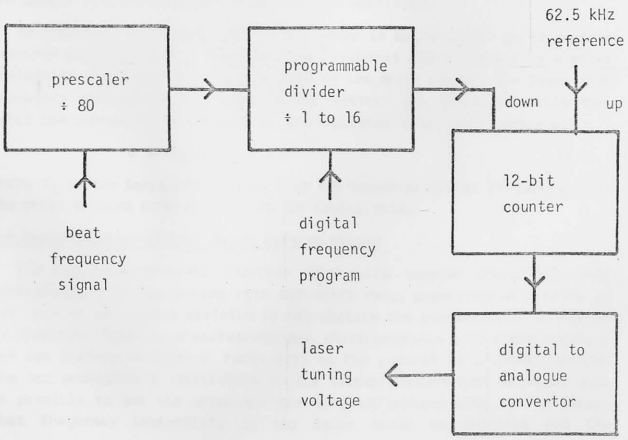


Fig. 5.2: Digital offset-lock system by Rowley

and hence with offset frequency. Although the 15:1 variation in the original system may have been acceptable, a 500:1 variation (for offset frequencies of 1 to 500 MHz) would certainly cause problems. Second, the laser tuning voltage must be generated with a resolution of at least 1 in $10^5$ for a resolution of 5 kHz in 500 MHz, which would require a digital-to-analogue convertor of at least 17 bits. Hence this system too was rejected in favour of the original approach desribed next.

5.3 Principles of microprocessor offset locking system

Digital frequency comparison may be achieved without the problems of Rowley's method by counting the laser difference frequency over a suitable crystal-controlled time interval and subtracting the count from a digital representation of the target offset. This yields the value of the required frequency correction. One possibility is then to integrate this value digitally (i.e. add it to a running-total) and to convert this to analogue form to give the laser tuning voltage; however, this would require a convertor with very high resolution (as for Rowley's method). Instead, the digital correction is converted to analogue form and this is integrated by analogue circuitry to generate the laser control signal (Fig. 5.3).

A refinement of this approach is to integrate the correction for a short time only and delay sampling the frequency again until some time after this period, so that each frequency sample includes the full effect of the previous correction. If the tuning rate of the laser (i.e. the frequency change for unit correction voltage) is accurately known, it then becomes possible to provide an exact correction to the laser after each sample, resulting in a response time for the control loop which is equal to the sample time (and therefore the fastest possible).

In practice, the tuning rate of the laser is not constant so it must be measured at intervals by observing the frequency change caused by a given correction. It is also possible to observe the drift rate of the laser (the frequency change for zero applied correction) and allow for this too. Hence the correction to be applied is calculated after each sample as:

$$c = (f_t - f - d) / r \qquad (5.1)$$

where $f_t$ is the target frequency, f is the measured offset frequency, d is the drift between samples and r is the tuning rate.

5.4 Implementation of the offset locking system

The algorithm desribed involves some quite complex operations (e.g. determination of the tuning rate and drift rate, detection of failure of the control loop, and a division in calculating the correction). The system is therefore based on a microprocessor, which provides a flexible solution and can perform additional tasks such as the control of a chart recorder and the provision of statistics on the system performance. It would also be possible to use the processor for data collection with the advantage that frequency instability in the laser could be detected and the

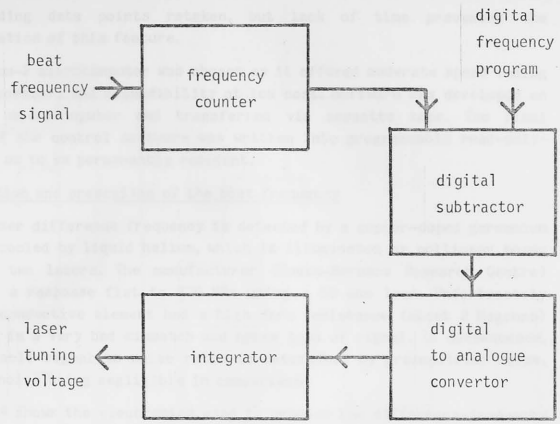


Fig. 5.3: Alternative digital offset-lock system

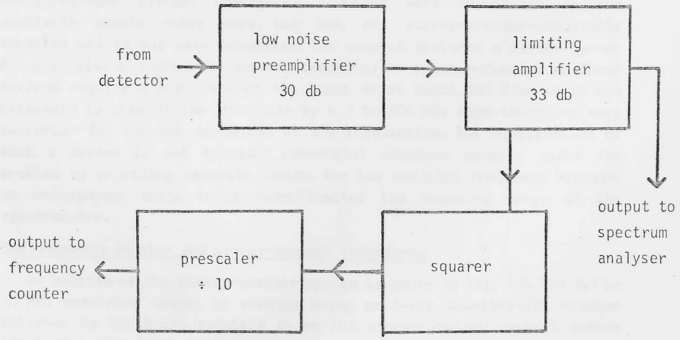


Fig. 5.4: Difference frequency signal processor

corresponding data points retaken, but lack of time prevented the implementation of this feature.

A Nascom-2 microcomputer was chosen as it offered moderate speed (using a Z80A processor) and expandibility at low cost. Software was developed on a larger microcomputer and transferred via cassette tape. The final version of the control software was written into programmable read-only-memory so as to be permanently resident.

5.5 Detection and prescaling of the beat frequency

The laser difference frequency is detected by a copper-doped germanium detector cooled by liquid helium, which is illuminated by collinear beams from the two lasers. The manufacturer (Santa-Barbara Research Centre) specified a response flat to 400 MHz using a 50 ohm load. Unfortunately the photoconductive element had a high dark resistance (about 2 Megohms) resulting in a very bad mismatch and hence loss of signal. In consequence, the available signal-to-noise ratio is determined by preamplifier noise, detector noise being negligible in comparison.

Fig. 5.4 shows the electronics used to process the difference-frequency signal. Commercial low-noise thick-film modules were used for the first two stages of amplification. Further amplifiers with good limiting characteristics were built to give more than 60 db total gain over a bandwidth of 500 MHz. A lower cutoff of 1 MHz was chosen to avoid flicker noise, which becomes appreciable below this frequency for wideband transistors. The amplifier chain yields a beat frequency signal of nearly a volt when the detector is illuminated by a few milliwatts from each beam, with signal-to-noise ratio greater than 30.

The frequency counter was built as an integral part of the microprocessor system. Commercial counters were unsuitable as the available sample rates were too low, and microprocessor-compatible versions are in any case expensive. The counter includes a divide-by-ten ECL prescaler to reduce the maximum frequency to a manageable value. These devices require a slew rate at the input of at least 100 V/us so it was necessary to precede the prescaler by a 1 to 500 MHz sine-to-square wave convertor for correct operation at low frequencies. The construction of such a device is not trivial; commercial counters usually avoid the problem by providing separate inputs for low and high frequency signals, an arrangement which would have limited the scanning range of the spectrometer.

5.6 Frequency counter and microprocessor interfaces

An outline of the microprocessor system is shown in Fig. 5.5. The 0.1 to 50 MHz prescaler output is counted using an 8-bit Schottky-TTL counter followed by two 8-bit counters in an LSI microprocessor support device (Z80A-CTC). Two more counters in the same integrated circuit define a programmable gate time referenced to the master processor clock, which was

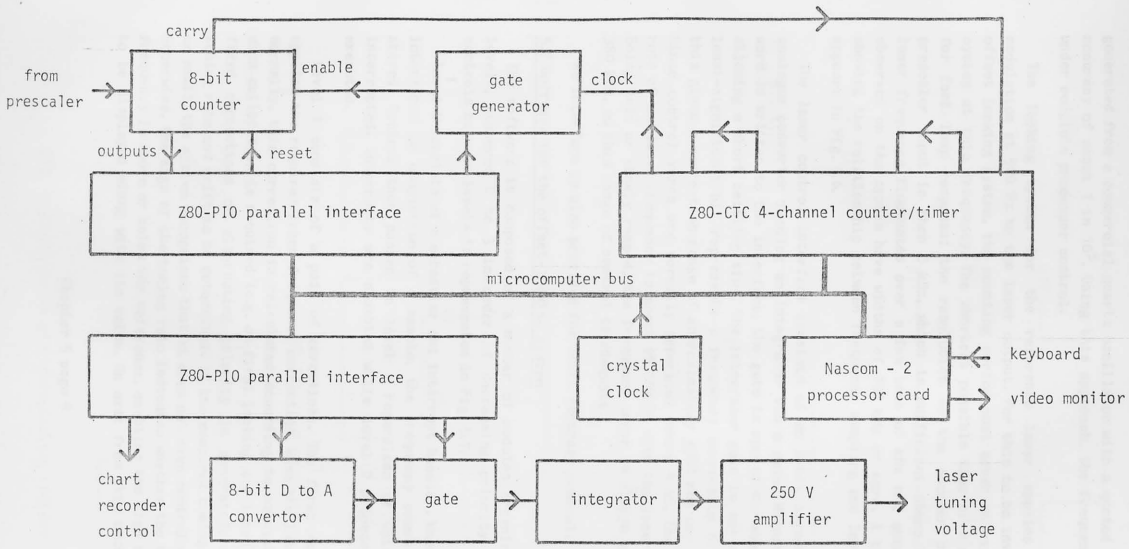


Fig. 5.5: Microcomputer system interface and frequency counter

generated from a commercial quartz oscillator with a quoted stability and accuracy of about 1 in $10^5$. Using this approach, the frequency counter is under complete processor control.

The locking system for the reference laser applies a frequency modulation at 500 Hz to the laser output. For this to be invisible to the offset locking system, the counting period must cover an exact number of cycles at this frequency. The shortest possible time of 2 ms was chosen for fast loop response; the resolution of the counter system at the prescaler input is then 5 kHz, which is sufficient since the reference laser frequency fluctuates over a few tens of kHz and absorption lines observed on the system have widths of 100 kHz or more. A timing diagram showing the relationship between frequency sampling and laser correction appears in Fig. 5.6.

The laser control interface consists of an 8-bit signed digital-to-analogue convertor feeding an integrator via a gate. Whenever a control word is written to the interface, the gate is opened for about 1 ms after allowing a short settling time. The integrator gain is set such that the least-significant bit represents a frequency correction of about 3 kHz; this gives a correction range of approximately $\pm$380 kHz per control word. Since control words are normally generated every 4 ms, the maximum slew rate of the laser frequency is about 95 MHz/s. When the laser frequency is being held or slowly ramped, the frequency error is always much less than 380 kHz, so this range of control is adequate.

An interface is also provided for chart recorder control.

## 5.7 Software for the offset-locking system

The software is composed of a number of modules organised into four levels, numbered 0 to 3 in order of decreasing priority. The flow of controls between levels is represented in Fig. 5.7.

Level 0 consists of a scheduler and interrupt handler. When the counter interrupts on completion of a sample, the frequency count is read and stored. Control then passes to level 1 regardless of which level was interrupted. Interrupts are disabled while level 0 processes are being executed.

Level 1 consists of a pair of coroutines. The first determines and applies the required laser frequency correction. When the laser is running normally, this correction is calculated according to equation (5.1), but when calibration is required (e.g. on first locking the laser) a series of fixed corrections of alternating polarity is generated, allowing the tuning rate and drift to be determined. If the measured tuning rate is zero or small, the system recognises that it does not have control of the laser; otherwise, the sign of the tuning rate indicates whether the tunable laser frequency is above or below the reference, enabling the sign of the offset to be displayed along with its value. On exit from this routine, another

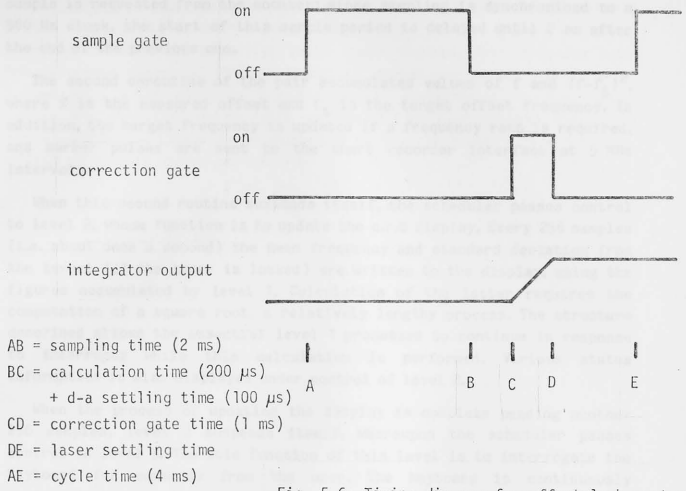


AB = sampling time (2 ms)
BC = calculation time (200 μs)
+ d-a settling time (100 μs)
CD = correction gate time (1 ms)
DE = laser settling time
AE = cycle time (4 ms)

Fig. 5.6: Timing diagram for offset-lock system

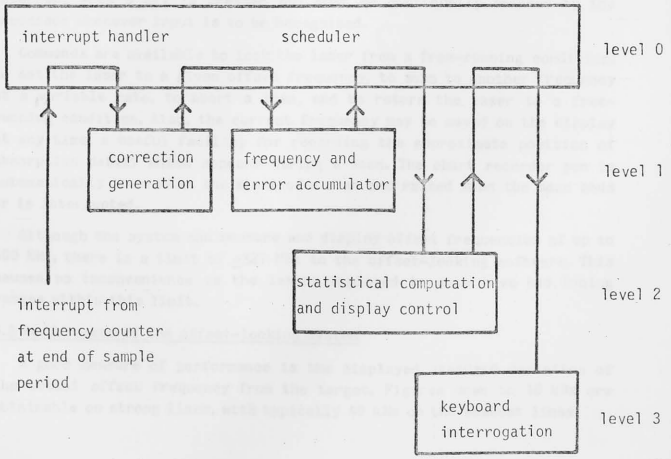


Fig. 5.7: Structure of offset-locking software

sample is requested from the counter; since sampling is synchronised to a 500 Hz clock, the start of this sample period is delayed until 2 ms after the end of the previous one.

The second coroutine of the pair accumulates values of f and $(f-f_t)^2$, where f is the measured offset and $f_t$ is the target offset frequency. In addition, the target frequency is updated if a frequency ramp is required, and marker pulses are sent to the chart recorder interface at 5 MHz intervals.

When this second routine suspends itself, the scheduler passes control to level 2, whose function is to update the c.r.t display. Every 256 samples (i.e. about once a second) the mean frequency and standard deviation from the target (if the laser is locked) are written to the display, using the figures accumulated by level 1. Calculation of the latter requires the computation of a square root, a relatively lengthy process. The structure described allows the essential level 1 processes to continue in response to interrupts while this calculation is performed. Various status information is also displayed under control of level 2.

When the process of updating the display is complete pending another 256 samples, level 2 suspends itself, whereupon the scheduler passes control to level 3. The sole function of this level is to interrogate the keyboard for commands from the user. The keyboard is continuously monitored whenever there are no more urgent tasks to attend to at lower levels. This approach is necessary since, like other low-cost microcomputers, the Nascom-2 has a keyboard which cannot generate an interrupt when a key is pressed but must be continually scanned by the processor whenever input is to be recognised.

Commands are available to lock the laser from a free-running condition, to set the laser to a given offset frequency, to scan to another frequency at a variable rate, to abort a scan, and to return the laser to a free-running condition. Also, the current frequency may be saved on the display at any time, a useful facility for recording the approximate position of absorption detail which appears during a scan. The chart recorder pen is automatically lowered at the start of a scan and raised when the scan ends or is interrupted.

Although the system can measure and display offset frequencies of up to 500 MHz, there is a limit of $\pm$327 MHz in the offset-locking software. This causes no inconvenience as the lasers employed to date have had tuning ranges within this limit.

5.8 Performance of the offset-locking system

A good measure of performance is the displayed standard deviation of the actual offset frequency from the target. Figures down to 10 kHz are obtainable on strong lines, with typically 40 kHz on the weakest lines.

The effect of increasing the gain of the reference laser stabilisation system (Chapter 4) to give a loop time-constant of less than 0.1 s is to increase the standard deviation above these figures. This suggests that the reference laser and its stabilisation system are the main sources of instability, which accounts for the poorer performance on weak lines (since the signal-to-noise ratio of the 4.3 μm fluorescence signal is worse). Hence the improvements discussed in Chapter 4 would have a direct effect on overall system performance.

## 6. THEORY OF MOLECULAR VIBRATION-ROTATION SPECTRA

### 6.1 Introduction

An exact solution of the complete molecular Hamiltonian is at present impossible for all but the simplest molecules, but the use of the Born-Oppenheimer approximation (Born & Huang, 1954) to separate the electronic from the nuclear terms is reasonable for most molecules in the electronic ground state. It is assumed that the electrons reach an equilibrium distribution much more rapidly than the heavier nuclei; hence, in a given electronic state, the potential energy of the molecule in free space may be considered a function of the nuclear coordinates only since the electrons will always be in the corresponding equilibrium state. In the following treatment, the motion of the electrons will therefore be ignored; their contribution to the energy of the system is included in the nuclear potential energy term.

### 6.2 Separation of vibration and rotation terms

A molecule of N nuclei has 3N position coordinates and an associated 3N momentum coordinates. Instead of using the coordinates of the individual nuclei, it is appropriate to use independent linear combinations of these in order to separate the various types of motion. Furthermore, it will be assumed that the molecule has a single equilibrium configuration, and all displacements will be expressed relative to this.

The first three coordinates used will be those describing motion of the centre of mass, i.e. $m_i x_i$, $m_i y_i$ and $m_i z_i$ (where the repeated suffix implies summation over all nuclei). These coordinates describe simple translations and are of no spectroscopic interest. The remaining coordinates will be chosen to preserve the centre of mass. If the molecule is non-linear, another three coordinates may be found to describe rotations. Initially, the molecular rotation and vibration will be taken to be independent.

The remaining 3N-6 coordinates (3N-5 for a linear molecule) describe vibrations. Since the equilibrium configuration was chosen as origin, the potential energy can have no linear dependence on these coordinates. For small vibrations in the majority of molecules, the second order term dominates the higher terms; these terms will therefore be neglected. The potential energy of the molecule may then be written:

$$V = V_{ij} q_i q_j \qquad (6.1)$$

where $q_i$ are the 3N-6 vibrational coordinates and summation convention is invoked.

It is possible to choose the coordinates $q_i$ as linear combinations of the nucear displacements $x_i$ such that the cross terms vanish, i.e.

$$V = V_i q_i^2 \qquad (6.2)$$

Such combinations are termed the normal coordinates of the molecule; the

symbols $q_i$ will henceforth denote them. Furthermore, they shall be mass-weighted such that the classical momentum conjugate to $q_i$ is $\dot{q}_i$. The vibrational part of the Hamiltonian may then be written:

$$H_{vib} = -\tfrac{1}{2}\hbar^2 \frac{\partial^2}{\partial q_i \partial q_i} + V_i q_i^2 \qquad (6.3)$$

Hence the choice of normal coordinates reduces the problem to a set of harmonic oscillators, each of which must have energy $(n + 1/2)\hbar\omega$; hence the energy associated with molecular vibration, neglecting the zero-point term, is:

$$E_{vib} = \hbar\omega_i n_i \qquad (6.4)$$

The vibrational states of a molecule may be denoted by the form $(n_1,n_2,\ldots n_{3N-6})$ where $n_i$ is the number of quanta in the $i_{th}$ mode. An alternative notation often used to describe simple excitations takes the form $n_1\nu_1+n_2\nu_2+\ldots$; thus a state (010..0) could be written simply $\nu_2$.

In molecules possessing appreciable symmetry, degenerate vibrational modes may exist; for example, the linear molecule $CO_2$ has two equivalent bending modes in mutually perpendicular planes. Any two independent linear combinations of these vibrations will serve as basis modes; in particular, if the two planar vibrations are combined with a $90^o$ phase difference, the resulting motion possesses angular momentum. Since this couples with the rotation of the molecule, it is appropriate to choose basis modes of this form. The excitation of a degenerate vibration is denoted $n^l$ where n is the total number of vibrational quanta involved and $l$ is the associated angular momentum; $l$ varies from -n to +n in steps of 2. This (n+1)-fold degeneracy arises from the fact that n quanta can be divided between two modes in n+1 ways.

In a similar manner, all vibrations perpendicular to the three-fold axis of a molecule such as $CH_3I$ are doubly degenerate and an angular momentum l of $\pm 1$ is associated with the singly excited state. These states are commonly denoted $v_i^{+l}$ and $v_i^{-l}$ and are degenerate only to a first approximation.

## 6.3 Effects of anharmonicity

The effect of third and higher order terms in the nuclear potential are readily observable in high-resolution spectra by the following effects. First, energy levels associated with a particular vibration are not quite evenly spaced; similarly, the energy of a combination mode is not quite equal to the sum of the energies of its component vibrations. Second, the degeneracy of the different $l$-components of a multiply-excited degenerate vibration is split to the extent that states of differing $|l|$ have slightly different energies (other terms also contribute to this effect). Third, the anharmonic terms will mix any two vibrations of the same symmetry which have an accidental near-degeneracy; this effect, known as Fermi resonance, causes mixing of the eigenfunctions and a shift of the two

energy levels away from each other. This type of interaction has already been mentioned (Chapter 1) in connection with the (100) and ($02^00$) states of $CO_2$.

Finally, anharmonicity allows various transitions to occur which would otherwise be forbidden, such as overtones of the form $0 \rightarrow 2v_i$; this transition will generally be somewhat weaker than $0 \rightarrow v_i$.

## 6.4 Energy of rotation

A rigorous treatment of molecular rotation is lengthy (Kroto, 1975); however, the main results may be obtained as follows. The molecule will be treated as a rigid rotor. Within this approximation, there is no potential energy associated with rotation in isotropic space and the Hamiltonian may be written classically as:

$$H = \tfrac{1}{2} I_{ij} \Omega_i \Omega_j \tag{6.5}$$

where I is the inertia tensor and $\Omega_i$ (i = 1 to 3) are the instantaneous angular velocities about three mutually perpendicular axes. These axes may be chosen such that the cross-terms vanish, i.e.

$$H = \tfrac{1}{2} I_i \Omega_i^2 \tag{6.6}$$

or, in terms of the angular momenta $J_a$, $J_b$, $J_c$,

$$H = AJ_a^2 + BJ_b^2 + CJ_c^2 \tag{6.7}$$

where $A = 1/(2I_a)$ etc.

By expressing the angular momenta in terms of position and momentum coordinates, the following commutation relations for the corresponding operators in quantum mechanics may be established:

$$[J_i, J_j] = i\varepsilon_{ijk} J_k \tag{6.8}$$

$$[J^2, J_i] = 0 \tag{6.9}$$

where $J^2 = J_i J_i$ is the total angular momentum of the molecule. Some particular cases will now be discussed.

## 6.5 Symmetric top molecules

We consider a molecule in which A > B = C (a prolate top). The Hamiltonian (6.7) may be written:

$$H = BJ^2 + (A-B)J_a^2 \tag{6.10}$$

Since $J^2$ commutes with $J_a$, there exist simultaneous eigenfunctions of both operators; the associated integral quantum numbers will be denoted j and k. The following relations may be established using ladder operators (Kroto, 1975):

$$J^2|j\ k\rangle = j(j+1)|j\ k\rangle \tag{6.11}$$

$$J_a|j\ k\rangle = k|j\ k\rangle \tag{6.12}$$

$$(J_b \pm iJ_c)|j\ k\rangle = [(j\pm k)(j\pm k+1)]^{1/2}|j\ k\pm 1\rangle \tag{6.13}$$

Since $0 \leq J_a^2 \leq J^2$ it follows from the first two of these that $j \geq 0$ and $|k| \leq j$. Hence the energy levels of the rigid symmetric rotor are:

$$E_{Jk} = BJ(J+1) + (A-B)k^2 \qquad (6.14)$$

where the conventional symbol J has been used in place of j, with J = 0, 1, 2, ... and k = -J, -(J-1), ... J. Each level has a degeneracy of 2J+1, which is the number of possible orientations of J with respect to a space-fixed axis. It is evident that the states (J,k) and (J,-k) have the same energy, so it is usual to label states by J and K, where K = |k|; levels with K > 0 are doubly degenerate in addition to the 2J+1 degeneracy.

By convention, the principal rotational constants are chosen such that $A \geq B \geq C$; hence the energy eigenvalues of an oblate top, in which $A = B \geq C$, are:

$$E_{JK} = BJ(J+1) + (B-C)K^2 \qquad (6.15)$$

A special case is the spherical top with A = B = C; the energies are simply BJ(J+1) with degeneracy $(2J+1)^2$.

## 6.6 Asymmetric top molecules

In the case of an asymmetric top it is no longer possible to find exact analytical solutions since the Hamiltonian cannot be written in terms of commuting operators. A technique commonly used is to express the eigenfunctions as linear combinations of those of a symmetric top; for example, if $A > B \tilde{-} C$ the Hamiltonian may be written:

$$H_r = \tfrac{1}{2}(B+C)J^2 + (A-\tfrac{1}{2}(B+C))J_a^2 + \tfrac{1}{2}(B-C)(J_b^2-J_c^2) \qquad (6.16)$$

A slightly different form of H is often used in numerical work, but the method of solution is similar. Since $J^2$ commutes with H, the eigenfunctions of H may be written as:

$$|j\ K_n'\rangle = a_{ni}|j\ K_i\rangle \qquad (6.17)$$

By writing $J_b$ and $J_c$ in terms of $J_b \pm iJ_c$, the matrix elements $\langle j\ K_i|H|j\ K_m\rangle$ may be evaluated from equations (6.11) to (6.13). Diagonalisation of the resulting matrix yields the coefficients $a_{ni}$ and the energy eigenvalues.

The diagonalisation process may be simplified by taking advantage of various symmetry properties of the matrix. The first two terms in H as expressed in equation (6.16) yield diagonal elements while the third creates elements which connect $|j\ K\rangle$ with $|j\ K\pm2\rangle$. Hence states of even and odd K are not coupled and two sub-matrices E and O may be extracted. Also, the basis states are degenerate in $\pm K$, enabling each sub-matrix to be split again (the Wang transformation). The four matrices may be individually diagonalised and then summed.

The energy levels of an asymmetric top are related to those of the limiting prolate and oblate symmetric tops as indicated in Fig. 6.1. In

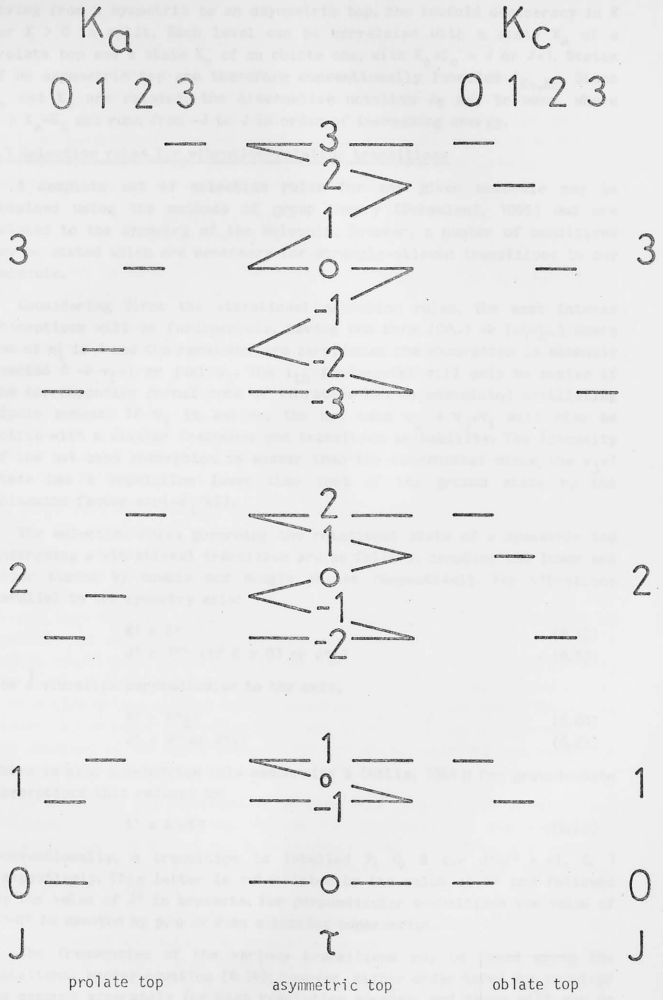


Fig. 6.1: Rotational energy levels of symmetric and asymmetric tops

moving from a symmetric to an asymmetric top, the twofold degeneracy in K for $K > 0$ is split. Each level can be correlated with a state $K_a$ of a prolate top and a state $K_c$ of an oblate one, with $K_a+K_c = J$ or $J+1$. States of an asymmetric top are therefore conventionally labelled $J_{Ka,Kc}$. Since $K_a$ and $K_c$ are related, the alternative notation $J_\tau$ may be used, where $\tau = K_a-K_c$ and runs from $-J$ to $J$ in order of increasing energy.

## 6.7 Selection rules for vibration-rotation transitions

A complete set of selection rules for any given molecule may be obtained using the methods of group theory (Schonland, 1965) and are related to the symmetry of the molecule. However, a number of conditions may be stated which are necessary for strongly-allowed transitions in any molecule.

Considering first the vibrational selection rules, the most intense absorptions will be fundamentals, having the form $(00..) \rightarrow (n_1'n_2'..)$ where one of $n_i'$ is 1 and the remainder are zero; hence the absorption is commonly denoted $0 \rightarrow v_i=1$ or just $\nu_i$. The $i_{th}$ fundamental will only be active if the corresponding normal mode of vibration has an associated oscillating dipole moment. If $\nu_i$ is active, the hot band $\nu_j \rightarrow \nu_j+\nu_i$ will also be active with a similar frequency and transition probability. The intensity of the hot band absorption is weaker than the fundamental since the $v_j=1$ state has a population lower than that of the ground state by the Boltzmann factor $\exp(-E_j/kT)$.

The selection rules governing the rotational state of a symmetric top undergoing a vibrational transition are as follows, denoting the lower and upper states by double and single primes respectively. For vibrations parallel to the symmetry axis:

$$K' = K'' \tag{6.18}$$

$$J' = J'' \text{ (if } K \neq 0) \text{ or } J''\pm1 \tag{6.19}$$

For a vibration perpendicular to the axis,

$$K' = K''\pm1 \tag{6.20}$$

$$J' = J'' \text{ or } J''\pm1 \tag{6.21}$$

There is also a selection rule concerning $l$ (Mills, 1964); for ground-state absorptions this reduces to:

$$l' = K'-K'' \tag{6.22}$$

Conventionally, a transition is labelled P, Q, R for $J'-J'' = -1, 0, 1$ respectively. This letter is subscripted by the value of K'' and followed by the value of J'' in brackets. For perpendicular transitions the value of $K'-K''$ is denoted by p, q or r as a leading superscript.

The frequencies of the various transitions may be found using the rotational energy equation (6.14); however, higher order terms are required to account accurately for high resolution spectra, and these will now be

discussed.

## 6.8 Centrifugal distortion and vibration-rotation interaction

At high values of J, rotating molecules distort appreciably under centrifugal forces so the rigid rotor approximation breaks down. In the case of a symmetric top, this distortion may be expressed by the addition of terms involving higher powers of J and K. Since the degree of distortion is independent of the sense of rotation, only even powers need be considered, hence the energy to fourth order terms is:

$$E_{JK} = BJ(J+1) + (A-B)K^2 - D_J J^2(J+1)^2 - D_{JK} J^2(J+1)K^2 - D_K K^4 \qquad (6.23)$$

Higher order terms involving the sextet constants $H_J$, $H_{JK}$, $H_{KJ}$ and $H_K$ are also needed for very accurate work.

Since the moments of inertia of a molecule vary with its normal coordinates in a non-linear way, the average moments of inertia depend to a significant degree on the vibrational state. For this reason, different values of A and B (and also the distortion constants D) apply in calculating the rotational sublevels of the initial and final states. One significant effect of this is that the frequencies of Q-branch transitions are not exactly independent of J, as exemplified by measurements on allene discussed in chapter 9.

Large perturbations may also be caused by Coriolis terms (Herzberg, 1945). If a molecule is rotating with frequency $\omega$ and simultaneously vibrating, the Coriolis force on each nucleus is $m\underline{\omega}x\underline{\dot{r}}$ where $\underline{\dot{r}}$ is the instantaneous velocity due to vibration, in the rotating frame. If a normal coordinate $q_i$ is expressed in terms of nuclear displacements $\underline{r}_i$, the forces generated by a particular vibrational mode in the presence of rotation may be established, and these may then be expressed in terms of normal coordinates again. In this way it can be shown that a vibration $v_i$ may excite a different mode $v_j$ in the presence of rotation; mixing of the states thus occurs and the energy levels of $v_i$ and $v_j$ are pushed apart. The effect is particularly serious if $v_i$ and $v_j$ have similar frequencies (i.e. the energies of the unperturbed states are close together); the resulting resonance may cause large frequency shifts.

In symmetric top molecules, a particularly large effect occurs since Coriolis forces couple the +1 and -1 components of the degenerate perpendicular vibrations $v_i$. In consequence, the components are split by an amount $4A\zeta_i K$, where $\zeta_i$ is the Coriolis constant associated with $v_i$ and lies between -1 and +1.

Finally, it has been shown (Amat & Henry, 1960) that centrifugal and Coriolis terms can split the twofold degeneracy associated with non-zero values of K, notably when $|K-l| = 3, 6$ .. in molecules having a threefold axis and when $|K-l| = 2, 4$ .. in molecules having a fourfold rotation or rotation-reflection axis; such a splitting has been observed in the allene

molecule (chapter 9).

## 6.9 Symmetry considerations

Any non-degenerate eigenfunction of a molecule must be symmetric or antisymmetric with respect to all the symmetry operators associated with the molecule, i.e. $O|\psi\rangle = \pm|\psi\rangle$ for each operator O. Hence, if there are n independent symmetry operators in the point group of a molecule (excluding the identity operator), each non-degenerate eigenfunction belongs to one of $2^n$ symmetry classes; this applies to rotational and vibrational as well as total eigenfunctions.

For non-linear molecules, species which are symmetric with respect to the principal rotation axis are denoted $A_1$, $A_2$, .. ($A_1$ is the totally symmetric species) while states which are antisymmetric with respect to this axis are denoted $B_1$, $B_2$ etc. For molecules with a centre of symmetry, the additional subscripts g and u denote symmetry or antisymmetry with respect to this operator.

In the case of degenerate states, each operator need only map one linear combination of the eigenfunctions to another such that the appropriate number of repetitions returns the original; for a doubly degenerate state the resulting symmetry classes are denoted $E_1$, $E_2$ etc.

The symmetry class of a product of two functions belonging to known classes can be established using a product table for the point group concerned; in this way, the symmetry of the total eigenfunction can be established. Application of Fermi-Dirac or Bose-Einstein statistics to identical nuclei in the molecule restricts the possible symmetry classes to which this eigenfunction may belong. This in turn restricts the possible combinations of electronic, nuclear, rotational and vibrational symmetry states. One effect of this is that the nuclear spin state affects the weighting of the vibration-rotation states, leading to intensity alternations in observed spectra.

As well as generating the complete set of symmetry selection rules, group theory may also be used to determine the possible Coriolis interactions within a molecule, and possible splitting of degeneracies. Thus group theory is an invaluable tool in medium- and high-resolution spectroscopy.

## 7. HYPERFINE STRUCTURE AND COLLISIONAL TRANSITIONS IN METHYL IODIDE

### 7.1 Introduction

On completion of the waveguide laser spectrometer, test runs were carried out using methyl iodide as the absorbing molecule. The $\nu_6$ perpendicular band of $CH_3I$ falls in the 10 $\mu$m region and the absorption is of medium strength. The spin of the iodine nucleus (I = 5/2) causes the transitions to split into a number of components; those with $\Delta F = \Delta J$ (where $\underline{F} = \underline{I}+\underline{J}$ and F takes values J-I, J-I+1, .. J+I) are stronger than other allowed components by a factor of about $J^2$ or more (Kroto, 1975). Thus the $\nu_6{}^rR_8(9)$ transition, which lies close to the 10P(8) $CO_2$ laser line, is split into six strong components; the corresponding values of F" are 13/2 to 23/2 (Fig. 7.1).

### 7.2 Comparison with previously published data

Fig. 7.2 shows the spectrum containing the four strong components of $\nu_6{}^rR_8(9)$. The measured offset frequencies are recorded in Table 7.1; these may be compared with the frequencies calculated from the data of Arimondo, Glorieux & Oka (1978), who used an r.f.-i.r. double-resonance technique to measure the quadrupole splittings of the upper and lower states of a number of vibration-rotation transitions. These calculated frequencies are also shown in Table 7.1; the origin was chosen such that the two sets of data have the same mean absolute frequency. In a different experiment, Arimondo & Glorieux (1979) measured the absolute frequencies of two of the components; these figures are reproduced in the final column of the table.

Table 7.1

Transitions observed in methyl iodide using 10P(8) laser line

| Measured/MHz | F | Calculated[+] | Reported[++] |
|---|---|---|---|
| 18.40 ± 0.05 | 23/2 | 18.405 | 18.0 ± 0.2 |
| 20.63 ± 0.05 | 13/2 | 20.623 | 20.6 ± 0.2 |
| 29.5 ± 0.5 | * | | |
| 33.0 ± 0.5 | * | | |
| 40.59 ± 0.05 | 21/2 | 40.583 | |
| 45.59 ± 0.05 | 15/2 | 45.570 | |
| 47.4 ± 0.5 | * | | |
| 51.0 ± 0.5 | * | | |
| 54.18 ± 0.05 | 19/2 | 54.165 | |
| 56.445 ± 0.05 | 17/2 | 56.428 | |

* Collision-induced

[+] from Arimondo, Glorieux & Oka (1978)

[++] by Arimondo & Glorieux (1979)

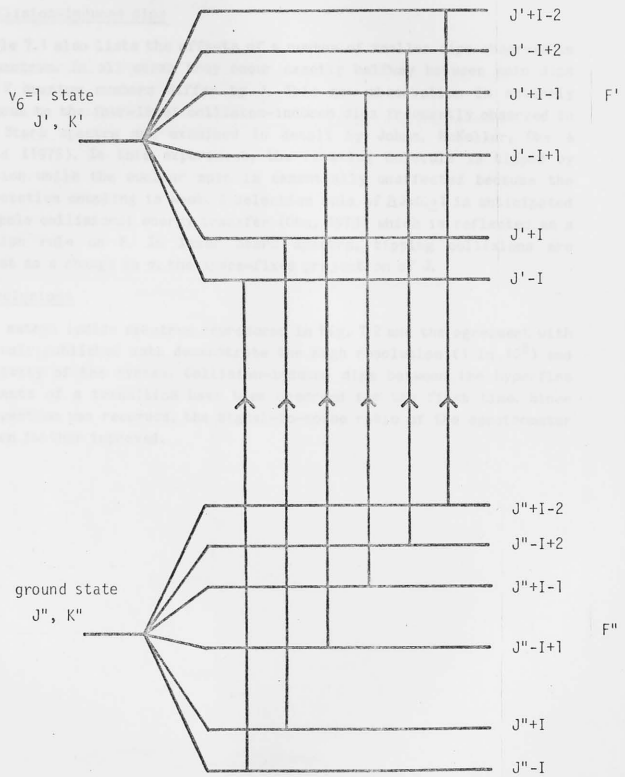


Fig. 7.1: Hyperfine splittings of methyl iodide energy levels, showing strongest components of a transition

In all cases, the agreement between the waveguide laser measurements and the double-resonance work is within the experimental error. The direct measurement of the F=23/2 component by Arimondo & Glorieux does not agree with the waveguide laser measurement, but the latter is supported by the double-resonance result.

## 7.3 Collision-induced dips

Table 7.1 also lists the offsets of a number of smaller dips observed in the spectrum. In all cases they occur exactly halfway between main dips whose F quantum numbers differ by 1. This new observation is entirely analogous to the four-level collision-induced dips frequently observed in laser Stark spectra and examined in detail by Johns, McKellar, Oka & Römheld (1975). In this experiment, the rotating molecule is tipped by collision while the nuclear spin is essentially unaffected because the spin-rotation coupling is weak. A selection rule of $\Delta J=0,\pm1$ is anticipated for dipole collisional energy transfer (Oka, 1973) which is reflected as a selection rule on F. In laser Stark spectra, tipping collisions are manifest as a change in m, the space-fixed projection of J.

## 7.4 Conclusions

The methyl iodide spectrum reproduced in Fig. 7.2 and the agreement with previously published data demonstrate the high resolution (1 in $10^8$) and sensitivity of the system. Collision-induced dips between the hyperfine components of a transition have been observed for the first time. Since this spectrum was recorded, the signal-to-noise ratio of the spectrometer has been further improved.

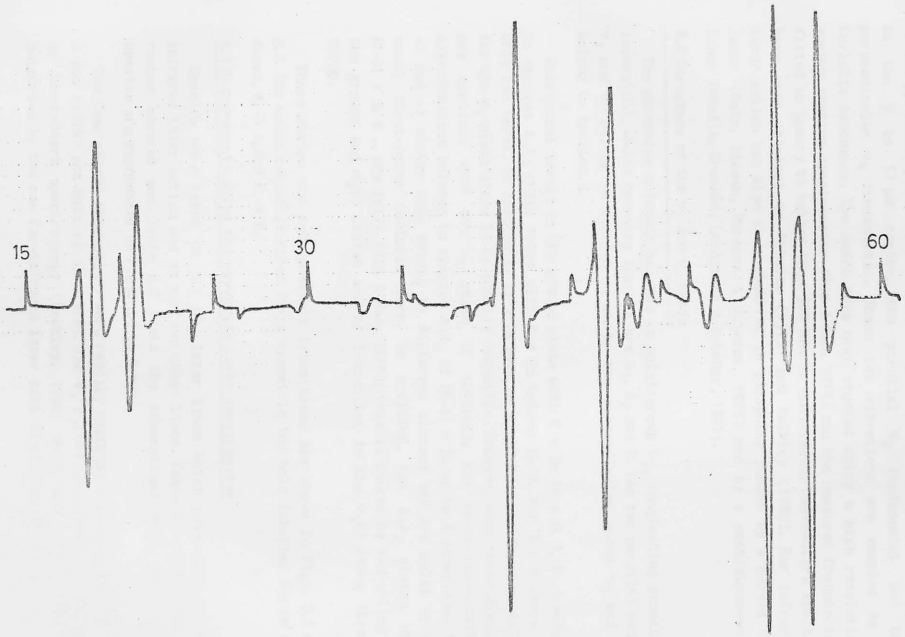


Fig. 7.2: Spectrum of methyl iodide (50 mtorr) taken on 10P(8) laser line, positive offset.

## 8. MEASUREMENTS ON PHOSPHINE

### 8.1 Introduction

The pyramidal phosphine molecule ($PH_3$) has two strong absorption bands in the 9 to 11 μm region, the parallel $\nu_2$ fundamental and the perpendicular $\nu_4$ fundamental. These two vibrations are coupled by a Coriolis resonance. The bands have been studied using a high resolution vacuum grating spectrometer (Yin & Rao, 1974) and the measured frequencies fitted to theory to better than 300 MHz in most cases. Laser-Stark spectra have been obtained by Shimizu (1975) and Rackley (1980). Far infrared laser action has also been observed in phosphine pumped by a pulsed $CO_2$ laser (Malk, Niesen, Parsons & Coleman, 1978) and by a continuous-wave laser (Shafik, Crocker, Landsberg & Butcher, 1981).

### 8.2 Structure of the $\nu_2$ and $\nu_4$ bands

The phosphine molecule belongs to point group $C_{3v}$ (neglecting possible inversion), whose symmetry species are $A_1$, $A_2$ and E. The two parallel modes $\nu_1$ and $\nu_2$ belong to species $A_1$ while the perpendicular modes $\nu_3$ and $\nu_4$ belong to species E.

Rotational levels in the ground state with K = 3n (n = 0, 1, 2 ..) belong to species $A_1A_2$ while those with K ≠ 3n belong to E. For K = 0 there is only one level, of species $A_1$ if J is even or $A_2$ if J is odd. The same holds for the $\nu_2$ state since it is totally symmetric. However, when these species are combined with the $\nu_4$ state (E species), the vibration-rotation eigenfunction belongs to species $A_1A_2$ if |K-l| = 3n or to E otherwise. The +l and -l states thus belong to different classes and are split by the usual first-order Coriolis term. In addition, the $A_1A_2$ states with |K-l| = 3, 6 .. are split (Yin & Rao, 1974); this is caused by K-doubling in the ground and $\nu_2$=1 states and by l-doubling in the $\nu_4$=1 state (Kroto, 1975).

These states and some possible transitions are shown in Figs. 8.1 and 8.2. The usual selection rules for a symmetric top hold (chapter 6); in all cases, $A_1 \rightarrow A_2$ and $E \rightarrow E$.

### 8.3 Measurements using the waveguide laser spectrometer

Spectra were taken on all $CO_2$ laser lines which give rise to far-infrared laser action and on various other lines. Table 8.1 summarises the ranges covered and Table 8.2 lists the absorptions seen. Some sample spectra are reproduced in Figs. 8.3 to 8.5.

The four strong absorptions were readily assigned using the data of Yin & Rao (1974) and Malk et al (1978). The $\nu_4{}^rP_2(10)$ assignment is supported by laser-Stark spectroscopy (Rackley, 1980) while the other three are supported by the c.w. far-infrared laser data (Shafik et al, 1981).

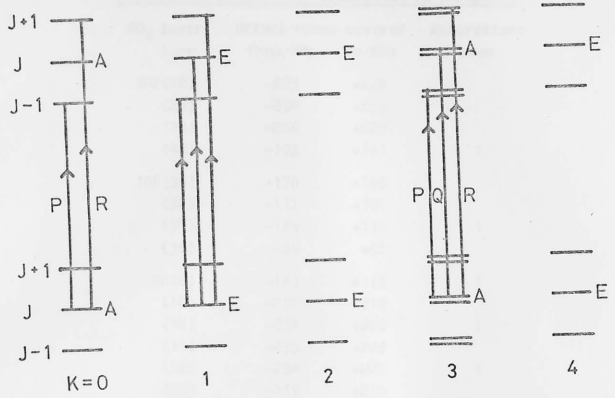


Fig. 8.1: Energy level diagram for ground and $v_2$=1 states of phosphine

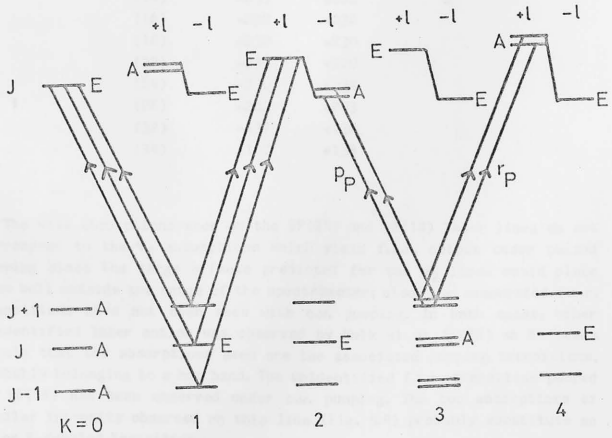


Fig. 8.2: Energy level diagram for ground and $v_4$=1 states of phosphine

Table 8.1

Frequencies scanned for absorption in phosphine

| $CO_2$ laser line | Offset range covered from/MHz | to/MHz | Absorptions seen |
|---|---|---|---|
| 10P(18) | -223 | +220 | |
| (20) | -234 | +233 | |
| (22) | -226 | +220 | |
| (42) | -103 | +101 | 1 |
| 10R(30) | -170 | +166 | |
| (32) | -117 | +106 | |
| (34) | -129 | +110 | 1 |
| (36) | -88 | +86 | |
| 9P(6) | -153 | +114 | 1 |
| (10) | -248 | +212 | |
| (12) | -234 | +228 | 1 |
| (14) | -235 | +228 | |
| (18) | -234 | +227 | 1 |
| (22) | -119 | +230 | |
| (24) | -230 | +228 | 1 |
| (26) | -234 | +228 | |
| 9R(10) | -223 | +219 | |
| (12) | -274 | +200 | |
| (14) | -235 | +228 | 2 |
| (16) | -232 | +230 | |
| (18) | -232 | +230 | |
| (22) | -235 | +220 | |
| (24) | -230 | +234 | |
| (26) | -202 | +203 | |
| (32) | -137 | +130 | |
| (34) | -167 | +138 | |

The weak absorptions seen on the 9P(24) and 9R(14) laser lines do not correspond to the $\nu_2$ absorptions which yield f.i.r. output under pulsed pumping since the large offsets predicted for the $\nu_2$ lines would place them well outside the range of the spectrometer; also, the associated f.i.r. transitions have not been seen with c.w. pumping. In both cases, other unidentified laser action was observed by Malk et al (1978) so it seems likely that the absorptions seen are the associated pumping transitions, probably belonging to a hot band. The unidentified f.i.r. transition pumped by 9R(14) has been observed under c.w. pumping. The two absorptions of similar intensity observed on this line (Fig. 8.4) probably constitute an l- or K-doubled transition.

Table 8.2

Absorptions measured in phosphine (frequencies in MHz)

| Laser line | Offset | Transition freq. | ± | Intensity[+] | Assignment |
|---|---|---|---|---|---|
| 10P(42)* | +95.66 | 27668370.14 | 0.1 | S | $\nu_2\ P_0(7)$ |
| 10R(34)* | -43.20 | 29511023.48 | 0.1 | S | $\nu_2\ Q_{12}(14)$ |
| 9P(24) | -185.95 | 31273061.20 | 0.2 | W | ? |
| 9P(18) | -173.945 | 31437886.23 | 0.1 | S | $\nu_4{}^rP_2(10)$ |
| 9P(12)* | -113.525 | 31595718.235 | 0.1 | S | $\nu_4{}^rP_0(9)$ |
| 9P(6) | +111.4 | 31746595.2 | 0.5 | W | $\nu_4{}^pP_1(7)$ ? |
| 9R(14)* | +23.70 | 32217114.96 | 0.2 | W | ? |
| | +164.44 | 32217255.70 | 0.2 | W | ? |

[+] absorptions marked S are 10 - 20 times stronger than those marked W

* f.i.r. laser action observed on these lines with c.w. pump

It is not clear whether the absorption observed on the 9P(6) line can be assigned to $\nu_4{}^pP_1(7)$ owing to its low strength (Fig. 8.5). Although a very small offset is predicted by Malk et. al. the difference between the frequencies calculated and observed by Yin & Rao is 400 MHz. Continuous-wave f.i.r. laser action has not been observed on this line.

## 8.4 Conclusions

Owing to the small number of coincidences between $PH_3$ absorptions and $CO_2$ laser lines there is insufficient data to improve on the existing constants for the $\nu_2$ and $\nu_4$ bands.

When molecules show f.i.r. laser action pumped by conventional c.w. $CO_2$ lasers (which have tunabilities of 50 MHz or less), it is usually assumed that the molecular absorption must lie within ±50 MHz of the $CO_2$ line centre. The measurements made indicate that this is not so; the offsets of f.i.r. laser pumping transitions from the 9P(12) and 10P(42) $CO_2$ line centres are -113.5 MHz and +95.7 MHz respectively, and both f.i.r. lines have been obtained using a conventional c.w. pump laser of modest power. These offsets correspond to about three times the Doppler half-width to half-maximum of the phosphine absorptions.

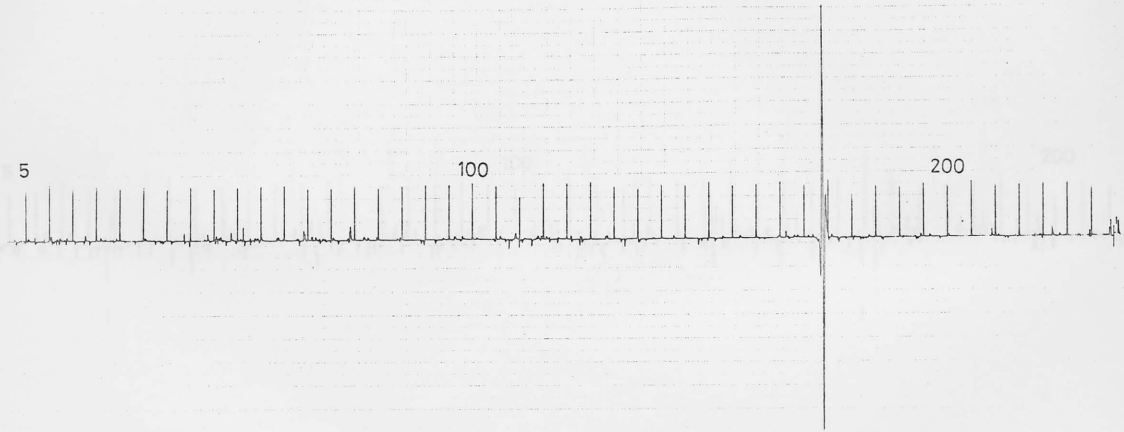


Fig. 8.3: Spectrum of phosphine (15 mtorr) taken on 9P(18) laser line, negative offset.

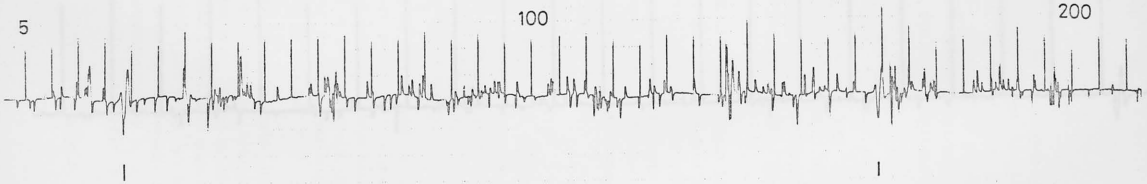


Fig. 8.4: Spectrum of phosphine (15 mtorr) on 9R(14) laser line, positive offset.

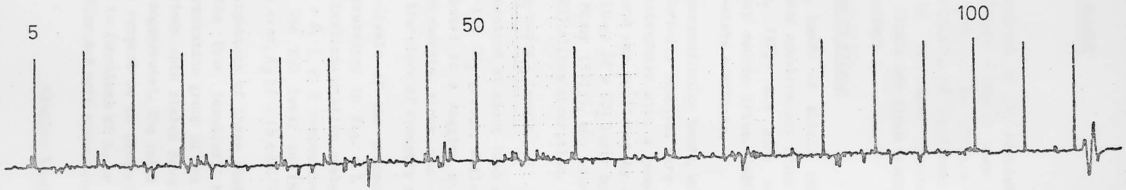


Fig. 8.5: Spectrum of phosphine (15 mtorr) taken on 9P(6) laser line, positive offset.

## 9. MEASUREMENTS ON ALLENE

### 9.1 Introduction

Infrared spectroscopy at the resolution afforded by a tunable laser source is particularly valuable when applied to molecules having no permanent dipole moment. The absence of a pure rotational spectrum prevents the determination of rotational constants and the observation of fine structure by microwave spectroscopy; similarly, laser-Stark spectroscopy is of little use since transitions in these molecules show no first-order Stark effect.

### 9.2 Previous studies of allene

The $\nu_5$ and $\nu_8$ bands of allene near 3.3 μm have been studied by conventional infrared spectroscopy (Maki & Toth, 1965), Raman spectroscopy (Butcher & Jones, 1973) and more recently using a tunable laser difference-frequency source (Pine, 1980). These measurements provide a good set of ground-state constants.

The $\nu_9$ and $\nu_{10}$ perpendicular bands, which lie in the 8.5 to 14 μm region and are strongly Coriolis coupled, were studied by Mills, Smith & Duncan (1965) using a spectrometer with a resolution of about 0.2 $cm^{-1}$. Further work on the $\nu_{10}$ band was published by Stone (1971). Q-switching of the 9P(34) and 9P(36) lines of a $CO_2$ laser by the allene molecule was observed by Meyer, Dupre & Meyer (1975), who attributed the effect on the former line to the $\nu_9{}^rR_2(23)$ allene absorption.

### 9.3 Theory of the $\nu_9$ and $\nu_{10}$ levels

The $\nu_9$ band is centred at about 1030 $cm^{-1}$ and involves predominantly a rocking motion of the $CH_2$ groups, while the $\nu_{10}$ band centred at about 850 $cm^{-1}$ is attributed to a wagging motion of these same groups. Both vibrations are degenerate since the two ends of the molecule are identical, and are therefore of symmetry species E.

Rotational sub-levels of the ground state and of either of these vibrations are represented in Fig. 9.1. Allene is a symmetric top with point group $D_{2d}$. Vibration-rotation states have symmetry $A_1A_2$, E, $B_1B_2$ or E for $|K-1|$ modulo 4 = 0, 1, 2, 3 respectively. States with K>0 are doubly degenerate, while the K=0 level in the vibrational ground state has symmetry $A_1$ if J is even, $A_2$ if J is odd.

The relative weightings of these states are affected by the possible spin states of the four identical hydrogen nuclei with $s=1/2$. By considering the permutation group of the molecule (Kroto, 1975) it may be shown that the sixteen spin states have symmetries $6A_1+B_1+3B_2+3E$ (the E states are doubly degenerate). The total molecular eigenfunction must be antisymmetric with respect to an interchange of any two of these nuclei, which restricts it to functions of $A_1$ or $B_1$ symmetry. This is achieved if the vibration-rotation and spin states pair up as follows: $A_1$ or $B_1$ with $A_1$

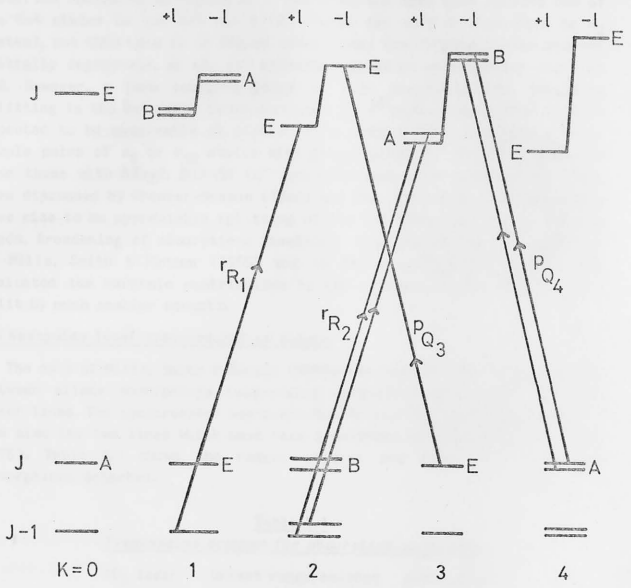


Fig. 9.1: Energy level diagram for ground and $v_9$=1 or $v_{10}$=1 states of allene

or $B_1$, $A_2$ or $B_2$ with $B_2$ (there are no $A_2$ spin states), E with E. Hence the weightings of the vibration-rotation states are $A_1$:$A_2$:$B_1$:$B_2$:E = 7:3:7:3:6.

The twofold degeneracy may be split by various high-order interactions. In the vibrational ground state, a term connecting pairs of states with $\Delta K=\pm 4$ is present (Amat & Henry, 1960), resulting in a splitting of the K=2 state. The splitting increases as $J^4$ for J>>K. The same term couples one of the K=4 states to the K=0 state ($A_1$ states can only be connected to $A_2$ states), but this term is of higher order since the coupled states are not initially degenerate, so the K=4 splitting would be much smaller than for K=2. However, a term coupling $\Delta K=\pm 8$ is also permitted; the resulting splitting in the K=4 state is proportional to $J^8$ when J>>K, so this term is expected to be observable at high J. In a similar way, l-doubling terms couple pairs of $\nu_9$ or $\nu_{10}$ states with $\Delta K=\pm 2$, $\Delta l=\Delta K$ ($q^+$ interactions) and also those with $\Delta K=\pm 2$, $\Delta l=-\Delta K$ ($q^-$ interactions). Such interactions have been discussed by Grenier-Besson (1960) and Oka (1967). These interactions give rise to an appreciable splitting of the K=1 states in the $\nu_9$ and $\nu_{10}$ bands. Broadening of absorptions involving these states has been reported by Mills, Smith & Duncan (1965) and by Stone (1971); the latter also evaluated the harmonic contribution to the $q^-$ term. States with K>1 are split by much smaller amounts.

## 9.4 Waveguide laser spectroscopy of allene

The data of Mills, Smith & Duncan (1965) was examined for close matches between allene absorptions (especially unresolved Q-branches) and $CO_2$ laser lines. The spectrometer was scanned over the $CO_2$ lines thus selected and also the two lines which have been Q-switched by allene (Meyer et.al., 1975). Table 9.1 shows the ranges covered and Table 9.2 lists the absorptions detected.

Table 9.1

Frequencies scanned for absorption in allene

| $CO_2$ laser line | Offset range covered from/MHz | to/MHz | Absorptions seen |
|---|---|---|---|
| 10P(32) | -145 | +145 | 1 |
| 10R(16) | -170 | +185 | 1* |
| (26) | -210 | +185 | 4 |
| (30) | -145 | +135 | |
| 9P(34) | -145 | +150 | 1* |
| (36) | -105 | +125 | 1 |

* doublet transition

Table 9.2

Absorptions measured in allene (frequencies in MHz)

| Laser line | Offset | Transition freq. | ± | Rel.Intens. | Assignment |
|---|---|---|---|---|---|
| 10P(32) | -45.7 | 27969404.1 | 0.5 | 21 | $\nu_{10}{}^{r}Q_{14}(J)$ |
| 10R(16) | +156.3 | 29178612.0 | 0.5 | 110 | $\nu_9{}^{P}Q_4(J)$* |
| | +163.0 | 29178618.7 | 0.5 | 50 | (doubled) |
| 10R(26) | -119.0 | 29370710.6 | 0.2 | 15 | $\nu_9{}^{P}Q_3(3)$ |
| | -45.0 | 29370784.6 | 0.2 | 30 | $\nu_9{}^{P}Q_3(4)$ |
| | +47.5 | 29370877.1 | 0.2 | 35 | $\nu_9{}^{P}Q_3(5)$ |
| | +158.45 | 29370988.1 | 0.2 | 12 | $\nu_9{}^{P}Q_3(6)$ |
| 9P(34) | -37.9 | 30983152.8 | 0.2 | 130 | $\nu_9{}^{r}R_2(23)$ |
| | -28.3 | 30983162.4 | 0.2 | 60 | (doubled) |
| 9P(36) | +81.5 | 30922996.9 | 0.5 | 15 | $\nu_9{}^{r}R_1(37)$ ? |

* J>18

## 9.5 Analysis of $\nu_9{}^{P}Q_3$ transitions

The 10R(26) $CO_2$ line showed a sequence of four absorptions with linearly increasing spacing (Figs. 9.2 and 9.3); these must be Q-branch transitions with J=3,4,5,6. The frequencies given by Mills indicate that the branch involved is $\nu_9{}^{P}Q_3$. The frequencies of these lines were fitted to the formula:

$$ {}^{P}Q_3(J) = \nu_{sub} + (B' - B'' - 4D''_{JK} + 9D''_{K})J(J+1) - (D'_J - D''_J)J^2(J+1)^2 \qquad (9.1) $$

The measurements gave:

$$ B'-B''-4D''_{JK}+9D''_{K} = 9.254 \pm 0.008 \text{ MHz} \qquad (9.2) $$

$$ D'_J-D''_J = 0.000125 \pm 0.00015 \text{ MHz} \qquad (9.3) $$

Taking $B'' = 8882.159 \pm 0.022$ MHz, $D''_J = 0.0026511 \pm 0.000007$ MHz and $D''_{JK} = 0.1595 \pm 0.0012$ MHz after Pine (1980), and assuming $D'_{JK}$ to be within ±15% of $D''_{JK}$, the following constants for the $v_9$=1 state are obtained:

$$ B' - B'' = 8.456 \pm 0.11 \text{ MHz} \qquad (9.4) $$

$$ B' = 8890.615 \pm 0.13 \text{ MHz} \qquad (9.5) $$

$$ D'_J = 0.002776 \pm 0.00015 \text{ MHz} \qquad (9.6) $$

## 9.6 K- and l-doubled transitions

The absorption on the 10R(16) line (Fig. 9.4) is believed to be a $\nu_9{}^{P}Q_4$ line as the laser frequency is only 0.13 $cm^{-1}$ above the frequency of this branch reported by Mills. If this assignment is correct, the absence of

another transition within the range covered and the value of B'-B" determined above indicate that J>18. A rough calculation comparing the frequencies of the $^{P}Q_4$ and $^{P}Q_3$ branches given by Mills suggests J=28±2.

Both this absorption and the one observed on 9P(34) assigned to $\nu_9\,^{r}R_2(23)$ by Meyer are doublets, the splittings being 6.7 and 9.6 MHz respectively. As shown on Fig. 9.1, both K-doubling of the lower state and l-doubling of the upper state are possible. The states involved are $A_1A_2$ or $B_1B_2$, and in both cases the observed intensity ratio is in good agreement with the theoretical value of 7:3.

9.7 Assignment of the remaining lines

The absorption seen on the 9P(36) laser line must be either a $\nu_9$ or a hot-band line. Since it is nearly as strong as the assigned $\nu_9$ lines, it is reasonable to assume J<50. It cannot belong to a Q-branch ($^{r}Q_3$ is nearest, 3 $cm^{-1}$ from the absorption frequency), so it must be a P- or R-branch transition. With B~0.3 $cm^{-1}$, the corresponding Q-branch must be less than 30 $cm^{-1}$ distant; this restriction leaves $^{r}R_1$, $^{r}R_2$, $^{r}R_3$, $^{r}P_4$ and $^{r}P_5$ as the possible candidates from $\nu_9$. The $^{r}R_2$ and $^{r}P_4$ splittings would certainly be observable at the required values of J, so these are ruled out. The remaining lines will not be split since the upper and lower states have E symmetry and cannot be doubled.

The frequencies of transitions in these branches were calculated using the constants given in the previous section. The sub-band origins were taken from the frequencies of the Q-branches given by Mills, corrected by -0.194 $cm^{-1}$; this correction was obtained by comparing the frequency quoted by Mills for the $^{r}R_2$ branch with the origin of this branch as measured by Meyer under higher resolution.

These calculations predicted the frequency of the $^{r}R_1(34)$ line to be just 0.018 $cm^{-1}$ below that of the observed transition, an error which is small compared to the line spacing of 0.6 $cm^{-1}$ and the 0.194 $cm^{-1}$ correction. The other branches yielded no transitions near the required frequency. It is therefore very probable that the observed transition is indeed $\nu_9\,^{r}R_1(34)$; the only other possibility is that it belongs to the $\nu_{11} \rightarrow \nu_{11}+\nu_9$ hot band.

A single transition was observed using the 10P(32) laser line, attributed to the $\nu_{10}\,^{r}Q_{14}$ branch; the centre frequency of this branch as given by Mills is 0.10 $cm^{-1}$ below the laser. An observable splitting due to K- or l-doubling is not expected as these effects are insignificant at high values of K.

9.8 Conclusions

Spectra obtained on the waveguide laser spectrometer have provided a measurement of B'- B" for the $\nu_9$ state which, in conjunction with the data given by Pine, yields a value of B' some 30 times more precise than previous measurements. This result has made possible the assignment of the

allene absorption which Q-switches the 9P(36) $CO_2$ laser line. Doubling of certain transitions has been observed in qualitative agreement with theory, but the relative importance of the various contributions is unresolved.

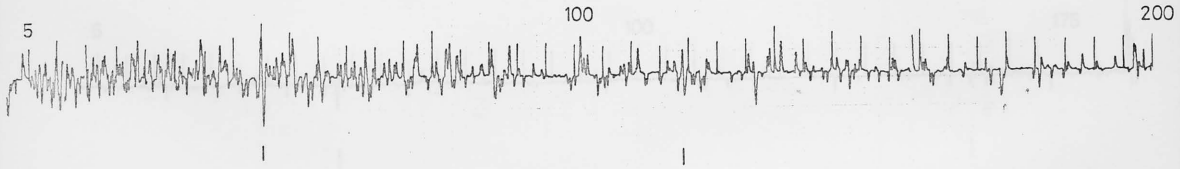


Fig. 9.2: Spectrum of allene (40 mtorr) taken on 10R(26) laser line, negative offset.

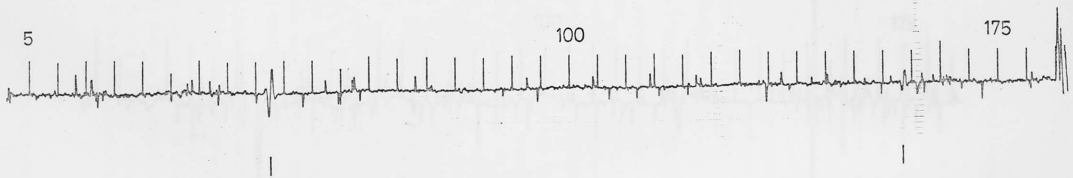


Fig. 9.3: Spectrum of allene (40 mtorr) taken on 10R(26) laser line, positive offset.

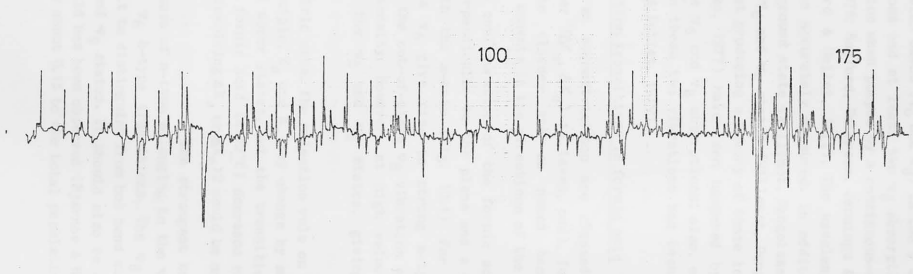


Fig. 9.4: Spectrum of allene (40 mtorr) taken on 10R(16) laser line, positive offset.

## 10. CORIOLIS RESONANCE IN FORMIC ACID

### 10.1 Introduction

The formic acid molecule is an asymmetric top with two strong fundamental absorption bands ($\nu_6$ and $\nu_8$) in the 9 to 10 μm region. Several of the $\nu_6$ absorptions and at least two $\nu_8$ absorptions give rise to far-infrared laser action when pumped by a continuous-wave $CO_2$ laser (Dyubko, Svich & Fesenko, 1976; Radford, Peterson, Jennings & Hucha, 1977; Deldalle, Dangoisse, Splingard & Bellet, 1977). The wavelengths of most of these emissions have been accurately measured. In addition, microwave data is available for the ground state (Willemot, Dangoisse, Monnanteuil & Bellet, 1980) and for the $\nu_6$ and $\nu_8$ states (Willemot, Dangoisse & Bellet, 1979). Previous attempts at producing a theory of these levels (Baskakov, Dyubko, Moskienko & Fesenko, 1977) have been hampered by the lack of precise frequencies for the $\nu_6$ and $\nu_8$ absorptions; also, evidence for a Coriolis interaction between these two vibrations has been presented (Dangoisse, Willemot, Deldalle & Bellet, 1979).

### 10.2 Vibration-rotation transitions in formic acid

Transitions in an asymmetric top are classed as a-, b- or c-type according to whether ($\Delta K_a$, $\Delta K_c$) is (even, odd), (odd, odd) or (odd,even) respectively. These classes are so named because they occur via oscillating dipole moments in the directions of the corresponding axes.

The equilibrium configuration of the formic acid molecule is planar with the c-axis perpendicular to the plane and a dipole moment which is almost aligned with the a-axis (Fig. 10.1). For this reason, in-plane vibrations such as $\nu_6$ give rise to strong a-type and weaker b-type transitions, while the out-of-plane $\nu_8$ vibration gives rise to a c-type band of lower intensity. However, at high values of $K_a$ the Coriolis interaction mixes the $\nu_6$ and $\nu_8$ states, giving rise to a-type $\nu_8$ transitions also.

As in the symmetric case, the selection rule on total angular momentum is $J'=J''\pm1,J''$. In principle, $K_a$ and $K_c$ may change by any values which couple suitable lower and upper states, but the transition moments for a near-symmetric top like formic acid ($A \gg B \gtrsim C$) decrease rapidly with increasing $\Delta K$. No transitions involving $\Delta K_a$ or $\Delta K_c > 2$ could be assigned in this work.

The strongest transitions in the 9 to 11 μm region are those of a-type belonging to the $\nu_6$ fundamental. Next in intensity are the $\nu_6$ b-type transitions. The $\nu_8$ transitions are much weaker and difficult to distinguish from hot band absorptions arising from the low-lying $\nu_7$ and $\nu_9$ states. It should also be remarked that a second isomer of formic acid has been observed (Bjarnov & Hocking, 1978), although it contributes only about 0.1% to the total population at room temperature.

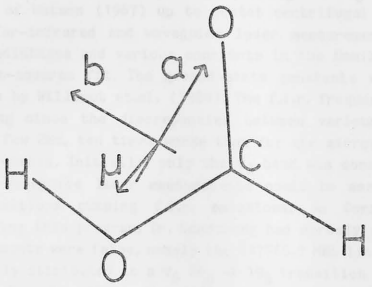


Fig. 10.1: Equilibrium configuration of the formic acid molecule. The c-axis is perpendicular to the plane of the paper.

## 10.3 Measurements using the waveguide laser spectrometer

Spectra of formic acid were obtained using all available 9R lines, most 9P lines and a few 10R lines of the $CO_2$ laser. The ranges covered and the lines observed are listed in Table 10.3 at the end of this chapter. Sample spectra are reproduced in Figs. 10.2 to 10.5. Many weak unassigned lines are present in the data.

## 10.4 Analysis

Dr. B.M. Landsberg kindly made available a computer program to calculate the frequencies of levels in the ground, $\nu_6$ and $\nu_8$ states using the Hamiltonian of Watson (1967) up to sextet centrifugal distortion terms. Microwave, far-infrared and waveguide laser measurements were compared with the predictions and various constants in the Hamiltonian floated to give a least-squares fit. The ground-state constants were fixed to the values given by Willemot et.al. (1980). The f.i.r. frequencies were given a low weighting since the discrepancies between various authors implied errors of a few MHz, ten times worse than for the microwave and waveguide laser measurements. Initially, only the $\nu_6$ band was considered and only a few of the waveguide laser measurements could be assigned, namely the strong transitions pumping f.i.r. emissions. No Coriolis terms were included. Using this program, Dr. Landsberg had already shown that certain f.i.r. assignments were false, namely the 447765.0 MHz line pumped by 9R(30) and previously attributed to a $\nu_6$ $20_8 \rightarrow 19_8$ transition (Baskakov, Dyubko, Moskienko & Fesenko, 1977), the 516538.7 MHz line pumped by 9R(22) and previously assigned to $\nu_6$ $23_{5,18} \rightarrow 22_{5,17}$ (Dangiosse, Willemot, Deldalle & Bellet, 1979) and the 561748.6 MHz emission pumped by 9R(16) and assigned by Baskakov et.al. to $\nu_8$ $25_{7,18} \rightarrow 24_{7,18}$. Neither these emissions nor any of those previously unassigned could be assigned to transitions in the $\nu_6$ or $\nu_8$ manifolds.

With these transitions removed, the resulting fit was fair, with errors of up to 16 MHz on the f.i.r. lines and 230 MHz on the $CO_2$ pumping frequencies. However, the quartet of infrared transitions involving the $v_6$=1 $33_{0,33}$ and $33_{1,33}$ levels (Figs. 10.2 & 10.3) showed a serious anomaly. The separation of these two levels was predicted to be 10 MHz greater than the experimentally observed value of 169.56 MHz, although the 137.59 MHz splitting of the ground state $34_{0,34}$ and $34_{1,34}$ levels was correctly predicted; this implied the existance of some perturbation to the $v_6$=1 state. The vibrational level nearest to $v_6$=1 is the $v_8$=1 level, and evidence for a Coriolis interaction between these vibrations has already been referred to.

Of the three possible types of Coriolis interaction in an asymmetric top, the c-type interaction does not couple an in-plane to an out-of-plane vibration. Dr. Landsberg therefore modified his program to include an a- or b-type Coriolis interaction. Invoking a b-type interaction made matters worse, but an a-type interaction with $2A\zeta_{6,8} \sim 24$ GHz removed the 10 MHz

error and greatly improved the fit as a whole. Although the Coriolis term does not have a large direct effect on levels of low $K_a$, it affects the 10 MHz splitting by causing the value of the rotational constant A to change, in order to maintain the fit at high $K_a$ values.

Accurate predictions of $\nu_6$ absorptions were then possible, so the computer was programmed to predict all transitions up to J=60, $K_a$=25 in the neighbourhood of a $CO_2$ laser line. Many more of the observed lines could then be assigned, and in several cases the laser tuning range was extended to search for a predicted transition. These lines were then included in the fit and the cycle repeated until no more assignments could confidently be made.

The assignment of the $30_{1,29} \leftarrow 30_{2,28}$ and $22_{14,8} \leftarrow 23_{14,9}$ lines posed some difficulty as the predicted frequencies were close together. Two absorptions of similar intensity were indeed observed near the 9R(38) laser line centre, but the two ways of assigning these lines gave equally good fits. The problem was resolved by painting two electrodes along the length of the cell (using a graphite suspension) and taking spectra with various potential differencies between these electrodes. The $30_{2,28}$ line was predicted to have a very small Stark effect in comparison with the $23_{14,9}$ line. The absorption line which was obliterated due to broadening by the inhomogeneous field produced with quite a small potential difference was therefore assigned to the latter. The other line was almost unaffected even at high fields, confirming its assignment as the $30_{2,28}$ transition.

The final $\nu_6$ fit (similar to the first part of the $\nu_6/\nu_8$ fit reproduced in Table 10.1) had a standard deviation of about 0.5 MHz. The most noticeable discrepancies in the calculated frequencies were those of the $19_{4,15} \leftarrow 19_{5,14}$ and $18_{4,15} \leftarrow 18_{5,14}$ lines, which showed an error in both absolute frequency and splitting. Also, the splitting between $33_{0,33}$ and $33_{1,33}$ in the $v_6$=1 state was slightly in error, but in the opposite sense to the original error without the a-type Coriolis term. The most probable explanation for this situation is an additional b-type Coriolis interaction, since the addition of even a small term of this type to the original Watson Hamiltonian had a pronounced effect on the splittings in the direction required to correct these errors, and it would be fortuitous if the b-type interaction were actually smaller still. Unfortunately, the time and computing resources needed to include both interactions were not available.

Attention was then shifted to the $\nu_8$ band, constraining the Coriolis coupling constant to the value derived from the $\nu_6$ fit. Three assigned $\nu_8$ absorptions were believed to lie close to $CO_2$ laser lines. Spectra taken on two of these lines (9P(16) and 9P(28)) were ambiguous since the transitions sought did not stand out from other weak absorptions; however, the 9P(38) line yielded a single absorption, close to the laser line, and so was assigned to the $23_{12,11} \leftarrow 23_{12,12}$ transition as required by the f.i.r. laser data. With this line and the f.i.r. and microwave data included,

a $\nu_8$ fit was performed with the other two lines represented by the $CO_2$ line centre frequencies at a weight of 0.0001.

The value of $H_K$ resulting from this fit was about 0.002 MHz, twenty times larger than the ground state or $\nu_6$ value. This was considered unacceptable. The main effect of this term in the fit was to shift the $23_{12}$ pump absorption to the $CO_2$ line from a position 7 GHz away. With $H_K$ constrained to zero or the ground state value, a good fit was obtained only after removing the $23_{12}$ absorption and f.i.r. emission; hence these assignments were rejected. Attempts to reassign these lines failed, although it was found that assignment to $23_{13}$ transitions produced a fit as good as the original, with $H_K$ having similar magnitude but opposite sign.

Table 10.2

Formic acid constants derived from fit (values in MHz)

| constant | value, $\nu_6$=1 | error | value, $\nu_8$=1 | error |
|---|---|---|---|---|
| $\nu_0$ | 33122629.0 | 1.0 | 30982555.0 | 41.0 |
| A | 77600.0 | 1.8 | 76977.7 | 1.8 |
| B | 12003.1709 | 0.0059 | 12001.620 | 0.018 |
| C | 10352.0457 | 0.0068 | 10419.641 | 0.017 |
| $D_J$ | 0.0102446 | 0.0000076 | 0.009764 | 0.000034 |
| $D_{JK}$ | -0.089313 | 0.000087 | -0.0702 | 0.0016 |
| $D_K$ | 1.7741 | 0.0013 | 1.266 | 0.031 |
| $\delta_J$ | 0.0020430 | 0.0000056 | 0.001819 | 0.000018 |
| $\delta_K$ | 0.04897 | 0.00027 | 0.0228 | 0.0028 |
| $H_J$ | 0.0000000162 | 0.0000000032 | | |
| $H_{JK}$ | -0.000000756 | 0.000000056 | | |
| $H_{KJ}$ | -0.00002574 | 0.00000083 | | |
| $H_K$ | 0.0000306 | 0.0000037 | | |
| $h_J$ | 0.0000000124 | 0.0000000029 | | |
| $2A\zeta_{6,8}$ | 23296.0 | 81.0 | | |

I^R representation.

The present $\nu_6/\nu_8$ fit is reproduced in Table 10.1 and the corresponding constants in Table 10.2. The error bounds quoted are those yielded by the fit and should not be taken too seriously since b-type and second order a-type Coriolis terms were not included. It is hoped that assignment of $\nu_8$ absorptions will be possible by starting with lines of low J and $K_a$ and/or doublets. Work in this area is continuing and the results will be published in due course.

| V' | J' | Ka' | Kc' | V" | J" | Ka" | Kc" | FREQUENCY | CALCULATED | OBS. - CALC. | WEIGHT |
|---|---|---|---|---|---|---|---|---|---|---|---|
| 1 | 9 | 2 | 7 | 1 | 9 | 2 | 8 | 9775,6700 | 9775,3373 | .3327 | 1,0000 |
| 1 | 3 | 1 | 2 | 1 | 3 | 1 | 3 | 9902,6100 | 9902,3352 | .2748 | 1,0000 |
| 1 | 17 | 3 | 14 | 1 | 17 | 3 | 15 | 12719,1000 | 12719,3943 | -.2943 | 1,0000 |
| 1 | 10 | 2 | 8 | 1 | 10 | 2 | 9 | 14440,8900 | 14440,7492 | .1408 | 1,0000 |
| 1 | 4 | 1 | 3 | 1 | 4 | 1 | 4 | 16501,8100 | 16501,3635 | .4665 | 1,0000 |
| 1 | 11 | 2 | 9 | 1 | 11 | 2 | 10 | 20486,2900 | 20486,4527 | -.1627 | 1,0000 |
| 1 | 1 | 0 | 1 | 1 | 0 | 0 | 0 | 22355,2400 | 22355,1757 | .0643 | 1,0000 |
| 1 | 5 | 1 | 4 | 1 | 5 | 1 | 5 | 24745,1200 | 24744,5781 | .5419 | 1,0000 |
| 1 | 12 | 2 | 10 | 1 | 12 | 2 | 11 | 27979,5500 | 27979,3519 | .1981 | 1,0000 |
| 1 | 20 | 3 | 17 | 1 | 20 | 3 | 18 | 30779,4300 | 30780,5138 | -1,0838 | 1,0000 |
| 1 | 6 | 1 | 5 | 1 | 6 | 1 | 6 | 34624,2200 | 34624,4766 | -.2566 | 1,0000 |
| 1 | 13 | 2 | 11 | 1 | 13 | 2 | 12 | 37169,7300 | 37169,5534 | .1766 | 1,0000 |
| 1 | 2 | 1 | 2 | 1 | 1 | 1 | 1 | 43686,2900 | 43689,9982 | -.2918 | 1,0000 |
| 1 | 2 | 0 | 2 | 1 | 1 | 0 | 1 | 44679,4800 | 44679,4736 | .0076 | 1,0000 |
| 1 | 7 | 1 | 6 | 1 | 7 | 1 | 7 | 46128,4900 | 46128,6948 | -.2048 | 1,0000 |
| 1 | 8 | 1 | 7 | 1 | 8 | 1 | 8 | 59235,4700 | 59235,1181 | .3519 | 1,0000 |
| 1 | 3 | 1 | 3 | 1 | 2 | 1 | 2 | 64570,7900 | 64574,5567 | -.2393 | 1,0000 |
| 1 | 3 | 0 | 3 | 1 | 2 | 0 | 2 | 66942,3100 | 66942,8946 | -.2154 | 1,0000 |
| 1 | 3 | 2 | 2 | 1 | 2 | 2 | 1 | 67067,2000 | 67066,7835 | .4765 | 1,0000 |
| 1 | 3 | 2 | 1 | 1 | 2 | 2 | 0 | 67189,7700 | 67189,2348 | .5352 | 1,0000 |
| 1 | 2 | 1 | 1 | 1 | 2 | 0 | 2 | 69181,8300 | 69181,0531 | .7769 | 1,0000 |
| 1 | 3 | 1 | 2 | 1 | 2 | 1 | 1 | 69521,8400 | 69521,3934 | .4466 | 1,0000 |
| 1 | 3 | 1 | 2 | 1 | 3 | 0 | 3 | 71768,1200 | 71768,3520 | -.2320 | 1,0000 |
| 1 | 4 | 1 | 3 | 1 | 4 | 0 | 4 | 75304,7500 | 75305,0111 | -.2611 | 1,0000 |
| 1 | 4 | 2 | 3 | 1 | 5 | 1 | 4 | 76852,4800 | 76851,6667 | .8133 | 1,0000 |
| 1 | 5 | 1 | 4 | 1 | 5 | 0 | 5 | 79902,6800 | 79902,9071 | -.2271 | 1,0000 |
| 1 | 7 | 0 | 7 | 1 | 6 | 0 | 6 | 156604,8000 | 156604,2051 | .5949 | 1,0000 |
| 1 | 7 | 5 | 3 | 1 | 6 | 5 | 2 | 156613,7800 | 156613,3541 | .4259 | 1,0000 |
| 1 | 7 | 4 | 3 | 1 | 6 | 4 | 2 | 156646,1000 | 156645,9691 | .1309 | 1,0000 |
| 1 | 7 | 3 | 5 | 1 | 6 | 3 | 4 | 156716,7600 | 156716,5743 | .2143 | 1,0000 |
| 1 | 7 | 3 | 4 | 1 | 6 | 3 | 3 | 156761,7500 | 156761,5677 | .1823 | 1,0000 |
| 1 | 8 | 2 | 6 | 1 | 7 | 2 | 5 | 188939,4300 | 188939,2134 | .2166 | 1,0000 |
| 1 | 9 | 2 | 7 | 1 | 8 | 2 | 6 | 201371,2800 | 201371,2305 | .0495 | 1,0000 |
| 1 | 17 | 3 | 15 | 1 | 16 | 3 | 14 | 381336,9800 | 381336,9819 | -.0019 | ,1000 |
| 1 | 18 | 3 | 16 | 1 | 17 | 3 | 15 | 403721,6000 | 403721,8851 | -.2851 | ,1000 |
| 1 | 18 | 0 | 18 | 1 | 17 | 0 | 17 | 402919,6000 | 402918,7235 | .8765 | ,1000 |
| 1 | 25 | 5 | 21 | 1 | 24 | 5 | 20 | 561724,0000 | 561725,4712 | -1,4712 | ,1000 |
| 1 | 26 | 5 | 22 | 1 | 25 | 5 | 21 | 584388,2000 | 584387,4926 | .7072 | ,1000 |
| 1 | 26 | 12 | 14 | 1 | 25 | 12 | 13 | 581930,8000 | 581929,5522 | .4378 | ,1000 |
| 1 | 30 | 1 | 29 | 1 | 29 | 1 | 28 | 653822,2000 | 653821,4903 | .7097 | ,1000 |
| 1 | 30 | 12 | 19 | 1 | 29 | 12 | 18 | 671419,5000 | 671418,2396 | 1,2604 | ,1000 |
| 1 | 32 | 0 | 32 | 1 | 31 | 0 | 31 | 672335,5000 | 672336,2039 | -,7039 | ,1000 |
| 1 | 33 | 0 | 33 | 1 | 32 | 0 | 32 | 692949,5000 | 692950,8489 | -1,3489 | ,1000 |
| 1 | 31 | 12 | 20 | 1 | 30 | 12 | 19 | 693787,5000 | 693787,6742 | .8258 | ,1000 |
| 1 | 32 | 12 | 21 | 1 | 31 | 12 | 20 | 716155,8000 | 716155,9147 | -.1147 | ,1000 |
| 1 | 33 | 9 | 25 | 1 | 32 | 9 | 24 | 739161,8000 | 739158,3488 | 2,8512 | ,1000 |
| 1 | 34 | 9 | 26 | 1 | 33 | 9 | 25 | 761607,6000 | 761605,9542 | 1,6458 | ,1000 |
| 1 | 44 | 6 | 39 | 1 | 43 | 6 | 38 | 991776,0000 | 991775,1488 | ,7512 | ,1000 |
| 1 | 48 | 12 | 28 | 0 | 48 | 13 | 27 | 31437987,3800 | 31437987,3445 | ,0355 | 1,0000 |
| 1 | 26 | 12 | 14 | 0 | 26 | 13 | 13 | 31491581,8500 | 31491582,9369 | -1,0869 | 1,0000 |
| 1 | 44 | 6 | 39 | 0 | 45 | 6 | 40 | 32204816,1300 | 32204815,1414 | ,9814 | 1,0000 |
| 1 | 29 | 12 | 17 | 0 | 28 | 13 | 16 | 32134182,9800 | 32134181,2385 | 1,7415 | 1,0000 |
| 1 | 21 | 3 | 18 | 0 | 22 | 4 | 19 | 32176205,8400 | 32176204,9789 | ,8611 | 1,0000 |
| 1 | 34 | 9 | 26 | 0 | 35 | 9 | 27 | 32296749,4500 | 32296749,5522 | -,1022 | 1,0000 |
| 1 | 33 | 0 | 33 | 0 | 34 | 1 | 34 | 32335224,2800 | 32335224,3027 | -,0227 | 1,0000 |
| 1 | 33 | 0 | 33 | 0 | 34 | 0 | 34 | 32335361,8700 | 32335361,8929 | -,0229 | 1,0000 |
| 1 | 33 | 1 | 33 | 0 | 34 | 1 | 34 | 32335393,8400 | 32335393,7746 | ,0654 | 1,0000 |
| 1 | 33 | 1 | 33 | 0 | 34 | 0 | 34 | 32335531,5000 | 32335531,3649 | ,1351 | 1,0000 |
| 1 | 32 | 12 | 20 | 0 | 33 | 12 | 21 | 32373175,8600 | 32373175,6356 | ,2244 | 1,0000 |
| 1 | 22 | 2 | 20 | 0 | 23 | 3 | 21 | 32373291,8400 | 32373291,2642 | ,5758 | 1,0000 |
| 1 | 6 | 4 | 2 | 0 | 7 | 5 | 3 | 32373315,2200 | 32373315,0746 | ,1454 | ,5000 |
| 1 | 6 | 4 | 3 | 0 | 7 | 5 | 2 | 32373315,2200 | 32373314,9150 | ,2850 | ,5000 |
| 1 | 25 | 5 | 21 | 0 | 25 | 6 | 20 | 32373323,7800 | 32373323,4675 | ,3124 | 1,0000 |
| 1 | 30 | 1 | 30 | 0 | 31 | 0 | 31 | 32418006,6800 | 32418006,6930 | -,0130 | 1,0000 |
| 1 | 18 | 8 | 10 | 0 | 17 | 9 | 9 | 32418191,3800 | 32418191,6432 | -,2632 | 1,0000 |
| 1 | 26 | 5 | 22 | 0 | 27 | 5 | 23 | 32481918,8400 | 32481917,5937 | 1,2463 | 1,0000 |
| 1 | 19 | 4 | 15 | 0 | 19 | 5 | 14 | 32516370,9200 | 32516373,5775 | -2,6575 | 1,0000 |
| 1 | 18 | 4 | 15 | 0 | 18 | 5 | 14 | 32516443,8100 | 32516444,2856 | -1,2756 | 1,0000 |
| 1 | 22 | 14 | 8 | 0 | 23 | 14 | 9 | 32647442,5200 | 32647442,4685 | ,0515 | 1,0000 |
| 1 | 30 | 1 | 29 | 0 | 30 | 2 | 28 | 32647452,8000 | 32647452,1041 | ,6959 | 1,0000 |
| 1 | 16 | 3 | 14 | 0 | 17 | 3 | 17 | 32676267,3800 | 32676265,1084 | 2,2716 | 1,0000 |
| 2 | 9 | 2 | 7 | 2 | 9 | 2 | 8 | 9158,9800 | 9158,7818 | ,1790 | 1,0000 |
| 2 | 3 | 1 | 2 | 2 | 3 | 1 | 3 | 9488,3500 | 9488,1823 | ,1677 | 1,0000 |
| 2 | 10 | 2 | 8 | 2 | 10 | 2 | 9 | 13527,4400 | 13527,2858 | ,1532 | 1,0000 |
| 2 | 4 | 1 | 3 | 2 | 4 | 1 | 4 | 15811,6800 | 15811,3268 | ,2732 | 1,0000 |
| 2 | 18 | 3 | 15 | 2 | 18 | 3 | 16 | 15987,1900 | 15987,0056 | ,1844 | 1,0000 |
| 2 | 11 | 2 | 9 | 2 | 11 | 2 | 10 | 19181,1900 | 19181,0588 | ,1312 | 1,0000 |
| 2 | 19 | 3 | 16 | 2 | 19 | 3 | 17 | 21484,5900 | 21484,8105 | -,2205 | 1,0000 |
| 2 | 1 | 0 | 1 | 2 | 0 | 0 | 0 | 22421,2600 | 22421,2228 | ,0372 | 1,0000 |
| 2 | 5 | 1 | 4 | 2 | 5 | 1 | 5 | 23718,6800 | 23718,2333 | ,4467 | 1,0000 |
| 2 | 12 | 2 | 10 | 2 | 12 | 2 | 11 | 26255,4700 | 26255,5534 | -,0834 | 1,0000 |
| 2 | 20 | 3 | 17 | 2 | 20 | 3 | 18 | 28299,1000 | 28298,9505 | ,2095 | 1,0000 |
| 2 | 6 | 1 | 5 | 2 | 6 | 1 | 6 | 33178,2000 | 33178,2088 | -,0120 | 1,0000 |
| 2 | 13 | 2 | 11 | 2 | 13 | 2 | 12 | 34859,7100 | 34859,4696 | ,2404 | 1,0000 |
| 2 | 2 | 1 | 2 | 2 | 1 | 1 | 1 | 43261,1200 | 43261,8285 | -,8914 | 1,0000 |
| 2 | 7 | 1 | 6 | 2 | 7 | 1 | 7 | 44203,2400 | 44202,8662 | ,3738 | 1,0000 |
| 2 | 2 | 0 | 2 | 2 | 1 | 0 | 1 | 44813,5500 | 44813,5824 | -,0324 | 1,0000 |
| 2 | 31 | 4 | 27 | 2 | 31 | 4 | 28 | 52935,1700 | 52935,1634 | ,0066 | 1,0000 |
| 2 | 8 | 1 | 7 | 2 | 8 | 1 | 8 | 56766,3400 | 56766,2781 | ,0619 | 1,0000 |
| 2 | 15 | 2 | 13 | 2 | 15 | 2 | 14 | 56935,1600 | 56935,4408 | -,2808 | 1,0000 |
| 2 | 3 | 1 | 3 | 2 | 2 | 1 | 2 | 64873,2800 | 64873,3344 | -,0544 | 1,0000 |
| 2 | 3 | 0 | 3 | 2 | 2 | 0 | 2 | 67148,5300 | 67148,2866 | ,2434 | 1,0000 |
| 2 | 3 | 2 | 2 | 2 | 2 | 2 | 1 | 67264,8900 | 67264,3151 | ,5749 | 1,0000 |
| 2 | 3 | 2 | 1 | 2 | 2 | 2 | 0 | 67379,8100 | 67378,7624 | 1,0476 | 1,0000 |
| 2 | 2 | 1 | 1 | 2 | 2 | 0 | 2 | 67913,5900 | 67913,5425 | ,0475 | 1,0000 |
| 2 | 3 | 1 | 2 | 2 | 2 | 1 | 1 | 69617,4200 | 69617,1324 | ,2876 | 1,0000 |
| 2 | 3 | 1 | 2 | 2 | 3 | 0 | 3 | 74382,4200 | 74382,3884 | ,0316 | 1,0000 |
| 2 | 4 | 1 | 3 | 2 | 4 | 0 | 4 | 73772,8900 | 73772,9038 | -,0138 | 1,0000 |
| 2 | 28 | 4 | 24 | 2 | 27 | 5 | 23 | 77128,4400 | 77128,4024 | ,0376 | 1,0000 |
| 2 | 5 | 1 | 4 | 2 | 5 | 0 | 5 | 78167,1700 | 78167,3433 | -,1733 | 1,0000 |
| 2 | 5 | 1 | 4 | 2 | 4 | 1 | 3 | 115926,2500 | 115926,2936 | -,0436 | 1,0000 |
| 2 | 7 | 1 | 7 | 2 | 6 | 1 | 6 | 151047,8400 | 151048,1642 | -,2642 | 1,0000 |
| 2 | 7 | 0 | 7 | 2 | 6 | 0 | 6 | 155363,1300 | 155363,2214 | -,0914 | 1,0000 |
| 2 | 7 | 2 | 6 | 2 | 6 | 2 | 5 | 156716,7600 | 156716,7463 | ,0137 | 1,0000 |
| 2 | 7 | 5 | 2 | 2 | 6 | 5 | 1 | 157659,9800 | 157660,1621 | -,1221 | 1,0000 |
| 2 | 7 | 4 | 4 | 2 | 6 | 4 | 3 | 157692,6400 | 157692,5629 | ,1371 | 1,0000 |
| 2 | 7 | 3 | 5 | 2 | 6 | 3 | 4 | 157161,5400 | 157161,5805 | -,0405 | 1,0000 |
| 2 | 7 | 3 | 4 | 2 | 6 | 3 | 3 | 157202,1700 | 157202,2373 | -,0673 | 1,0000 |
| 2 | 8 | 2 | 6 | 2 | 7 | 2 | 5 | 181331,7400 | 181331,8472 | -,1072 | 1,0000 |
| 2 | 8 | 1 | 7 | 2 | 7 | 1 | 6 | 185059,8300 | 185059,9718 | -,1418 | 1,0000 |
| 2 | 11 | 4 | 8 | 2 | 10 | 4 | 7 | 247475,8000 | 247475,9009 | -,0009 | ,1000 |
| 2 | 30 | 4 | 26 | 2 | 29 | 4 | 25 | 885316,8000 | 885316,6834 | ,1166 | ,1000 |
| 2 | 30 | 4 | 26 | 0 | 30 | 3 | 28 | 31491427,4000 | 31491426,8241 | 10,7459 | ,0001 |
| 2 | 11 | 4 | 8 | 0 | 12 | 3 | 10 | 31159508,3000 | 31159519,0459 | -10,7459 | ,0001 |

STANDARD DEVIATION OF FIT = ,3639650+00

Table 10.2: Computer fit of microwave, f.i.r. and i.r. transitions in HCOOH. The ground, $v_6$=1 and $v_8$=1 states are denoted by V=0,1,2 respectively.

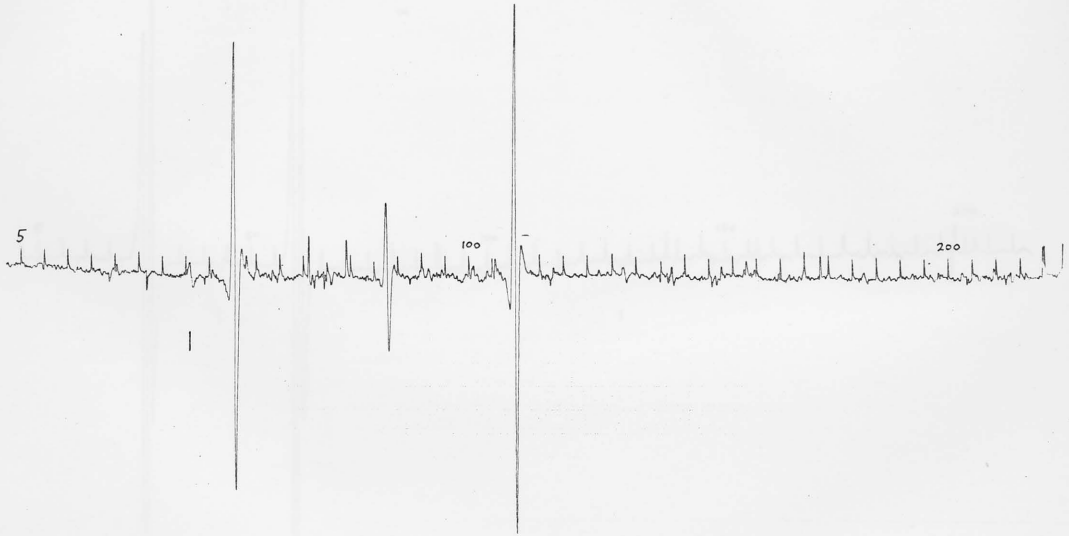


Fig. 10.2: Spectrum of formic acid (40 mtorr) taken on 9R(20) laser line, negative offset.

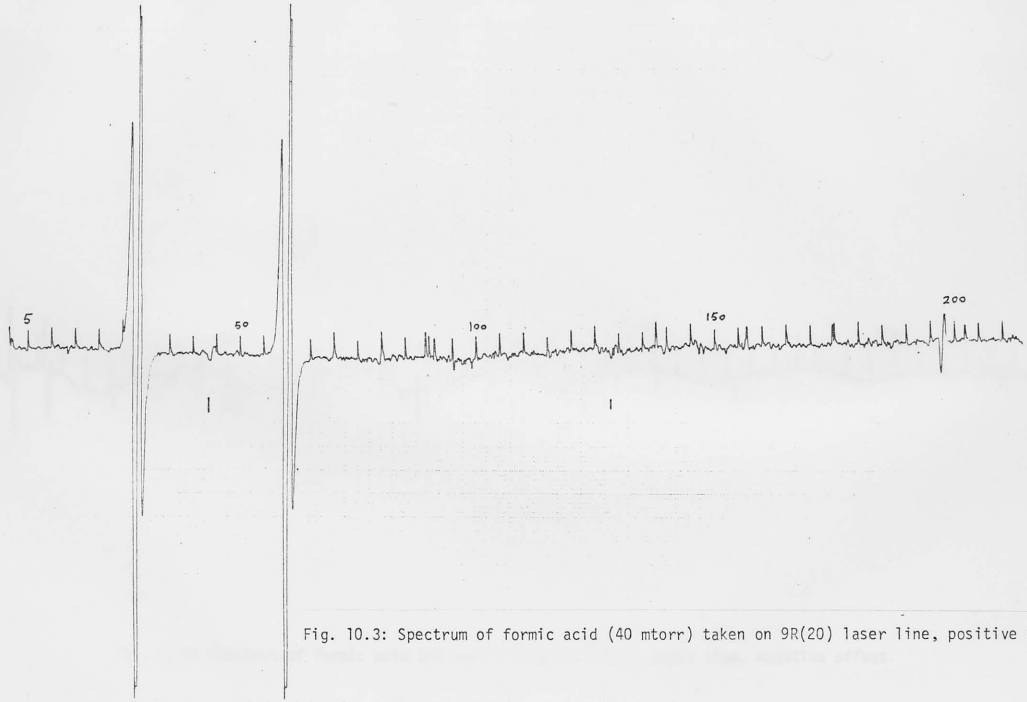


Fig. 10.3: Spectrum of formic acid (40 mtorr) taken on 9R(20) laser line, positive offset.

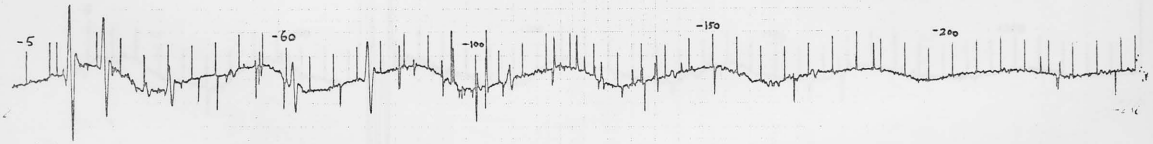


Fig. 10.4: Spectrum of formic acid (60 mtorr) taken on 9P(16) laser line, negative offset.

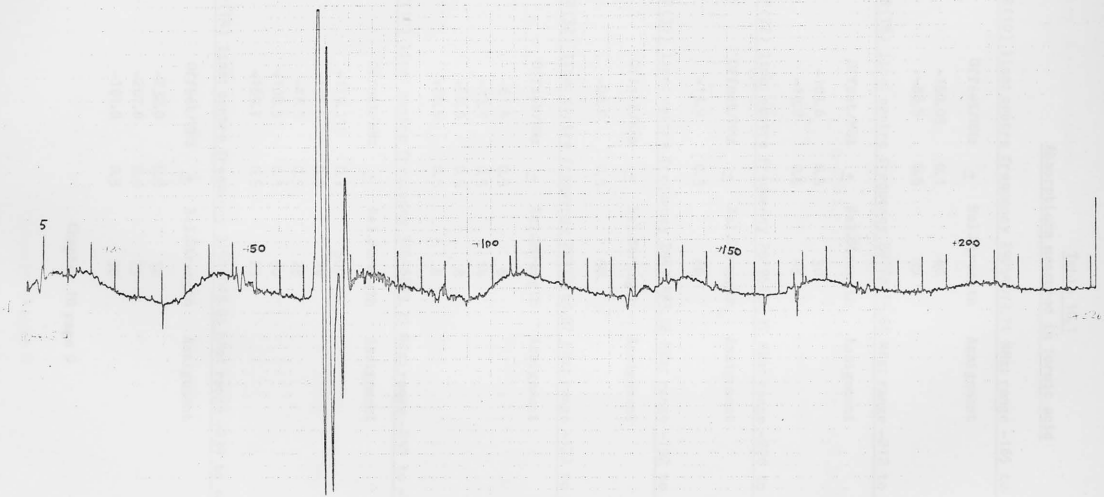


Fig. 10.5: Spectrum of formic acid (60 mtorr) taken on 9P(16) laser line, positive offset.

Table 10.1

Absorptions measured in formic acid

10R(10) line: centre frequency 29054072.71 MHz: range -165 to +148 MHz

| Offset/MHz | ± | Rel.Strength | Assignment |
|---|---|---|---|
| -150.05 | 0.1 | 40 | |
| -88.5 | 0.5 | 25 | |

10R(16) line: centre frequency 29178455.68 MHz: range -212 to +201 MHz

| Offset/MHz | ± | Rel.Strength | Assignment |
|---|---|---|---|
| -103.6 | 0.5 | 30 | |
| -19.2 | 0.5 | 48 | |

10R(22) line: centre frequency 29296136.37 MHz: range -206 to +213 MHz

| Offset/MHz | ± | Rel.Strength | Assignment |
|---|---|---|---|
| +14.9 | 0.3 | 80 | |

10R(30) line: centre frequency 29442483.32 MHz: range -192 to +183 MHz

| Offset/MHz | ± | Rel.Strength | Assignment |
|---|---|---|---|
| -86.0 | 0.5 | 50 | |

10R(32) line: centre frequency 29477160.87 MHz: range -172 to +163 MHz

| Offset/MHz | ± | Rel.Strength | Assignment |
|---|---|---|---|
| -61.4 | 0.5 | 8 | |
| -33.4 | 0.5 | 14 | |
| +58.0 | 0.5 | 8 | |
| +86.5 | 0.5 | 8 | |

9P(10) line: centre frequency 31646843.39 MHz: range -249 to +213 MHz

| Offset/MHz | ± | Rel.Strength | Assignment |
|---|---|---|---|
| -179.115 | 0.1 | 500 | |
| -137.5 | 0.5 | 34 | |
| -46.5 | 0.5 | 28 | |
| +108.5 | 0.5 | 90 | |
| +169.7 | 0.5 | 23 | |

9P(14) line: centre frequency 31544028.88 MHz: range -234 to +228 MHz

| Offset/MHz | ± | Rel.Strength | Assignment |
|---|---|---|---|
| -232.0 | 0.5 | 12 | |
| -207.0 | 0.5 | 25 | |
| -181.0 | 0.5 | 30 | |

Table 10.1 (continued)

| | | |
|---|---|---|
| -141.0 | 0.5 | 5 |
| -120.0 | 0.5 | 35 |
| -118.5 | 0.5 | 6 |
| -72.5 | 0.5 | 45 |
| -48.235 | 0.1 | 240 |
| +60.1 | 0.5 | 32 |
| +109.5 | 0.5 | 10 |
| +174.8 | 0.5 | 22 |

9P(16) line: centre frequency 31491437.39 MHz: range -238 to +226 MHz

| Offset/MHz | ± | Rel.Strength | Assignment |
|---|---|---|---|
| -171.2 | 1.0 | 4 | |
| -141.8 | 1.0 | 3 | |
| -107.0 | 0.5 | 8 | |
| -77.7 | 0.5 | 30 | |
| -61.8 | 0.5 | 20 | |
| -47.8 | 1.0 | 2 | |
| -35.6 | 0.5 | 17 | |
| -30.8 | 1.0 | 6 | |
| -21.8 | 0.5 | 42 | |
| -14.7 | 0.5 | 58 | |
| +4.5 | 0.5 | 11 | |
| +47.0 | 0.5 | 10 | |
| +64.460 | 0.1 | >3000 | $\nu_6\ {}^{26}12,14 \leftarrow {}^{26}13,13$ |
| +68.515 | 0.1 | 95 | |
| +128.7 | 0.5 | 9 | |

9P(18) line: centre frequency 31438060.18 MHz: range -231 to +224 MHz

| Offset/MHz | ± | Rel.Strength | Assignment |
|---|---|---|---|
| -135.38 | 0.1 | 110 | |
| -75.9 | 0.2 | 40 | |
| -72.805 | 0.1 | >400 | $\nu_6\ {}^{40}12,28 \leftarrow {}^{40}13,27$ |
| -62.4 | 0.2 | 8 | |
| +56.6 | 0.2 | 80 | |
| +71.8 | 0.5 | 5 | |

9P(20) line: centre frequency 31383900.41 MHz: range -141 to +134 MHz

| Offset/MHz | ± | Rel.Strength | Assignment |
|---|---|---|---|
| -105.25 | 0.5 | 5 | |
| -40.5 | 0.5 | 18 | |

Table 10.1 (continued)

9P(22) line: centre frequency 31328961.50 MHz: range -217 to +159 MHz

| Offset/MHz | ± | Rel.Strength | Assignment |
|---|---|---|---|
| -180.8 | 0.5 | 2 | |
| -57.8 | 0.5 | 40 | |
| -15.7 | 0.5 | 20 | |

9P(24) line: centre frequency 31273247.15 MHz: range -150 to +150 MHz

| Offset/MHz | ± | Rel.Strength | Assignment |
|---|---|---|---|
| -62.3 | 0.2 | 6 | |
| -61.1 | 0.2 | 4 | |
| -2.3 | 0.3 | 9 | |
| +102.7 | 0.5 | 8 | |

9P(26) line: centre frequency 31216761.31 MHz: range -234 to +229 MHz

| Offset/MHz | ± | Rel.Strength | Assignment |
|---|---|---|---|
| -46.0 | 0.5 | 15 | |
| -36.8 | 0.5 | 25 | |
| +7.2 | 0.5 | 51 | |
| +95.7 | 0.5 | 4 | |
| +102.2 | 0.5 | 15 | |

9P(28) line: centre frequency 31159508.16 MHz: range -234 to +228 MHz

| Offset/MHz | ± | Rel.Strength | Assignment |
|---|---|---|---|
| -68.2 | 0.5 | 8 | |
| -56.0 | 0.5 | 8 | |
| -39.5 | 0.5 | 43 | |
| +21.3 | 0.5 | 11 | |
| +49.0 | 0.5 | 7 | |
| +76.8 | 0.5 | 14 | |
| +111.6 | 0.5 | 13 | |
| +139.3 | 1.0 | 7 | |
| +167.0 | 1.0 | 7 | |

9P(30) line: centre frequency 31101492.18 MHz: range -187 to +202 MHz

| Offset/MHz | ± | Rel.Strength | Assignment |
|---|---|---|---|
| +28.8 | 0.5 | 8 | |
| +50.0 | 0.5 | 20 | |

9P(32) line: centre frequency 31042718.06 MHz: range -170 to +165 MHz

| Offset/MHz | ± | Rel.Strength | Assignment |
|---|---|---|---|

No lines seen.

Table 10.1 (continued)

9P(34) line: centre frequency 30983190.75 MHz: range -115 to +127 MHz

| Offset/MHz | ± | Rel.Strength | Assignment |
|---|---|---|---|
| +24.8 | 0.5 | 110 | |
| +42.0 | 1.0 | 6 | |
| +121.3 | 1.0 | 250 | |

9P(36) line: centre frequency 30922915.42 MHz: range -125 to +125 MHz

| Offset/MHz | ± | Rel.Strength | Assignment |
|---|---|---|---|
| -96.5 | 0.5 | 12 | |
| -88.8 | 0.5 | 25 | |
| +23.35 | 0.2 | 38 | |
| +79.3 | 0.5 | 3 | |

9P(38) line: centre frequency 30861897.50 MHz: range -112 to +112 MHz

| Offset/MHz | ± | Rel.Strength | Assignment |
|---|---|---|---|
| +5.64 | 0.2 | 80 | |

9R(4) line: centre frequency 32004017.38 MHz: range -81 to +76 MHz

| Offset/MHz | ± | Rel.Strength | Assignment |
|---|---|---|---|
| -28.300 | 0.1 | 8 | |
| -1.250 | 0.05 | 150 | $\nu_6\ ^{44}6,39 \leftarrow {}^{45}6,40$ |
| +68.950 | 0.05 | 85 | |

9R(6) line: centre frequency 32048236.24 MHz: range -133 to +139 MHz

| Offset/MHz | ± | Rel.Strength | Assignment |
|---|---|---|---|
| -79.155 | 0.1 | 90 | |
| +57.0 | 0.5 | 4 | |

9R(8) line: centre frequency 32091652.66 MHz: range -187 to +200 MHz

| Offset/MHz | ± | Rel.Strength | Assignment |
|---|---|---|---|
| -147.2 | 0.5 | 8 | |
| -132.600 | 0.1 | 140 | |
| -57.1 | 0.5 | 15 | |
| -41.6 | 0.5 | 30 | |
| -8.3 | 0.5 | 5 | |
| +20.135 | 0.1 | 90 | |
| +78.455 | 0.1 | 35 | |
| +87.1 | 0.5 | 12 | |
| +89.3 | 0.5 | 12 | |
| +133.350 | 0.1 | 45 | |
| +162.0 | 0.5 | 3 | |

Table 10.1 (continued)

9R(10) line: centre frequency 32134266.885 MHz: range -152 to +145 MHz

| Offset/MHz | ± | Rel.Strength | Assignment |
|---|---|---|---|
| -109.7 | 0.5 | 8 | |
| -84.0 | 0.5 | 7 | $\nu_6\ ^{29}12,17 \leftarrow {}^{28}13,16$ |
| +64.2 | 0.5 | 7 | |
| +87.5 | 0.5 | 20 | |
| +140.6 | 0.5 | 4 | |
| +144.1 | 0.5 | 7 | |

9R(12) line: centre frequency 32176079.48 MHz: range -264 to +201 MHz

| Offset/MHz | ± | Rel.Strength | Assignment |
|---|---|---|---|
| -216.5 | 0.5 | 7 | |
| -172.7 | 0.5 | 14 | |
| -137.0 | 0.5 | 7 | |
| -93.8 | 0.5 | 37 | |
| -64.4 | 0.5 | 8 | |
| +126.355 | 0.1 | 500 | $\nu_6\ ^{21}3,18 \leftarrow {}^{22}4,19$ |

9R(14) line: centre frequency 32217091.26 MHz: range -169 to +179 MHz

| Offset/MHz | ± | Rel.Strength | Assignment |
|---|---|---|---|
| +43.5 | 1.0 | 28 | |

9R(16) line: centre frequency 32257303.33 MHz: range -182 to +174 MHz

| Offset/MHz | ± | Rel.Strength | Assignment |
|---|---|---|---|
| +25.815 | 0.1 | 100 | |
| +79.315 | 0.1 | 85 | |

9R(18) line: centre frequency 32296717.04 MHz: range -149 to +144 MHz

| Offset/MHz | ± | Rel.Strength | Assignment |
|---|---|---|---|
| -126.5 | 0.5 | 3 | |
| -107.37 | 0.1 | 105 | |
| -89.0 | 0.5 | 2 | |
| -72.0 | 0.5 | 19 | |
| +32.42 | 0.1 | >1000 | $\nu_6\ ^{34}9,26 \leftarrow {}^{35}9,27$ |
| +50.55 | 0.1 | 100 | |
| +79.17 | 0.1 | 100 | |
| +117.2 | 0.5 | 4 | |
| +131.39 | 0.1 | 1000 | |

Table 10.1 (continued)

9R(20) line: centre frequency 32335334.03 MHz: range -223 to +214 MHz

| Offset/MHz | ± | Rel.Strength | Assignment |
|---|---|---|---|
| -109.745 | 0.05 | 90 | $\nu_6\ 33_{0,33} \leftarrow 34_{1,34}$ |
| -82.8 | 0.5 | 5 | |
| -50.28 | 0.1 | 18 | |
| -41.0 | 1.0 | 3 | three-level dip |
| +19.8 | 1.0 | 2 | |
| +27.845 | 0.05 | 260 | $\nu_6\ 33_{0,33} \leftarrow 34_{0,34}$ |
| +43.840 | 0.05 | 1 | collision-induced |
| +48.5 | 1.0 | 0.5 | |
| +50.5 | 1.0 | 1 | |
| +59.815 | 0.05 | 250 | $\nu_6\ 33_{1,33} \leftarrow 34_{1,34}$ |
| +79.0 | 1.0 | 0.5 | |
| +129.0 | 1.0 | 4 | three-level dip |
| +197.5 | 1.0 | 25 | $\nu_6\ 33_{1,33} \leftarrow 34_{0,34}$ |

9R(22) line: centre frequency 32373156.19 MHz: range -157 to +198 MHz

| Offset/MHz | ± | Rel.Strength | Assignment |
|---|---|---|---|
| -131.7 | 0.5 | 12 | |
| -123.8 | 0.5 | 4 | |
| -112.3 | 0.5 | 32 | |
| -105.0 | 0.5 | 28 | |
| -78.5 | 0.5 | 6 | |
| -69.0 | 0.5 | 2 | |
| -51.1 | 0.5 | 20 | |
| -32.8 | 0.5 | 8 | |
| -17.3 | 0.5 | 7 | |
| +10.7 | 0.5 | 7 | |
| +11.5 | 0.5 | 2 | |
| +19.67 | 0.1 | 1500 | $\nu_6\ 32_{12,20} \leftarrow 33_{12,21}$ |
| +65.5 | 0.5 | 5 | |
| +81.0 | 0.5 | 5 | |
| +81.5 | 0.5 | 20 | |
| +89.0 | 0.5 | 5 | |
| +108.7 | 0.5 | 1 | |
| +112.4 | 0.5 | 1 | |
| +134.85 | 0.5 | 43 | $\nu_6\ 22_{2,20} \leftarrow 23_{3,21}$ |
| +138.7 | 0.5 | 3 | |
| +153.96 | 0.1 | 50 | |
| +159.0 | 0.5 | 1 | $\nu_6\ 6_{4,2} \leftarrow 7_{5,3}$ and $6_{4,3} \leftarrow 7_{5,2}$ |
| +167.585 | 0.1 | 25 | $\nu_6\ 25_{5,21} \leftarrow 25_{6,20}$ |

Table 10.1 (continued)

9R(24) line: centre frequency 32410185.685 MHz: range -214 to +229 MHz

| Offset/MHz | ± | Rel.Strength | Assignment |
|---|---|---|---|
| -179.085 | 0.1 | 2000 | $\nu_6\ ^{30}{}_{1,30} \leftarrow {}^{31}{}_{0,31}$ |
| -141.4 | 0.5 | 40 | |
| -130.0 | 0.5 | 3 | |
| -128.7 | 0.5 | 4 | |
| -123.5 | 0.5 | 2 | |
| -116.2 | 0.5 | 15 | |
| -111.5 | 0.5 | 5 | |
| -96.5 | 0.5 | 4 | |
| -42.9 | 0.5 | 28 | |
| -30.4 | 0.5 | 50 | |
| -24.3 | 0.5 | 55 | |
| -20.5 | 0.5 | 120 | |
| +6.70 | 0.1 | 130 | $\nu_6\ ^{18}{}_{8,10} \leftarrow {}^{17}{}_{9,9}$ |
| +58.5 | 0.5 | 16 | |
| +72.5 | 0.5 | 5 | |
| +86.4 | 0.5 | 20 | |
| +93.7 | 0.5 | 44 | |
| +117.9 | 0.5 | 30 | |
| +122.97 | 0.1 | 2000 | |
| +135.1 | 0.5 | 47 | |
| +150.0 | 0.5 | 7 | |
| +178.9 | 0.5 | 15 | |
| +186.0 | 0.5 | 20 | |
| +200.0 | 0.5 | 5 | |

9R(26) line: centre frequency 32446424.93 MHz: range -189 to +185 MHz

| Offset/MHz | ± | Rel.Strength | Assignment |
|---|---|---|---|
| -112.5 | 0.5 | 10 | |
| -110.9 | 0.5 | 6 | |
| -58.3 | 0.5 | 9 | |
| -37.1 | 0.5 | 84 | |
| -32.9 | 0.5 | 85 | |
| +34.4 | 0.5 | 90 | |
| +42.7 | 0.5 | 11 | |
| +49.2 | 0.5 | 76 | |
| +104.05 | 0.1 | >120 | |
| +152.8 | 0.5 | 27 | |

Table 10.1 (continued)

9R(28) line: centre frequency 32481876.59 MHz: range -154 to +154 MHz

| Offset/MHz | ± | Rel.Strength | Assignment |
|---|---|---|---|
| -64.0 | 0.1 | 110 | |
| +3.86 | 0.1 | 42 | |
| +18.41 | 0.1 | 110 | |
| +20.675 | 0.1 | 100 | |
| +41.45 | 0.1 | >2000 | $\nu_6$ $26_{5,22} \leftarrow 27_{5,23}$ |
| +107.0 | 0.2 | 35 | |

9R(30) line: centre frequency 32516543.61 MHz: range -184 to +182 MHz

| Offset/MHz | ± | Rel.Strength | Assignment |
|---|---|---|---|
| -172.685 | 0.1 | 400 | $\nu_6$ $19_{4,15} \leftarrow 19_{5,14}$ |
| -161.6 | 0.5 | 20 | |
| -140.60 | 0.1 | >2000 | $\nu_6$ $18_{4,15} \leftarrow 18_{5,14}$ |
| -97.9 | 0.5 | 8 | |
| -61.395 | 0.1 | >1000 | |
| -39.54 | 0.1 | >2000 | |
| -33.0 | 0.5 | 3 | |
| -28.0 | 0.5 | 2 | |
| +9.6 | 0.5 | 23 | |
| +31.8 | 0.5 | 27 | |
| +48.00 | 0.1 | 700 | |

9R(32) line: centre frequency 32550429.14 MHz: range -115 to +115 MHz

| Offset/MHz | ± | Rel.Strength | Assignment |
|---|---|---|---|
| -24.97 | 0.1 | 190 | |
| -13.35 | 0.2 | 48 | |
| -4.5 | 0.5 | 7 | |
| +4.45 | 0.1 | 35 | |
| +100.7 | 0.5 | 10 | |

9R(34) line: centre frequency 32583536.61 MHz: range -207 to +155 MHz

| Offset/MHz | ± | Rel.Strength | Assignment |
|---|---|---|---|
| -199.0 | 0.5 | 3 | |
| +58.7 | 0.5 | 23 | |
| +73.5 | 0.5 | 33 | |
| +120.0 | 0.5 | 16 | |

9R(36) line: centre frequency 32615869.675 MHz: range -104 to +103 MHz

| Offset/MHz | ± | Rel.Strength | Assignment |
|---|---|---|---|
| -76.3 | 0.5 | 5 | |
| +4.58 | 0.1 | 270 | |

Table 10.1 (continued)

| | | |
|---|---|---|
| +30.01 | 0.1 | 98 |
| +32.78 | 0.1 | 102 |

9R(38) line: centre frequency 32647432.22 MHz: range -138 to +146 MHz

| Offset/MHz | ± | Rel.Strength | Assignment |
|---|---|---|---|
| -45.1 | 0.5 | 3 | |
| +10.30 | 0.1 | 81 | $\nu_6\ 22_{14,8} \leftarrow 23_{14,9}$ |
| +19.58 | 0.1 | 39 | $\nu_6\ 30_{1,29} \leftarrow 30_{2,28}$ |

9R(40) line: centre frequency 32678228.36 MHz: range -56 to +56 MHz

| Offset/MHz | ± | Rel.Strength | Assignment |
|---|---|---|---|
| -21.0 | 0.2 | 280 | $\nu_6\ 18_{3,16} \rightarrow 19_{3,17}$ |

## 11. CONCLUSIONS

It has been demonstrated here and elsewhere that waveguide carbon dioxide lasers can be used as spectral sources for high resolution spectroscopy. The resolution obtained here is some 100 times better than that achievable by any Doppler-limited spectrometer. Elsewhere, even higher resolution has been demonstrated in spectra of strongly-absorbing molecules (van Lerberghe, Avrillier & Borde, 1978).

Further development of spectrometers of this type should proceed in the direction of increased spectral coverage. Methods of improving the laser tuning range have already been discussed in chapter 2. Another approach is to operate the laser on other lines of carbon dioxide (e.g. the sequence band lines) or other molecules such as carbon monoxide, or other isotopes of these molecules. A long waveguide laser with auxilliary mode selection would be particularly suited to these investigations as operation on weaker transitions would then be possible.

At the present time, the tunability of an individual line is only about 1% of the typical line separation; in consequence, the easily-recognised band structures produced by broadband spectrometers do not appear. Furthermore, many simple molecules which absorb in the 9 to 11 μm region have few absorptions accessible to the spectrometer; allene and phosphine are examples. In such cases, a broadband spectrum is usually an essential prerequisite for line identification; waveguide laser and Fourier-transform spectrometers are thus complementary. Microwave and far-infrared measurements can also be very helpful in this respect.

The most profitable applications of waveguide laser spectrometers would seem to be in those areas where lower resolution is inadequate. Two examples have been presented in this thesis. First, the hyperfine structure of transitions is usually sub-Doppler in scale (as for methyl iodide); observation of this structure yields new knowledge and may also assist in assignment of lines, since well-documented formulae relate the hyperfine pattern to the rotational state (Kroto, 1975). Other fine structure such as K-doubling is similarly helpful. Second, molecules having a very dense spectrum cannot readily be understood from conventional spectra, since the typical spacing between absorption lines may be below the instrument resolution even when using a good Fourier-transform instrument. This applies particularly to molecules having overlapping absorption bands and to asymmetric tops; formic acid provides an excellent example of both.

With theoretical models improving and computers becoming larger and faster, the number of molecules which may profitably be studied at high resolution is ever increasing. It is my hope that others will continue this work, and that the spectrometer which has absorbed much of my effort over these past years will not lie idle.

REFERENCES


Abrams R L & Bridges W B, 1973:

'Characteristics of sealed-off waveguide $CO_2$ lasers', IEEE J.Quantum Electron. QE9 940.

Abrams R L, 1974

'Gigahertz tunable waveguide $CO_2$ laser', Appl.Phys.Letts. 25 304.

Amat G & Henry L, 1960:

'Résonances et dédoublements du type K dans les molécules a symétrie axiale', J.Phys.Radium 21 728.

Arimondo E & Glorieux P, 1979:

'Saturated absorption experiments on a dressed molecule: application to the spectroscopy of the $v_6$ band of $CH_3I$', Phys.Rev.A 19 1067.

Arimondo E, Glorieux P & Oka T, 1978:

'Radio-frequency spectroscopy inside a laser cavity; "pure" nuclear quadrupole resonance of gaseous $CH_3I$', Phys.Rev.A 17 1375.

Avrillier S & Verdonck J, 1977:

'Coupling losses in laser resonators containing a hollow rectangular dielectric waveguide', J.Appl.Phys. 48 4937.

Baskakov O I, Dyubko S F, Moskienko M V & Fesenko L D, 1977:

'Identification of active transitions in formic acid vapour laser', Sov.J.Quantum Electron. 7 445.

Bjarnov E & Hocking W H, 1978:

'The structure of the other rotamer of formic acid, cis-HCOOH', Z.Naturforsch 33a 610.

Born M & Huang K, 1954:

'Dynamical Theory of Crystal Lattices', Oxford University Press.

Bridges T J, Burkhardt E G & Smith P W, 1972:

'$CO_2$ waveguide lasers', Appl.Phys.Lett. 20 403.

Butcher R J & Jones W J, 1973:

'The Raman spectrum of allene', J.Raman Spectrosc. 1 393.

Dangoisse D, Willemot E, Deldalle A & Bellet J, 1979:

'Assignment of the HCOOH cw-submillimetre laser', Opt.Commun. 28 111.

Degnan J J & Hall D R, 1973:

'Finite-aperture waveguide laser resonators', IEEE J.Quantum Electron. QE9 901.

Deldalle A, Dangoisse D, Splingard J P & Bellet J, 1977:

'Accurate measurements of c.w. optically pumped f.i.r. laser lines of formic acid molecule and its isotopic species $H^{13}COOH$, HCOOD and DCOOD', Opt.Commun. 22 333.

Duley, W W 1976:

'$CO_2$ lasers: effects and applications', Academic Press, New York.

Dyubko S F, Svich A V & Fesenko L D, 1976:

'Submillimetre HCOOH, DCOOH, HCOOD and DCOOD laser', Sov.Phys.Tech.Phys. 20 1536.

Evans D E, Prunty S L & Sexton M C, 1980:

'A boron nitride cw carbon dioxide waveguide laser for optically pumping heavy water', Infrared Phys. 20 21.

Freed C, Bradley L C & O'Donnell R G, 1980:

'Absolute frequencies of lasing transitions in seven $CO_2$ isotopic species', IEEE J.Quantum Electron. QE16 1195.

Freed C & Javan A, 1970:

'Standing-wave saturation resonances in the $CO_2$ 10.6 μm transitions observed in a low-pressure room-temperature absorber gas', Appl.Phys.Letts. 17 53.

Freed C & O'Donnell R G, 1977:

'Advances in $CO_2$ laser stabilisation using the 4.3 μm fluorescence technique', Metrologia 13 151.

Grenier-Besson M L, 1960:

'Résonances et dédoublements rotationels du type l dans les molécules a symétrie axiale', J.Phys.Radium 21 555.

Hall D R, Gorton E K & Jenkins R M, 1977:

'10 μm propagation losses in hollow dielectric waveguides', J.Appl.Phys. 48 1212.

Hall J L, 1973:

'The lineshape problem in laser-saturated molecular absorption', Lectures in Theoretical Physics (ed. Mahanthappa K T & Brittin W E B), Gordon & Breach, New York.

Hauck J P & Huffmann E H, 1980:

'Three-watt near room-temperature CO waveguide laser', Rev.Sci.Instrum. 51 1265.

Herlemont F, Lyszyk M, Lemaire J, Lambeau Ch & Fayt A, 1979:

'Laser spectroscopy of ethylene with waveguide $CO_2$ and $N_2O$ lasers', J.Mol.Spectrosc. 74 400.

Herzberg G, 1945:

'Infrared and Raman Spectra', van Nostrand, Princeton.

Johns J W C, McKellar A R W, Oka T & Römheld M, 1975:

'Collision-induced Lamb dips in laser Stark spectroscopy', J.Chem.Phys. 62 1488.

Kroto H W, 1975:

'Molecular Rotation Spectra', Wiley, London.

Laakmann K D & Steier W H, 1976:

'Waveguides: characteristic modes of hollow rectangular dielectric waveguides', Appl.Optics 15 1334.

Leeb W R, 1975:

'Tunability characteristics of waveguide $CO_2$ lasers with internal etalons', Appl.Opt. 14 1706.

Leeb W R, 1976:

'Tunable metal film filters as narrowband ir laser reflectors', Appl.Opt. 15 681.

van Lerberghe A, Avrillier S & Borde C J, 1978:

'High stability cw waveguide $CO_2$ laser for high resolution saturation spectroscopy', IEEE J.Quantum Electron. QE14 481.

Letokhov V S & Chebotayev V P, 1977:

'Nonlinear Laser Spectroscopy', Springer Series in Optical Sciences vol. 4, Springer-Verlag, Berlin.

Lyszyk M, Herlemont F & Lemaire J, 1977:

'On the tuning range of a cw double-discharge Pyrex waveguide $^{12}C^{16}O_2$ laser', J.Phys.E 10 1110.

Maki A G & Toth R A, 1965:

'Infrared measurements on allene and allene-$d_4$', J.Mol.Spectrosc. 17 136.

Marcatili E A J & Schmeltzer R A, 1964:

'Hollow metallic and dielectric waveguides for long distance optical transmission and lasers', Bell Syst.Tech.J. 43 1783.

Malk E G, Niesen J W, Parsons D F & Coleman P D, 1978:

'Laser emission in the 83-223 μm region from $PH_3$ with laser line assignments', IEEE J.Quantum Electron. QE14 544.

Meyer F, Dupre J & Meyer C, 1975:

'Passive Q-switching of a $CO_2$ laser by allene molecule', J.Mol.Spectrosc. 55 28.

Meyer T W, Rhodes C K & Haus H A, 1975:

'High resolution line broadening and collisional studies in $CO_2$ using nonlinear spectroscopic techniques', Phys.Rev.A 12 1993.

Mills I M, 1964:

'Selection rules for rovibronic transitions in symmetric top molecules', Mol.Phys. 7 549.

Mills I M, Smith W L & Duncan J L, 1965:

'Coriolis perturbations in the infrared spectrum of allene', J.Mol.Spectrosc. 16 349.

Oka T, 1967:

'Vibration-rotation interaction in symmetric top molecules and the splitting between $A_1$ and $A_2$ levels', J.Chem.Phys. 47 5410.

Oka T, 1973:

'Advances in Atomic & Molecular Physics' vol. 9, Academic Press, New York.

Papanayou A, 1976:

'Measurements and analysis of a carbon dioxide boron nitride channel laser', R & D Tech. report ECOM-4430, US Army Electronics Command, New Jersey.

Pine A S, 1980:

'Tunable laser survey of molecular air pollutants: Doppler-limited spectra of the C-H stretching bands of formaldehyde, ethylene, ethane and allene', Final Report, Lincoln Laboratory, Massachusetts Institute of Technology.

Rackley S A, 1980:

Unpublished results; for a description of the apparatus used see: 'Stabilisation of $CO_2$ lasers using the Stark effect' by S.A.Rackley, PhD. thesis, Cambridge University (1980).

Radford H E, Petersen F R, Jennings D A & Mucha J A, 1977:

'Heterodyne measurements of submillimetre laser spectrometer frequencies [for magnetic resonance spectroscopy]', IEEE J.Quantum Electron. QE13 92.

Rowley W R C, 1977:

'A digital frequency offset-lock system designed for use with stabilised lasers', NPL Quantum Metrology Report Qu40.

Schonland D, 1965:

'Molecular Symmetry', van Nostrand, London.

Shafik S, Crocker D, Landsberg B M & Butcher R J, 1981:

'Phosphine far infrared cw laser transitions; optical pumping at more than 100 MHz from resonance', IEEE J.Quantum Electron. (to be published).

Shimizu F, 1975:

'Stark spectroscopy of $PH_3$ by 10 μm $CO_2$ and $N_2O$ lasers', J.Phys.Soc.Jap. 38 293.

Shotton K C & Rowley W R C, 1975:

'An electronic servocontrol system for stabilised lasers and similar applications', NPL Quantum Metrology Report Qu28.

Stone J M R, 1971:

'The infrared spectrum of the $\nu_{10}$ band of allene', J.Mol.Spectrosc. 38 503.

Thomas J E, Kelly M J, Monchalin J P, Kurmit N A & Javan A, 1980:

'Stable $CO_2$ and $N_2O$ laser design', Rev.Sci.Instrum. 51 240.

Watson J K G, 1967:

'Determination of centrifugal distortion coefficients in asymmetric-top molecules', J.Chem.Phys. 46 1935.

Willemot E, Dangoisse D & Bellet J, 1979:

'Microwave spectrum of the vibrational excited states $\nu_6$ and $\nu_8$ of formic acid', J.Mol.Spectrosc. 77 161.

Willemot E, Dangoisse D, Monnanteuil N & Bellet J, 1980:

'Microwave spectra of molecules of astrophysical interest XVIII: formic acid', J.Phys.Chem.Ref.Data 9 59.

Woods P T & Joliffe B W, 1976:

'Stable single-frequency carbon dioxide lasers', J.Phys.E 9 395.

Yin P K L & Rao K N, 1974:

'$\nu_2$ and $\nu_4$ fundamentals of phosphine occurring at 8-12 μm', J.Mol.Spectrosc. 51 199.